United States, National Bur. of Standards

SECTION C

A UNITED STATES DEPARTMENT OF COMMERCE PUBLICATION

JOURNAL OF RESEARCH

of the NATIONAL BUREAU OF STANDARDS

Volume 75C Nos. 3&4 July - Dec. 1971

ENGINEERING

Engineering and Instrumentation

U.S. DEPARTMENT OF COMMERCE
National Bureau of Standards

Journal of Research
of the
National Bureau of Standards

C. Engineering and Instrumentation

July–Dec. • 1971

VOLUME • 75C

NUMBERS • 3 & 4

Editor: Martin Greenspan

Associate Editors: G. F. Montgomery, R. V. Smith, A. F. Schmidt

Publication dates:
Feb. 15, May 15, Aug. 15, Nov. 15, 1971

J. Res. Nat. Bur. Stand. (U.S.), C
CODEN: JNBCA 75C (3 & 4) 145–219 (1971)

JOURNAL OF RESEARCH

The National Bureau of Standards Journal of Research reports research and development in the fields of activity shown at right. Also included from time to time are survey articles on topics closely related to the Bureau's scientific and technical program.

The Journal is published in three separate sections as follows:

A. Physics and Chemistry

Contains papers of interest primarily to scientists working in these fields. Issued six times a year. Annual subscription: domestic, $9.50; foreign, $11.75. Single copy, varies.

B. Mathematical Sciences

Presents studies and compilations designed mainly for the mathematician and the theoretical physicist. Issued quarterly. Annual subscription: domestic, $5.00; foreign, $6.25. Single copy, $1.25.

C. Engineering and Instrumentation

Reports research and development results of interest chiefly to the engineer and the applied scientist. Issued quarterly. Annual subscription: domestic, $5.00; foreign, $6.25. Single copy, $1.25.

The National Bureau of Standards[1] was established by an act of Congress March 3, 1901. The Bureau's overall goal is to strengthen and advance the Nation's science and technology and facilitate their effective application for public benefit. To this end, the Bureau conducts research and provides: (1) a basis for the Nation's physical measurement system, (2) scientific and technological services for industry and government, (3) a technical basis for equity in trade, and (4) technical services to promote public safety. The Bureau consists of the Institute for Basic Standards, the Institute for Materials Research, the Institute for Applied Technology, the Center for Computer Sciences and Technology, and the Office for Information Programs.

THE INSTITUTE FOR BASIC STANDARDS provides the central basis within the United States of a complete and consistent system of physical measurement; coordinates that system with measurement systems of other nations; and furnishes essential services leading to accurate and uniform physical measurements throughout the Nation's scientific community, industry, and commerce. The Institute consists of a Center for Radiation Research, an Office of Measurement Services and the following divisions:

Applied Mathematics—Electricity—Heat—Mechanics—Optical Physics—Linac Radiation[2]—Nuclear Radiation[2]—Applied Radiation[2]—Quantum Electronics[3]—Electromagnetics[3]—Time and Frequency[3]—Laboratory Astrophysics[3]—Cryogenics[3].

THE INSTITUTE FOR MATERIALS RESEARCH conducts materials research leading to improved methods of measurement, standards, and data on the properties of well-characterized materials needed by industry, commerce, educational institutions, and Government; provides advisory and research services to other Government agencies; and develops, produces, and distributes standard reference materials. The Institute consists of the Office of Standard Reference Materials and the following divisions:

Analytical Chemistry—Polymers—Metallurgy—Inorganic Materials—Reactor Radiation—Physical Chemistry.

THE INSTITUTE FOR APPLIED TECHNOLOGY provides technical services to promote the use of available technology and to facilitate technological innovation in industry and Government; cooperates with public and private organizations leading to the development of technological standards (including mandatory safety standards), codes and methods of test; and provides technical advice and services to Government agencies upon request. The Institute also monitors NBS engineering standards activities and provides liaison between NBS and national and international engineering standards bodies. The Institute consists of the following technical divisions and offices:

Engineering Standards Services—Weights and Measures—Flammable Fabrics—Invention and Innovation—Vehicle Systems Research—Product Evaluation Technology—Building Research—Electronic Technology—Technical Analysis—Measurement Engineering.

THE CENTER FOR COMPUTER SCIENCES AND TECHNOLOGY conducts research and provides technical services designed to aid Government agencies in improving cost effectiveness in the conduct of their programs through the selection, acquisition, and effective utilization of automatic data processing equipment; and serves as the principal focus within the executive branch for the development of Federal standards for automatic data processing equipment, techniques, and computer languages. The Center consists of the following offices and divisions:

Information Processing Standards—Computer Information—Computer Services—Systems Development—Information Processing Technology.

THE OFFICE FOR INFORMATION PROGRAMS promotes optimum dissemination and accessibility of scientific information generated within NBS and other agencies of the Federal Government; promotes the development of the National Standard Reference Data System and a system of information analysis centers dealing with the broader aspects of the National Measurement System; provides appropriate services to ensure that the NBS staff has optimum accessibility to the scientific information of the world, and directs the public information activities of the Bureau. The Office consists of the following organizational units:

Office of Standard Reference Data—Office of Technical Information and Publications—Library—Office of International Relations.

---

[1] Headquarters and Laboratories at Gaithersburg, Maryland, unless otherwise noted; mailing address Washington, D.C. 20234.
[2] Part of the Center for Radiation Research.
[3] Located at Boulder, Colorado 80302.

U.S. DEPARTMENT OF COMMERCE
Peter G. Peterson, Secretary
NATIONAL BUREAU OF STANDARDS
Lewis M. Branscomb, Director

Order all publications from the Superintendent of Documents
U.S. Government Printing Office, Washington, D.C. 20402.

Use of funds for printing this publication approved by the Director of the Bureau of the Budget (June 22, 1966).

JOURNAL OF RESEARCH of the National Bureau of Standards—C. Engineering and Instrumentation
Vol. 75C, Nos. 3 and 4, July–December 1971

Thermal Voltage Converters and Comparator for Very Accurate AC Voltage Measurements

E. S. Williams

Institute for Basic Standards, National Bureau of Standards, Washington, D.C. 20234

(July 22, 1971)

A new fourteen-range set of thermal voltage converters and a thermoelement comparator are used to measure ac-dc difference, and a-c voltages relative to external d-c standards, with 20 ppm (parts-per-million) accuracy at audio frequencies. The imprecision is less than 2 ppm. Corrections relative to the very stable middle ranges can be redetermined for every range by a seven-step intercomparison of certain adjacent ranges.

Key words: AC-DC difference; comparator; thermoelement; transfer voltmeter; voltage measurements.

1. Introduction

An a-c voltage at audio frequencies is measured most accurately at the present time by using a thermal voltage converter (TVC) to compare it with a stable and accurately measured d-c voltage, which is nominally equal to it. The basic d-c standards are then, in effect, "transferred" to the a-c measurement. The TVC may be simply a thermoelement (TE) in series with an appropriate multiplier resistor. The output emf of the TE is ordinarily monitored with a null detector and a balancing circuit, which may be a Lindeck potentiometer. A balancing circuit and a null detector are included in most commercial multi-range models.

Before the TVC is used for a-c voltage measurements it must be tested for ac-dc difference or frequency influence so that corrections may be applied. The set of TVCs and the new TE comparator described in this paper were developed primarily for making these tests. However they may also be used for a-c voltage measurements as explained in section 9. For ac-dc difference measurements the TE comparator, whose read out instrument may be either a nanovoltmeter or a galvanometer, provides a considerable advantage over other methods in overcoming the difficulties caused by power supply instability and inexact voltage control.

The 14-range set of TVCs (designated No. 7) consists of six resistor units and two TEs, and extends from 1 to 1000 V. The TEs are rated at 2.5 and 5.0 mA, and each one may be attached to any one of the resistors by a coaxial connector (see fig. 1). This permits each resistor to be used for two voltage ranges, as shown in table 1. Certain adjacent ranges of the set can be intercompared, and the ac-dc differences of all the ranges can be determined relative to any one range. This set is otherwise similar to an earlier set [1][1], which consisted of two 5-mA TEs and 12 series resistors, and covered a range from 0.5 to 500 V. The earlier set, designated No. 1, has been extended to 1000 V with one additional resistor as part of the present project. It is evaluated in a 14-step intercomparison in which each range is compared, at reduced voltage, with the next lower one.

In a well designed TVC the ac-dc difference is not affected by changes in the applied voltage. Therefore, an ac-dc difference determined for the 100-V range at 60 V can be applied as a correction when this resistor is used at 200 V to test the nominal 300-V range of the next higher resistor. Experience has shown this step-up procedure to be feasible. However if the higher voltage ranges are not carefully built the ac-dc differences can change due to self-heating effects to be described later.

2. Design and Construction

The two TEs are mounted in 2-in brass tubes (see figs. 1 and 2, upper right) with coaxial connectors for attaching to a resistor. The 2.5 mA-TE has a 400 Ω heater and is used alone as the 1-V range. The 5 mA-TE has a 125 Ω heater and a 275 Ω resistor is added inside its enclosure to make a 400 Ω, 2-V range.

The middle ranges (six ranges, 3 to 60 V) make use of three resistors—0.8 kΩ, 3.6 kΩ, and 12 kΩ (see table 1). Each of these is a 2W metal-film resistor mounted coaxially in a 3-in brass cylinder 4 1/2 in long with coaxial connectors at each end.

[1] Figures in brackets indicate the literature references on page 153.

FIGURE 1. *New set of thermal voltage converters.*

The simple symmetrical geometry of these units permits approximate calculations of their reactances [2]. The calculations are inexact because of the necessary assumptions as to end-effects, and they neglect any small residual reactances of the resistors themselves. They do indicate however, that the frequency error of each resistor unit (without the TE) should be less than 1 ppm at 50 kHz, even for tubes smaller than 2 in in diameter. (The 3-in tube was chosen for the higher ranges where more space is necessary and was therefore used for the middle ranges also.)

The higher voltage ranges have larger resistor assemblies to avoid excessive temperature rise. The 100–200 V unit has a 40 kΩ spiraled metal-film resistor five inches long.[2] The 300–600 and 500–1000 V units have resistors of tin oxide deposited on a 0.81-in glass tube 6 in long. A small voltage coefficient was anticipated in these resistors, but measurements have shown it to be negligible.

[2]This experimental resistor is not ordinarily available commercially. Four 40 kΩ metal film resistors in series-parallel can also be satisfactory.

TABLE 1. *NBS thermal voltage converter set No. 7*

Fourteen voltage ranges (column 2) are formed with six series resistors and two TEs (F 1 and F 2).

Series resistor	*Voltage range*	*TE*	*Total resistance*
kΩ		*mA*	*kΩ*
.....	1	2.5 (F 1)	0.4
.....	2	5.0 (F 2)	0.4
	3	2.5	1.2
0.8.....	6	5.0	1.2
	10	2.5	4.0
3.6.....	20	5.0	4.0
	30	2.5	12.4
12.....	60	5.0	12.4
	100	2.5	40.4
40.....	200	5.0	40.4
	300	2.5	120.4
120.....	600	5.0	120.4
	500	2.5	200.4
200.....	1000	5.0	200.4

Errors in these ranges are caused mainly by capacitance between the resistor assembly and the outer casing, which permits alternating current to bypass the TE to ground. Therefore more a-c than d-c voltage is required for a given TE output. Frequency compensation could be provided by placing relatively small capacitors in parallel with part of the resistance. However, such capacitors probably would not be sufficiently stable over a long period of time and might be affected by temperature changes which occur in the resistor enclosure.

Compensation was therefore provided (as in the earlier set No. 1) with an inner shield which is connected to the input and surrounds the high- or input-end of the resistor (see "S" in fig. 2). The shield is positioned, relative to the resistor, to control the capacitance currents and provide optimum high-frequency

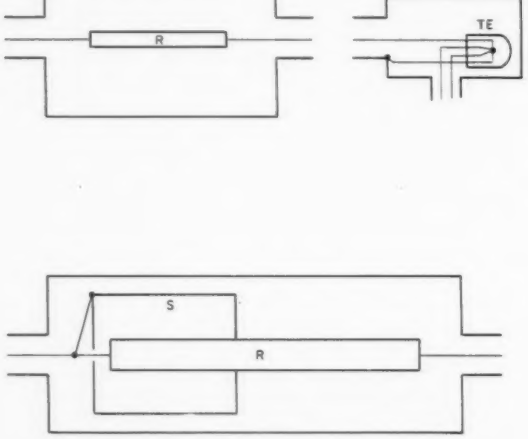

FIGURE 2. *Essentials of thermal voltage converters.*
Thermoelement (TE) enclosure, low voltage unit with resistor (R), and high voltage unit (100 to 1000 V) with resistor (R) and frequency compensation shield (S).

compensation; perfect compensation is possible only at one frequency.

3. 1000-V TVC

As stated earlier the corrections for the high and low voltage ranges are determined relative to the middle range by intercomparison tests. It is necessary therefore that the ac-dc difference of all ranges be unaffected by voltage level. The voltage effect is rare in low and middle ranges, but it can be troublesome at higher ranges where the heat generated by the resistor is appreciable. All intercomparison tests were initially made at two voltage levels in order to evaluate this effect—or to prove its absence. If, for example, the nominal 600-V range is compared with the 1000-V range at both 400 and 600 V, and the same results are obtained, it is unlikely that the 600-V range is affected by the voltage increase (the 1000-V range is very probably unaffected at these voltages). However both ranges are in question until we are assured that the 1000-V range is also free of this effect.

The highest range, then presents a special problem. It is more likely to change due to increased voltage (heating) and there is no higher range to compare it with. If it is compared with another 1000-V TVC at two or more voltages and no change is observed it is possible that both have the same voltage effect. However this is unlikely if TVCs are of somewhat different design. If intercomparisons of several units of difference design show no change between rated voltage and a lower voltage we may safely assume this effect is negligible in each one.

Five 1000-V TVCs (table 2) have therefore been built, each with differing components, and a network of intercomparison tests was made as described in the next section. The original set of TVCs [1] was included in these tests.

TABLE 2. *Five 1000-V TVCs*

Unit	*Resistance*	*Voltage range with TE*		*Resistor assembly*
		F 1	*F* 2	
	kΩ			
A	400	1000		Four 100 kΩ wire-wound resistors in series, each 1 3/8 in long.
B	400	1000		Four 100 kΩ wire-wound resistors in series, each 1 3/8 in long.
C	200	500	1000	Four 200 kΩ metal-film resistors in series-parallel, each 2 in long.
D	200	500	1000	One 200 kΩ tin oxide resistor 6 in long.
E	400	1000		Four 400 kΩ metal-film resistors in series-parallel, each 2 in long.

The five 1000-V TVCs are designated alphabetically (A through E)[3] and all except "A" have the inner shield, as described below, for frequency compensation. The resistor in unit "A" is mounted concentrically in a set of six brass rings whose potentials are maintained by a capacitance divider. The whole assembly is mounted in a 4-in brass cylinder 7 in long.

Self-heating of a TVC may affect either the frequency compensation or the resistor itself. Apparently the dielectric losses in the insulation between conductors can be affected by heating and change the impedance of the resistor. This change occurred within a few minutes after a voltage increase or decrease in several resistor types, which were therefore discarded.

The frequency compensating shield may be moved, relative to the resistor, by thermal expansion of mounting parts and cause a change in ac-dc difference. This occurred in some of our early units and the change was slow, taking up to an hour. Later shields were therefore mounted very rigidly since a small displacement will have a large effect on the frequency influence.

The shield now in use is in two parts. A brass cylinder, with one end closed, is mounted firmly against the outer end piece (input end) with a polystyrene insulator one-half inch thick (fig. 3). A movable tube fits tightly inside this cylinder and the shield length adjustment is made by pushing this piece forward with a small rod inserted through the end piece and the insulator. The rod is removed after each adjustment.

The shield is most effective at the leading edge where the voltage difference is greatest between the resistor and the shield. Therefore the movable part of the shield is cut at an angle, so that only part of it (see fig. 3) extends outside the fixed cylinder. Thereby the effect of small position changes is reduced. Even so, the compensation is affected by approximately 0.01 percent per millimeter of position change in some typical units.

The shield length adjustment is made in small steps, and tests are made after each adjustment. When optimum compensation is achieved, the unit is opened and the shield parts are locked together with three screws through their overlapping portions.

4. TE and TVC Tests

As stated earlier the middle ranges are the most accurate, and they are the base from which higher and lower ranges are tested. However they are no more accurate than the TE used with them. Before being installed in a TVC the TEs are therefore compared with one of a group of carefully selected TE standards which were made according to NBS specifications. This group contains twelve elements made by four manufacturers, and are rated from 5 to 20 mA. [1] They have either Karma or Evanohm [4] heaters to reduce

[3] Unit "D" is assigned to this set (No. 7).

[4] Certain commercial products and instruments are identified in this paper in order to specify adequately the experimental procedure. In no case does such identification imply recommendation or endorsement by the National Bureau of Standards, nor does it imply that the products or equipment identified are necessarily the best available for the purpose.

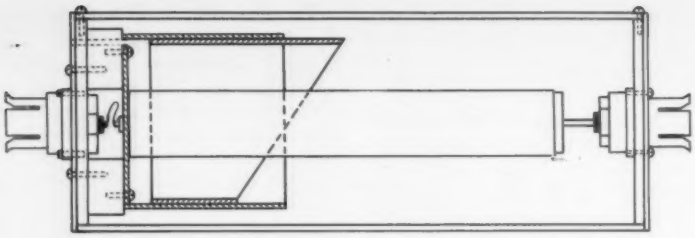

FIGURE 3. *Cross section of high voltage TVC.*
Input end is at the left. Fixed and adjustable shield parts are supported by a polystyrene insulator one-half inch thick.

thermoelectric effects in the heaters. They also have small reverse d-c differences (less than 200 ppm), high bead resistances (over 1000 MΩ), and small ac-dc differences. An additional two are multi-junction elements of different design. All of these TEs have been intercompared as current converters with agreement to better than 3 ppm. Theoretical calculations, taking into consideration all known sources of error, also indicate that the error should not exceed a few ppm at audio frequencies. Because of this and because of the excellent agreement between these thermoelements of different design and construction, we may safely assume that the average ac-dc difference of the group is 0 to ±2 ppm.

The low-frequency performance of a TVC depends on the TE since the reactance of the resistor is entirely negligible even at a few kilohertz. The accuracy of a TE at low frequency is mainly dependent on the length of the heater. A very short heater permits heat to flow more readily to the support stems and cooling to occur between current peaks. However most commercial TEs have errors less than 10 ppm at 20 Hz and some have errors less than 10 ppm even at 5 Hz.

In testing selected commercial TEs for the TVCs at audio frequencies we often find a small ac-dc difference (up to 4 ppm) which is independent of frequency but dependent on heater current. It ordinarily decreases at lower heater currents. When these TEs are used in a TVC the ac-dc difference will therefore be slightly voltage dependent. In the step-up test process, where the TVC is alternately used at 50 and 100 percent of rated current, this relatively small thermoelement error is introduced at every step of the process. If the process is a long one, as in the 12-resistor set, there could be a significant accumulation of error. TVCs in the new set are intercompared by testing each resistor once with one TE at reduced current (60 or 67%), and again with rated current on the other TE. If these TEs differ in ac-dc difference at these currents, there will again be an accumulation of error.

This is one of the advantages of the set with only six resistors. If the 20-V range is the starting point (it is probably the most stable), we have only four steps up to the 1000-V range, and three steps down to the 1-V range. The other advantages are that less time is required for the intercomparisons and there are fewer units to construct.

Intercomparison data for this set of TVCs are listed in table 3 as well as determinations made using TVC set No. 1. (Test methods are discussed in later sections of the paper). The middle ranges differ by 2 ppm or less even though the resistance varies from 1200 to 12000 Ω. Since the resistance enters into the theoretical calculation of ac-dc difference, this agreement is an additional indication of accuracy.

Step-down tests show that the two lowest voltage ranges usually have a positive correction (i.e., more a-c than d-c voltage is required for a given TE output) of 5 ppm or less at 50 kHz. There is no resistor in series with the TE at the 1 V range, and at the 2-V range the TE is a large part of the total impedance. These ranges are therefore affected more by the small reactance of the TE. The corrections for these ranges are more likely to change if a TE is replaced than for the higher ranges. A step-down test from the middle range is therefore advisable when TE replacements are made.

The five 1000-V TVCs were compared with the 300- and 500-V ranges of TVC set No. 1 and the 600-V range of the new set No. 7. The corrections are listed in table 4 for 20 and 50 kHz and all values are averaged.

TABLE 3. *AC-DC difference*

TVC-a	TVC-b	Applied voltage	AC-DC difference (ppm)					
			20 kHz			50 kHz		
			$\delta_a-\delta_b$	δ_x	δ	$\delta_a-\delta_b$	δ_x	δ
F1		1		−3	−3		+1	−3
F2	F1	1	+1			0		
F2		2		−2	−2		+1	−2
F1–3	F2	2	+1			−1		
F1–3		3		−1	+1		0	−2
F2–6		6		−1	0		0	−3
F1–10	F2–6	6	+1			+1		
F1–10		10		0	+1		+1	+1
F2–20		20		0	0		+1	+1
F1–30	F2–20	20	−1			−2		
F1–30		30		−1	+1		−1	+2
F2–60		60		−1	0		−1	0
F1–100	F2–60	60	−1			−4		
F1–100		100		−2	0		−5	−2
F2–200		200		−2	−1		−5	−6
F1–300	F2–200	200	−2			+6		
F1–300		300		−4	−3		+1	+4
F2–600		600		−4	−4		+1	+1
F1–500	F2–600	500	−2			+26		
F1–500		500		−6	−3		+27	+30
F2–1000		1000		−6			+27	

Table 5 lists intercomparison data for the same frequencies for seven pairings of the five 1000-V TVCs. Values for 600 and 1000 V do not differ significantly and so they are all averaged together.

Corrections (δ) for each range of the new TVC set are listed as determined in comparison with TVC Set No. 1. Intercomparison data($\delta_a - \delta_b$) are also listed and a computed correction (δ_s) based on the intercomparison, starting with the average of the measured ac-dc differences of the 10- and 20-V ranges. The TVCs are identified as the combination of a TE (F1 or F2) with the appropriate resistor; i.e., F2–600 forms the 600-V range.

Averages of the corrections for the five 1000-V TVCs listed in table 4 are shown in the circles in figure 4, and the connecting lines show the intercomparison values from table 5. The agreement between the various units is illustrated by this figure.

Each of the values listed in tables 4 and 5 is the average of at least four separate determinations. An analysis of the data taken in a series of 26 intercomparison tests (an average of 5 determinations with each one), involving all ranges at two frequencies and usually two voltages, showed an imprecision ($3\,\sigma_a$, where σ_a is the standard deviation of the average of five determinations) of only 1.4 ppm.

TABLE 4. *Ac-dc difference corrections for five 1000-volt TVC (A–E)*
The standard instruments are the 300- and 500-V units of Set No. 1 and the 600-V range of Set No. 7.

Standard	Volts	A	B	C	D	E
AC-DC difference at 20 kHz (ppm)						
500–1	500		−20	−9	−4	−12
300–1	300				−4	−10
600–7	600	−3	−22		−2	−12, −10
		−8			−3	−10
Ave.		−6	−21	−9	−3	−11
AC-DC difference at 50 kHz (ppm)						
500–1	500	+21	−6	+11	+30	−3
300–1	300				+30	−4
600–7	600	+30	−9		+30	−6
		+23			+32	−6
Ave.		+25	−7	+11	+30	−5

TABLE 5. *Relative ac-dc differences for seven pairings of members of the five 1000-V TVCs*

Volts	$\delta_A-\delta_B$	$\delta_B-\delta_C$	$\delta_C-\delta_D$	$\delta_D-\delta_E$	$\delta_E-\delta_A$	$\delta_A-\delta_C$	$\delta_A-\delta_D$
AC-DC difference at 20 kHz (ppm)							
600	−11	+14	+2	−7	+7	+3	0
1000	−17	+13	0	−6	0	+9	+5
600	−16	+17		−10			−2
1000	−17						+5
Ave.	−15	+15	+1	−7	+4	+6	+2
AC-DC difference at 50 kHz (ppm)							
600	−20	+14	+10	−33	+28	−15	+3
1000	−22	+6	+2	−33	+35	−14	+4
600	−25			−37		−15	+2
1000	−24						+1
Ave.	−23	+10	+6	−34	+32	−15	+2

5. Thermal Compensation

The coaxial connector between the TE and the series resistor provides a low-reactance connection for minimum frequency error. Tests and calculations show the error is less than 1 ppm at 50 kHz. However, it also permits heat to flow freely from the resistor, which dissipates up to five watts on the 1000-V range, to the TE which has a temperature coefficient of emf of approximately 0.2 percent/° C (at constant input current).

Heat conduction through the center conductor of this connector was reduced, at 300 V and higher, by replacing the two polystyrene insulators in the coaxial connectors (one in the resistor output and one in the TE input) with two made of boron nitride. This material is a good electrical insulator and yet it conducts heat well enough to provide an effective heat sink for this conductor. It is used in both ends of the high voltage resistors to improve the heat flow from the resistor to the relatively heavy brass casing. This also helps to reduce the temperature rise in the resistor.

Heat flow through the outer part of these connectors will gradually raise the temperature of the TE casing, and this also causes a heating drift. The increase in temperature of the TE bulb is slowed by mounting it in a short section of brass tubing to increase the thermal mass and this tube is thermally insulated from the TE casing. Thermal compensation is also added by attaching a 10-Ω thermistor to the tube containing the TE and connecting it in series with the TE output. A resistor appropriately chosen to complete the compensation circuit (see Fig. 7 and appendix I) will draw current through the thermistor sufficient to compensate for the temperature increase.

This resistor value may be computed for TEs with average temperature coefficients as in appendix I. However, temperature coefficients differ considerably and, for best results, it is usually necessary to match the resistor to the TE and thermistor combination. A suitable value can be found by substituting a variable resistor outside the TE casing and adjusting it for minimum warmup drift on a 1000-V range. However, if the TVC is to be used with a TE comparator similar to the one to be described, it will frequently be connected

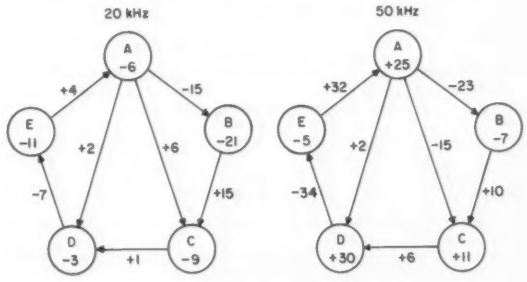

FIGURE 4. *Intercomparisons of 1000-volt TVCs.*
Ac-dc difference corrections (ppm) from table 4 for five 1000-V TVCs are shown in the circles and the relative differences from table 5 are shown on the interconnecting lines. The algebraic difference between any pair should be equal to the figure on the connecting line within experimental error.

across a 1000-Ω divider, and this will affect the compensation by about 20 percent. A value about 10 percent higher than the one chosen experimentally should provide a satisfactory compromise and reduce the drift by a factor of five or more. With the compensation and the large thermal time constant of the TE in its casing, the drift can be reduced to less than 5 ppm/minute under typical laboratory condition. The error from this is almost completely eliminated by taking a sequence of readings with a-c, d-c, reversed d-c, and a-c voltage applied, as described in the next section.

6. TVC Test Methods

A brief review of other comparison methods may be useful before describing the TE comparator. Figure 5 shows two TVCs connected in parallel. The separate balancing circuits (or Lindeck Potentiometers) (B) and null detectors (D) may or may not be built in. Stable a-c and d-c voltage supplies are connected to the two TVCs by the ac-dc switch. The switching arrangement shown is typical and convenient, although others, such as reversing the d-c supply by a separate switch, are satisfactory. The d-c supply must have an ungrounded output and it should be possible to ground either terminal as the voltage is reversed. The reversed d-c differences of the TVC can rarely, if ever, be neglected in these tests.

For convenience and clarity, we shall call one TVC the "standard" and the other the "test." Normally the one with known ac-dc difference corrections is the standard, and the test TVC is usually treated differently in the test procedures, as explained below.

There are two procedures for this intercomparison. One might be called a null-balancing method. With a-c voltage applied to both TVCs, the balancing circuits of the test and standard instruments are adjusted to null the detectors. The d-c supply is then switched to the TVCs, and the voltage is adjusted to obtain a null balance first on the detector of the test instrument and then on the standard. Each d-c voltage is carefully measured, and the small difference between the two should equal the difference between the a-c voltage and one direction of d-c voltage. The measurement is then repeated with reversed d-c voltage, and an average is taken.

This method is tedious and time consuming, an accurate d-c voltage standard is required, and if there is any drift in either instrument output due to warmup or other reasons, as there very often is, the data may lack both accuracy and precision.

A more satisfactory procedure and one that will minimize the effect of drift may be called a deflection method. Both balancing circuits are adjusted to near null, and then a-c and d-c voltages are applied in the succession indicated in figure 5 (AC, DC+, DC−, AC). For each input the power supply is adjusted to set the test instrument detector to null. The deflection of the standard TVC detector is read for each setting, and the difference between the average reading on a-c voltage and d-c voltage is an indication of relative ac-dc difference. If the readings are made at nearly equal time intervals, and if the drift rate is reasonably constant (even though fairly large), the determinations can be made with satisfactory precision.

If the detector of the standard TVC is a galvanometer the reading may be in divisions or millimeters, but they can be converted to volts or percent ac-dc differences by calibrating the detector scale in one of several ways. A calibration factor can be determined simply and directly by making a small measured change in the d-c input and observing the detector response.

If the detector is a microvoltmeter and if the balancing circuit is a Lindeck potentiometer indicating the millivolt output of the thermoelement, the calibration step can be eliminated. With the four deflection readings on the detector the difference between the average reading on a-c voltage (E_a) and those on d-c voltage (E_d) is computed from the differences of the corresponding readings of the microvoltmeter. The ac-dc difference of the test instrument is

$$\delta_t = \delta_s + \frac{E_{sa} - E_{sd}}{n_s E_{sd}}$$

where the subscript s indicates that these values come from the standard instrument, and δ_s is the ac-dc difference correction for the standard.[5]

The factor n relates small changes in thermoelement heater current (ΔI) (at a fixed frequency) to corresponding changes in output emf ($\Delta E/E = n\Delta I/I$ approximately). For a TVC we may substitute $n\Delta V/V$ for the right hand expression, so that $n = V\Delta E/E\Delta V$. The value of n is 2 if the thermoelement has a square law response, possibly at very low heater currents, but it is usually 1.7 to 1.9 at rated current. Determinations of n should therefore be made in a d-c test at five or more current levels by measuring the values indicated. A plot of n against E can be made so that values corresponding to any emf can be found for substitution in the equation above (see sec. 8).

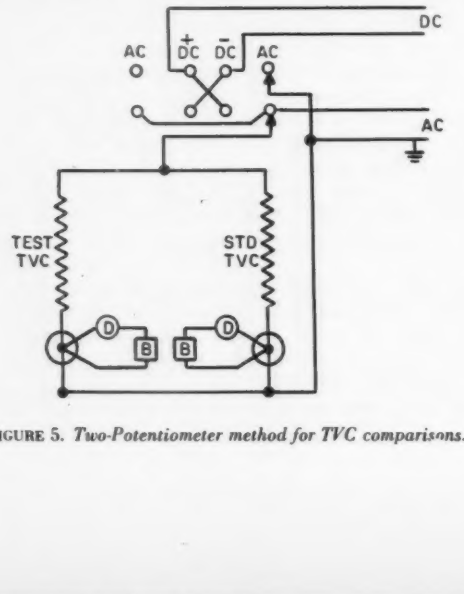

FIGURE 5. *Two-Potentiometer method for TVC comparisons.*

[5] See eq 3 of appendix II. This general formula is applicable here also.

7. TE Comparator

There are several variations of basic comparator circuits which are used to minimize the difficulty caused by power supply instability [1, 3]. They employ a voltage divider circuit to which two emfs are connected. The divider is adjusted to null a detector, and at this point the divider setting corresponds to the ratio of the emfs. If one emf (E_t) is held constant as a-c and then d-c voltage is applied to the TVCs, the other emf (E_s) will change if there is a relative ac-dc difference in the TVCs at the frequency ($\delta_t \neq \delta_s$). The resulting unbalance in the divider will produce a change in the detector deflection proportional to the ac-dc difference. However, small fluctuations in the power supply will produce nearly equal proportional changes in the emfs and therefore the detector will not be affected appreciably. The stabilizing effect depends on how well matched the time constants and response characteristics of the TEs are, but the effect usually affords a significant advantage. Also, the monitored emf need not be held constant so exactly as with a simple balancing circuit.

In the new comparator (fig. 6) the higher of the two emfs is connected across a 1000-Ω Kelvin-Varley divider, and the lower one is connected to the variable tap. The detector is brought to null by adjusting the divider. A Lindeck potentiometer and the same detector (with key k_1) is used to monitor the test TVC output (E_t). The detector is labeled "N" in the diagram because the use of a nanovoltmeter is suggested.

The test procedure is similar to that already mentioned. Preliminary settings of the potentiometer and divider are first made so the readings of the nanovoltmeter will fall near mid-scale. Then with a-c voltage applied, the key k_1 (labeled "SET" on the instrument, figs. 8 and 9) is depressed and the appropriate power supply is adjusted for a null on the detector. Key k_2 (READ) is then depressed and the detector indication is read. The two-step procedure is repeated for two directions of d-c voltage and for a second a-c input. The average indication in nanovolts [6] (N_a) for a-c input and the average for d-c input (N_d) is computed and the ac-dc difference of the test instrument is

$$\delta_t = \delta_s + \frac{N_d - N_a}{n_s E_s} \qquad \text{(appendix II eq 5)}$$

Figure 6 shows the test TVC output (E_t) connected to the high emf terminal (E_H in fig. 8). If E_t is smaller than E_s it will be necessary to interchange them, but this is a minor inconvenience. If E_t is connected to the E_L terminal the potentiometer is switched to that input with switch S_2 (fig. 8) and E_t is monitored as before. The same switch also reverses the polarity of the detector, and therefore the sign of the indication. The slightly modified equation for δ_t is eq 11 in appendix II.

A galvanometer may also be used as a detector but since the circuit resistance is relatively high a photoelectric amplifier is necessary for sufficient sensitivity. The scale must be linear over the portion to be used and a scale calibration is also necessary to relate the readings in divisions or millimeters to a voltage change. The calibration can be made quite easily however by moving switch S_1 from READ to CAL with k_2 closed and observing the resulting deflection change. This increases the resistance of the 1000-Ω divider by 0.5 Ω and changes the divider current by 0.05 percent. The

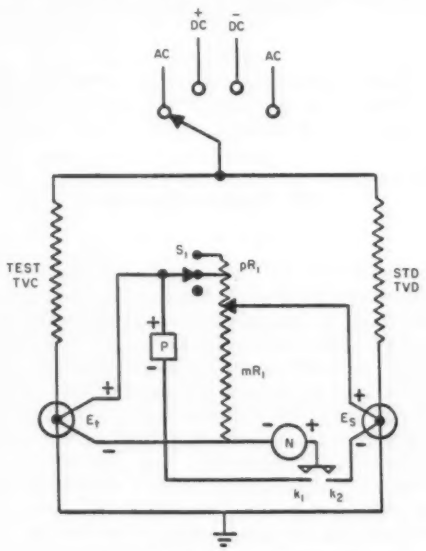

FIGURE 6. *New TE comparator.*

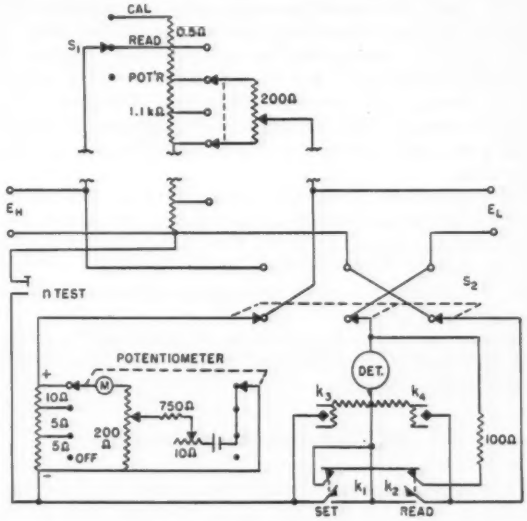

FIGURE 8. *New TE comparator.*

[6] $\delta_t - \delta_s$ is conveniently in parts-per-million if E_t is in millivolts and $N_d - N_a$ is in nanovolts.

FIGURE 9. *Photograph of TE comparator.*

voltage applied to the galvanometer circuit is changed by the same amount and the deflection change D_1 is used in eq 10 and 12 in appendix 2 to determine δ_t. A measurement of E_s is made only to find the corresponding value of n_s from a plot as before.

8. *n* Tests

Measurements of n are conveniently made with the comparator. The thermoelement to be tested is connected to the E_L input and the E_H input is unused. A key labeled "n TEST" (fig. 6) is locked down and switch S_2 is moved to E_H connecting the potentiometer voltage across the divider. The divider is set arbitrarily but preferably near full range and the potentiometer is adjusted to null the detector. The input voltage is then changed by a small measured amount $\Delta V/V$, and the resulting change in TE output (ΔE) is measured by observing the change in indication of the detector (nanovolts or microvolts).[7] Switch S_2 is then moved to E_L and a measurement of TE output (E) is made with the potentiometer. The values for each factor of the equation given above ($n = V\Delta E/E\Delta V$) are then known and n is calculated from this equation.

If a galvanometer is used as the detector a measurement of D_1 is made as described above, and the deflection change resulting from the measured change in input voltage (ΔV) is designated D_2. Then $n = 0.05\ D_2/qD_1$, where q is the percentage change in input voltage ($100\ \Delta V/V$).

Determinations of n need be accurate only to a few percent, and, since they are quite stable, retesting is not usually necessary.

9. AC Voltage Measurements

As suggested earlier, the comparator may be used with one TVC to measure an a-c voltage such as the input to a digital voltmeter or the output of a calibrated a-c voltage supply. Switch S_1 has a third position marked "POT'R" which disconnects the divider from the E_H input. If a TVC output is connected to E_H, and switch S_2 is moved to that input, the potentiometer and detector can be used to measure the TVC output and changes in it. The circuit is as figure 5 without the test TVC. The d-c voltage is accurately measured and nominally equal to the a-c voltage.

It is suggested that d-c voltage be applied to the TVC first and a detector reading taken. Then, at nearly equal time intervals, a second reading is taken with a-c voltage and a third with reversed d-c voltage. The difference between the average of the readings with a d-c voltage (E_d) and the one with a-c voltage (E_a) is related to the input voltage difference very much as before.

$$V_{ac} = V_{dc}\left(1 + \frac{E_a - E_d}{nE} + \delta_s\right)$$

With a nanovoltmeter the emfs are read directly, but if the detector is a galvanometer a scale sensitivity factor must be determined.

10. Design Details

The case of the TE comparator has thermal insulation and electrostatic shielding, and the comparator is carefully built to minimize thermal emfs and contact resistances. The switch decks of the Kelvin-Varley divider and S_1 and S_2 have enclosed silver contacts and the keys k_1 and k_2 are of a low-thermal type. The back contacts on these keys connect a 100-Ω shunt across the detector to reduce sensitivity and noise until one key or the other is depressed. The fine control for the divider is a ten-turn helical resistor with a special low-thermal sliding contact. The resolution of the uncalibrated divider is not quite sufficient for setting an exact null on the detector, but setting within a few divisions is adequate in the ordinary use of the instrument.

[7] A small change in the input to a TVC can be measured with a volt box and potentiometer or by a setting with a calibrated d-c voltage supply. It is also convenient to use a resistor with a shorting switch in series with a TVC to introduce a small current change (ΔI) in the thermoelement heater (i.e., 20 Ω with a 40-kΩ, 200-V TVC will give $100\ \Delta I/I = 0.05$ percent which is equivalent to $100\ \Delta V/V$).

11. Conclusion

The use of one resistor unit for two TVC voltage ranges has reduced by about half the time required, over previous TVC sets, to make a complete intercomparison test. Changes in any member of the set are readily detected since frequent intercomparison tests are more feasible.

The TE comparator combines the stabilizing feature of other comparators with much of the simplicity of the single Lindeck potentiometer or balancing circuit. It is relatively inexpensive to build and calculations are simplified and direct, especially where the detector is a nanovoltmeter. Repeated tests have shown that the imprecision is less than 2 ppm and ac-dc transfer accuracies, with the TVC set, are 10 ppm at audio frequencies and 20 ppm up to 50 kHz.

This work was supported in part by the Army Metrology and Calibration Center, Redstone, Alabama. Their encouragement and support are gratefully acknowledged. The author also acknowledges the help of C. B. Childers and A. G. Perrey who made many of the exacting measurements described here.

12. References

[1] Hermach, F. L. and Williams, E. S., Thermal converters for audiofrequency voltage measurements of high accuracy, IEEE Transactions on Instrumentation and Measurement, **IM-15,** No. 4, 260–268, (Dec. 1966).

[2] Hermach, F. L. and Williams, E. S., Thermal voltage converters for accurate voltage measurements to 30 mcgacycles per second, Trans. AIEE (Communication and Electronics), **79,** Pt. I, 200–206, (July 1960).

[3] Turgel, Raymond S., A comparator for thermal ac-dc transfer standards, ISA Transactions, **6,** No. 4, 286–292, (1967).

13. Appendix I

The temperature coefficient of emf, β, of the average TE is about -0.2 percent/° C, with constant input current. Thus a corresponding decrease in the resistance, $R = R_c + R_t + R_s$ (see fig. 7) is required to maintain a constant voltage across the resistor R_s. For a 1 degree increase in temperature, the change in thermistor resistance, $\Delta R_t = \alpha R_t/100$ where α is the temperature coefficient of the thermistor in percent/° C – typically about -4 percent/° C. Therefore, for thermal compensation,

$$\beta = 100\Delta R_t/R = \alpha R_t/R$$

$$\text{and } R = \alpha R_t/\beta$$

With the typical values listed we find $R = 200\ \Omega$, and, subtracting R_c and R_t, the value for R_s is 180 Ω.

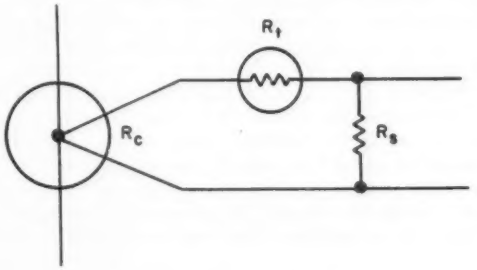

FIGURE 7. *Thermal compensation for TE.*

R_c TE output resistance (about 10Ω).
R_t Thermistor resistance (about 10Ω).
R_s Series resistor to complete compensation circuit. (R_c and R_t have negligible temperature coefficients.)

14. Appendix II

Development of Equations[4]

The ac-dc difference of a TVC is defined as

$$\delta = \frac{V_a - V_d}{V_d} \tag{1}$$

where V_a is the a-c voltage and V_d the average of the two directions of dc-voltage required to produce the same output emf. In the circuit of figure 6 the a-c and d-c voltages are adjusted to give the same emf E_t, of the TVC under test, as indicated by a null on the detector N with k_1 closed. The same voltages are applied to the standard TVC. Then,

$$V_a = V_d(1+\delta_t) = V'_d(1+\delta_s) \tag{2}$$

where V'_d is the d-c voltage required to produce the same output emf of the standard as V_a, and the subscripts, t and s, refer to the test and standard instruments respectively. If $V'_d - V_d << 1$, then, closely enough

$$\delta_t - \delta_s = \frac{V'_d - V_d}{V_d}.$$

From the definition of n given in the paper

$$\delta_t - \delta_s = \frac{E_{sa} - E_{sd}}{n_s E_{sd}} \tag{3}$$

With the polarities as shown in figure 6,

$$N = mE_t - E_s \tag{4}$$

where N is the detector voltage with k_2 closed and k_1 open, and m is the divider ratio (with the detector resistance $R_d >> R_1$).

Thus.

$$\delta_t = \delta_s + \frac{N_d - N_a}{n_s E_{sd}} \tag{5}$$

where the subscript a and d have the same meaning as before.

[4] These equations were developed by F. L. Hermach.

If a galvanometer is used as the detector, the current through it with k_2 closed is, by Thevenin's Theorem,

$$I_{gb}=\frac{mE_t-E_s}{R_e} \tag{6}$$

where R_e is the resistance of the galvanometer circuit with E_t and $E_s=0$. With E_t and E_s held constant and pR_1 inserted by means of S_1,

$$I_{gc}=\frac{mE_t/(1+p)-E_s}{R_e'} \tag{7}$$

where R_e' is the resistance of the galvanometer circuit.

Since $mE_t-E_s<<E_s$ and $p<<1$, we have to a sufficient degree of approximation,

$$I_{gb}-I_{gc}=\frac{E_sp}{R_e}=\frac{(D_b-D_c)}{S}=\frac{D_1}{S} \tag{8}$$

where D_b and D_c are the resulting galvanometer deflections and S is the galvanometer current sensitivity.

In the ac-dc test, with mE_t constant,

$$I_{ga}-I_{gd}=\frac{E_{sd}-E_{sa}}{R_e}=\frac{D_a-D_d}{S} \tag{9}$$

Thus, from (3), (8) and (9),

$$\delta_t=\delta_s+\frac{p(D_d-D_a)}{n_sD_1} \tag{10}$$

The test and standard TVCs may be interchanged if $E_t<E_s$. If E_t is applied to the E_L input of figure 8 and held constant, with the detector and potentiometer connected as shown in the figure, a similar analysis leads to the following equations:

$$\delta_t=\delta_s+\frac{N_d-N_a}{n_sE_t} \tag{11}$$

and

$$\delta_t=\delta_s+\frac{p(D_d-D_a)}{n_sD_1} \tag{12}$$

The characteristic n is determined from

$$n=\frac{\Delta E/E}{\Delta V/V} \tag{13}$$

by applying known changes in input voltage and observing the changes in output emf with a high resistance voltmeter, as described in the text. If a galvanometer is used as the detector instead of the voltmeter its sensitivity is determined by inserting pR_1 as described. From equations similar to (8) and (9)

$$\frac{\Delta E_s}{E_s}=\frac{p\Delta D}{D_1} \tag{14}$$

If the thermocouple resistance of the test TVC, R_{tc}, is significant, p in equation (7) should be replaced by p', the fraction of R_1+R_{tc} inserted by S_1. Similarly if the potentiometer resistance R_p is significant, p in equation (14) should be replaced by p'', the fraction of R_1+R_p inserted by S_1.

(Paper 75C3&4-321)

JOURNAL OF RESEARCH of the National Bureau of Standards—C. Engineering and Instrumentation
Vol. 75C, Nos. 3 and 4, July–December 1971

Formulation and Experimental Verification of an Axisymmetric Finite-Element Structural Analysis

R. A. Mitchell, R. M. Woolley, and C. R. Fisher*

Institute for Basic Standards, National Bureau of Standards, Washington, D.C. 20234

(September 29, 1971)

A finite-element structural analysis is described for application to problems in which geometry and loading are axisymmetric and material properties are isotropic elastic. An attempt to minimize restrictions imposed on the shape and orientation of the triangular finite-elements has been largely successful. This facilitates use of the analysis, with automatic finite-element mesh generation, in parameter or optimization studies. A series of laboratory tests to verify the analysis are described in which the magnitude and distribution of boundary loading was known within narrow limits.

Key words: Axisymmetric; elastic; experiment; finite-element analysis; force transducer; stiffness matrix; structural analysis.

1. Introduction

In the structural optimization of a force transducer of the elastic column type, one is concerned with relationships between surface strains and such parameters as boundary loading, dimensions, and material properties. Finite-element analysis is probably the most versatile structural analysis method currently available for studying these relationships. The finite-element formulation described here was developed for application to such optimization problems in which both the geometry and loading are axisymmetric and the materials are isotropic elastic. This class of problems is analytically two-dimensional. Ring-shaped finite elements of triangular cross section and a global Cartesian coordinate system are used in the analysis. This approach generally follows the outlines given by Clough [1, 2],[1] Rashid [2, 3, 4], and Wilson [5].

For efficient structural optimization it is necessary to program the computer to generate automatically the mesh that subdivides a structure into a network of finite elements. To facilitate this, an attempt has been made in this formulation to keep to a minimum the restrictions imposed on shape and orientation of the triangular elements. Explicit integration, used here to develop general formulas for the stiffness of finite elements, yields logarithmic terms which require special treatment to avoid excessive errors when one side of a triangular element is oriented at a small non-zero angle with respect to the axis of symmetry. The special treatment adopted here is to expand the logarithmic integrals into rapidly converging infinite series. Although the stiffness integrals are rather intricate in both the logarithmic and the series forms, they do avoid the need for numerical integration.

An experimental verification of the analysis was obtained by a series of tests conducted on the structural body of a force transducer (load cell) made of 18 percent nickel 250 grade maraging steel. Axial compressive load was applied to the load-cell body. The load was distributed over a small circular area at the top and over a narrow ring-shaped area at the bottom. Thus, the location of applied load was known within narrow limits. Strains on the surface of the load-cell body, known to vary significantly with load location or distribution, were measured and found to be in good agreement with the finite-element analysis.

2. Finite-Element Formulation

In a finite-element analysis the continuum structure is subdivided into a network of elements that are connected to adjacent elements only at common nodal points. Elastic displacements within the individual elements are assumed to be defined by generalized functions that assure displacement compatibility along common boundaries of adjacent elements. The stiffness matrix of each element, relating nodal point forces and displacements, is then computed in terms of the assumed displacement functions, dimensions, and material properties of the element. The stiffness matrix for the entire structure, relating

* Present address: Naval Scientific and Technical Intelligence Center, Washington, D.C. 20390

[1] Figures in brackets indicate literature references at end of paper.

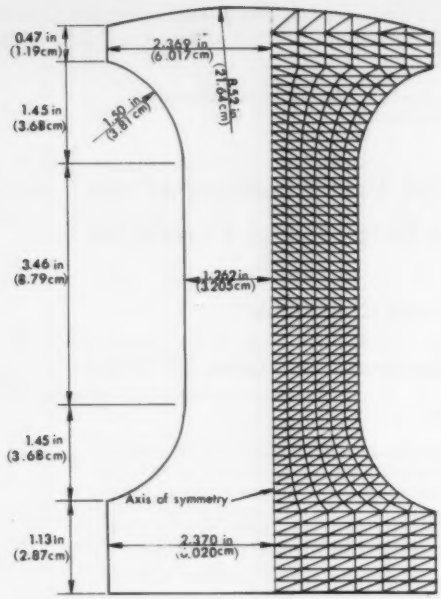

FIGURE 1. *Longitudinal cross section of load-cell body used in laboratory tests*

applied external forces to nodal point displacements throughout the structure, is formed by superposing the element stiffness matrices.

A longitudinal cross section of the load-cell body used in the laboratory tests is shown in figure 1. The figure illustrates a triangular finite element mesh. A similar but finer mesh was used for the analyses that were correlated with the laboratory tests.

The triangular cross section of a general element is shown in figure 2. Each nodal point (actually, a nodal circle in the axisymmetric case) has independent displacement components in the r and z directions. The generalized displacement functions assumed for this formulation are given by

$$\begin{Bmatrix} u \\ v \end{Bmatrix} = \begin{bmatrix} 1 & r-r_i & z-z_i & 0 & 0 & 0 \\ 0 & 0 & 0 & 1 & r-r_i & z-z_i \end{bmatrix} \begin{Bmatrix} \alpha_1 \\ \alpha_2 \\ \alpha_3 \\ \alpha_4 \\ \alpha_5 \\ \alpha_6 \end{Bmatrix} \tag{1}$$

in which

u = displacement in the r direction of any point in the element,

v = displacement in the z direction of any point in the element,

and

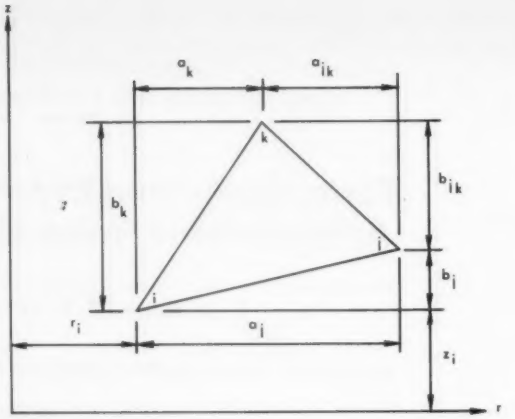

FIGURE 2. *Cross section of a general axisymmetric finite element.*

α_n = a generalized coordinate.

A generalized coordinate, α_n, represents either the r or z component of displacement of nodal point i or a rate of change of a displacement component with respect to r or z. The assumed displacement functions give linear variations in displacement along element boundaries and, therefore, complete displacement compatibility between adjacent elements. Stresses within adjacent elements are not, in general, in equilibrium along common boundaries, but the resultant forces acting at nodal points are required to be in equilibrium. Substitution of nodal point coordinates (defined in fig. 2) into eq (1) gives the nodal point displacements in terms of the generalized coordinates.

$$\begin{Bmatrix} u_i \\ u_j \\ u_k \\ v_i \\ v_j \\ v_k \end{Bmatrix} = \begin{bmatrix} 1 & 0 & 0 & 0 & 0 & 0 \\ 1 & a_j & b_j & 0 & 0 & 0 \\ 1 & a_k & b_k & 0 & 0 & 0 \\ 0 & 0 & 0 & 1 & 0 & 0 \\ 0 & 0 & 0 & 1 & a_j & b_j \\ 0 & 0 & 0 & 1 & a_k & b_k \end{bmatrix} \begin{Bmatrix} \alpha_1 \\ \alpha_2 \\ \alpha_3 \\ \alpha_4 \\ \alpha_5 \\ \alpha_6 \end{Bmatrix}, \tag{2}$$

or

$$\{w\} = [A]\ \{\alpha\}\cdot \tag{3}$$

Element strains are obtained by applying the definitions of strain from elasticity theory [6] to eq (1) as follows:

$$\begin{Bmatrix} \epsilon_r \\ \epsilon_\theta \\ \epsilon_z \\ \gamma_{rz} \end{Bmatrix} = \begin{Bmatrix} \dfrac{\partial u}{\partial r} \\ \dfrac{u}{r} \\ \dfrac{\partial v}{\partial z} \\ \dfrac{\partial u}{\partial z} + \dfrac{\partial v}{\partial r} \end{Bmatrix} = \begin{bmatrix} 0 & 1 & 0 & 0 & 0 & 0 \\ \dfrac{1}{r} & \dfrac{r-r_i}{r} & \dfrac{z-z_i}{r} & 0 & 0 & 0 \\ 0 & 0 & 0 & 0 & 0 & 1 \\ 0 & 0 & 1 & 0 & 1 & 0 \end{bmatrix} \begin{Bmatrix} \alpha_1 \\ \alpha_2 \\ \alpha_3 \\ \alpha_4 \\ \alpha_5 \\ \alpha_6 \end{Bmatrix}, \tag{4}$$

or $$\{\epsilon\} = [\,B\,(r,z)]\,\{\alpha\}\,. \tag{5}$$

The assumed stress-strain relationship for isotropic elastic materials is

$$\begin{Bmatrix}\sigma_r\\ \sigma_\theta\\ \sigma_z\\ \tau_{rz}\end{Bmatrix} = \frac{\nu E}{(1+\nu)(1-2\nu)}\begin{bmatrix}\frac{1-\nu}{\nu} & 1 & 1 & 0\\ 1 & \frac{1-\nu}{\nu} & 1 & 0\\ 1 & 1 & \frac{1-\nu}{\nu} & 0\\ 0 & 0 & 0 & \frac{1-2\nu}{2\nu}\end{bmatrix}\begin{Bmatrix}\epsilon_r\\ \epsilon_\theta\\ \epsilon_z\\ \gamma_{rz}\end{Bmatrix}, \tag{6}$$

or $$\{\sigma\} = [D]\,\{\epsilon\}\,, \tag{7}$$

in which E = Modulus of elasticity
and ν = Poisson's ratio.

By a process of equating internal to external virtual work, using eqs (3), (5), and (7), the general equation for nodal point stiffness of an element can be shown to be (see ref 1, 2, 3 and 7)

$$[k] = [A^{-1}]^T\left(\int_{\text{Volume}} [B]^T[D][B]dV\right)[A^{-1}], \tag{8}$$

or $$[k] = [A^{-1}]^T[\bar{k}][A^{-1}]. \tag{9}$$

In eq (8), dV is a differential volume within the element. Integration is performed over the volume of the element, and the superscripts T and -1 indicate matrix transposition and inversion, respectively. The stiffness matrix $[k]$ relates the six components of force $\{f\}$ acting at the three nodal points of a triangular element to the six components of nodal point displacement $\{w\}$ by

$$\{f\} = [k]\,\{w\}. \tag{10}$$

Using r, $z-z_i$, and θ as the variables of integration, and defining the integrals of the functions of these variables by

$$I(f(r,z-z_i,\theta)) \equiv 2\pi\int_r\int_{z-z_i} f(r,z-z_i)rd(z-z_i)dr, \tag{11}$$

the nonzero elements of $[\bar{k}]$, eq (9), are

$$\bar{k}_{11} = \frac{(1-\nu)E}{(1+\nu)(1-2\nu)}I\left(\frac{1}{r^2}\right)$$

$$\bar{k}_{12} = \bar{k}_{21} = \frac{E}{(1+\nu)(1-2\nu)}I\left(\frac{1}{r}\right) - \frac{(1-\nu)Er_i}{(1+\nu)(1-2\nu)}I\left(\frac{1}{r^2}\right)$$

$$\bar{k}_{13} = \bar{k}_{31} = \frac{(1-\nu)E}{(1+\nu)(1-2\nu)}I\left(\frac{z-z_i}{r^2}\right)$$

$$\bar{k}_{16} = \bar{k}_{61} = \frac{\nu E}{(1-\nu)(1-2\nu)}I\left(\frac{1}{r}\right)$$

$$\bar{k}_{22} = \frac{2E}{(1+\nu)(1-2\nu)}I\,(1) - \frac{2Er_i}{(1+\nu)(1-2\nu)}I\left(\frac{1}{r}\right) + \frac{(1-\nu)Er_i^2}{(1+\nu)(1-2\nu)}I\left(\frac{1}{r^2}\right)$$

$$\bar{k}_{23} = \bar{k}_{32} = \frac{E}{(1+\nu)(1-2\nu)}I\left(\frac{z-z_i}{r}\right) - \frac{(1+\nu)Er_i}{(1+\nu)(1-2\nu)}I\left(\frac{z-z_i}{r^2}\right)$$

$$\bar{k}_{26} = \bar{k}_{62} = \frac{2\nu E}{(1+\nu)(1-2\nu)}I(1) - \frac{\nu Er_i}{(1+\nu)(1-2\nu)}I\left(\frac{1}{r}\right)$$

$$\bar{k}_{33} = \frac{E}{2(1+\nu)}I(1) + \frac{(1-\nu)\,E}{(1+\nu)(1-2\nu)}I\left(\frac{(z-z_i)^2}{r^2}\right)$$

$$\bar{k}_{35} = \bar{k}_{53} = \frac{E}{2(1+\nu)}I(1)$$

$$\bar{k}_{36} = \bar{k}_{63} = \frac{\nu E}{(1+\nu)(1-2\nu)}I\left(\frac{z-z_i}{r}\right)$$

$$\bar{k}_{55} = \frac{E}{2(1+\nu)}I(1)$$

$$\bar{k}_{66} = \frac{(1-\nu)\,E}{(1+\nu)(1-2\nu)}I(1).$$

For explicit integration of eq (11) in the $r-z$ plane, the notation shown in figure 2 is used with the constraints

$$r_i \leqq r_k,$$

$$r_i < r_j,$$

if $r_i = r_k$ then $z_i < z_k$.

Since r_j may be less than, equal to, or greater than r_k, four possible sets of integration limits, cases 1 through 4 in figure 3, are considered. These are:

Case 1:

$$I_1(f(r,z-z_i)) = 2\pi\int_{r_i}^{r_k}\int_{z_{ij}}^{z_{ik}} f(r,z-z_i)rd(z-z_i)dr \tag{12}$$

Case 2:

$$I_2(f(r,z-z_i)) = 2\pi\int_{r_k}^{r_j}\int_{z_{ij}}^{z_{jk}} f(r,z-z_i)rd(z-z_i)dr \tag{13}$$

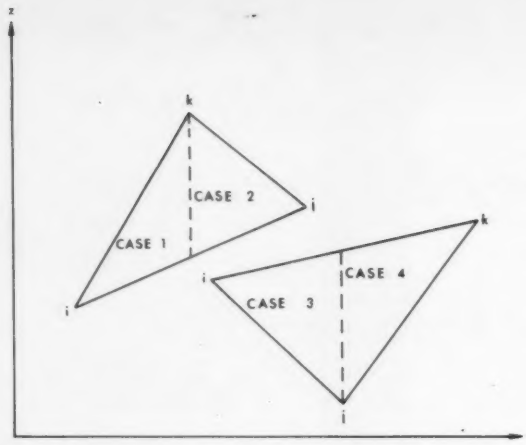

FIGURE 3. *Four different integration limit cases.*

Case 3:

$$I_3(f(r,z-z_i))=2\pi\int_{r_i}^{r_j}\int_{z_{ij}}^{z_{ik}} f(r,z-z_i)\,r\,d(z-z_i)\,dr \quad (14)$$

Case 4:

$$I_4(f(r,z-z_i))=2\pi\int_{r_j}^{r_k}\int_{z_{jk}}^{z_{ik}} f(r,z-z_i)\,r\,d(z-z_i)\,dr \quad (15)$$

in which the limit notation z_{ij} represents the value of $z-z_i$ along line $i-j$. Three of the functions in $[\bar{k}]$ integrate directly, for either orientation of side $j-k$, to

$$I(1)=\frac{2}{3}\,\pi A(r_i+r_j+r_k),$$

$$I\left(\frac{1}{r}\right)=2\pi A,$$

and

$$I\left(\frac{z-z_i}{r}\right)=\frac{2}{3}\,\pi A(b_j+b_k),$$

in which $A=\frac{1}{2}(a_jb_k-a_kb_j)$ = area of the element cross section.

The integrals of the other three functions in $[\bar{k}]$, for the four cases shown in figure 3, are

$$I_1\left(\frac{1}{r^2}\right)=\frac{4\pi A}{a_j}\left(1-\frac{r_i}{a_k}\ln\frac{r_k}{r_i}\right)$$

$$I_2\left(\frac{1}{r^2}\right)=-\frac{4\pi A}{a_j}\left(1-\frac{r_j}{a_{jk}}\ln\frac{r_j}{r_k}\right)$$

$$I_3\left(\frac{1}{r^2}\right)=\frac{4\pi A}{a_k}\left(1-\frac{r_i}{a_j}\ln\frac{r_j}{r_i}\right)$$

$$I_4\left(\frac{1}{r^2}\right)=-\frac{4\pi A}{a_k}\left(1-\frac{r_k}{a_{jk}}\ln\frac{r_j}{r_k}\right)$$

$$I_1\left(\frac{z-z_i}{r^2}\right)=2\pi A\left(\frac{a_jb_k+a_kb_j}{a_j^2}\right)\left[\frac{1}{2}-\frac{r_i}{a_k}\left(1-\frac{r_i}{a_k}\ln\frac{r_k}{r_i}\right)\right]$$

$$I_2\left(\frac{z-z_i}{r^2}\right)$$

$$=\frac{2\pi A}{a_{jk}^2}\left[2A-2b_{jk}r_i+r_i^2\left(\frac{a_jb_k+a_kb_j-2a_jb_j}{a_j^2}\right)\right]\ln\frac{r_j}{r_k}$$

$$+\frac{\pi A}{a_j^2}\left[\frac{2a_j^2b_{jk}}{a_{jk}}-a_jb_k-a_kb_j-2r_i\left(\frac{a_jb_k+a_kb_j-2a_jb_j}{a_{jk}}\right)\right]$$

$$I_3\left(\frac{z-z_i}{r^2}\right)=2\pi A\left(\frac{a_jb_k+a_kb_j}{a_k^2}\right)\left[\frac{1}{2}-\frac{r_i}{a_j}\left(1-\frac{r_i}{a_j}\ln\frac{r_j}{r_i}\right)\right]$$

$$I_4\left(\frac{z-z_i}{r^2}\right)$$

$$=\frac{2\pi A}{a_{jk}^2}\left[2A-2b_{jk}r_i-r_i^2\left(\frac{a_jb_k+a_kb_j-2a_kb_k}{a_k^2}\right)\right]\ln\frac{r_j}{r_k}$$

$$+\frac{\pi A}{a_k^2}\left[\frac{2a_k^2b_{jk}}{a_{jk}}-a_jb_k-a_kb_j+2r_i\left(\frac{a_jb_k+a_kb_j-2a_kb_k}{a_{jk}}\right)\right]$$

$$I_1\left(\frac{(z-z_i)^2}{r^2}\right)=4\pi A\left(\frac{a_j^2b_k^2+a_k^2b_j^2+a_ja_kb_jb_k}{a_j^3}\right)\left[\frac{1}{9}-\frac{r_i}{6a_k}+\frac{r_i^2}{3a_k^2}\left(1-\frac{r_i}{a_k}\ln\frac{r_k}{r_i}\right)\right]$$

$$I_2\left(\frac{(z-z_i)^2}{r^2}\right)=\frac{4\pi A}{3a_{jk}^3}\left[4A^2-6Ab_{jk}r_i+3b_{jk}^2r_i^2+r_i^2\left(\frac{4A^2+3a_ja_{jk}b_jb_{jk}}{a_j^3}\right)\right]\ln\frac{r_j}{r_k}$$

$$+\frac{2\pi A}{a_{jk}^2}\left[b_{jk}(2A+a_jb_j-a_kb_k)-2b_{jk}^2r_i+r_i(a_j+a_k)\left(\frac{4A^2+3a_ja_{jk}b_jb_{jk}}{a_j^3}\right)\right]$$

$$-\frac{4\pi A}{9}\left(1+3\frac{r_jr_k}{a_{jk}^2}\right)\left(\frac{4A^2+3a_ja_{jk}b_jb_{jk}}{a_j^3}\right)$$

$$I_3\left(\frac{(z-z_i)^2}{r^2}\right)=4\pi A\left(\frac{a_j^2b_k^2+a_k^2b_j^2+a_ja_kb_jb_k}{a_k^3}\right)\left[\frac{1}{9}-\frac{r_i}{6a_j}+\frac{r_i^2}{3a_j^2}\left(1-\frac{r_i}{a_j}\ln\frac{r_j}{r_i}\right)\right]$$

$$I_4\left(\frac{(z-z_i)^2}{r^2}\right)=\frac{4\pi A}{3a_{jk}^3}\left[4A^2-6Ab_{jk}r_i+3b_{jk}^2r_i^2+r_i^3\left(\frac{4A^2+3a_ka_{jk}b_kb_{jk}}{a_k^3}\right)\right]\ln\frac{r_j}{r_k}$$

$$+\frac{2\pi A}{a_{jk}^2}\left[b_{jk}(2A+a_jb_j-a_kb_k)-2b_{jk}^2r_i+r_i(a_j+a_k)\left(\frac{4A^2+3a_ka_{jk}b_kb_{jk}}{a_k^3}\right)\right]$$

$$-\frac{4\pi A}{9}\left(1+3\frac{r_jr_k}{a_{jk}^2}\right)\left(\frac{4A^2+3a_ka_{jk}b_kb_{jk}}{a_k^3}\right).$$

The logarithmic terms in the above integrals require special treatment to avoid excessive errors in numerical computations. By a limiting process employing L'Hospital's rule it can be shown that, as r_i or both r_i and r_k tend to zero, the limit of the logarithmic term is zero. Therefore, if one or two nodal points of an element lie on the z axis, the logarithmic terms are omitted from the computation. A more difficult computational problem is presented when one side of a finite element is oriented at a small nonzero angle relative to the z axis. To permit the use of elements with a side so oriented, the logarithmic terms can be expanded in the series (Peirce's formula 768 [8])

$$\ln(1+\chi)=\chi-\frac{\chi^2}{2}+\frac{\chi^3}{3}-\frac{\chi^4}{4}+\ldots+(-1)^{n-1}\frac{\chi^n}{n}+\ldots$$

which converges in the interval $-1<\chi<1$. This gives the following alternate forms of the integrals:

$$I_1'\left(\frac{1}{r^2}\right)=\frac{4\pi A}{a_j}\sum_n\frac{(-1)^{n+1}}{n+1}\left(\frac{a_k}{r_i}\right)^n$$

$$I_2'\left(\frac{1}{r^2}\right)=-\frac{4\pi A}{a_j}\sum_n\frac{1}{n+1}\left(\frac{a_{jk}}{r_j}\right)^n$$

$$I_3'\left(\frac{1}{r^2}\right)=\frac{4\pi A}{a_k}\sum_n\frac{(-1)^{n+1}}{n+1}\left(\frac{a_j}{r_i}\right)^n$$

$$I_4'\left(\frac{1}{r^2}\right)=-\frac{4\pi A}{a_k}\sum_n\frac{(-1)^{n+1}}{n+1}\left(\frac{a_{jk}}{r_k}\right)^n$$

$$I_1'\left(\frac{z-z_i}{r^2}\right)=2\pi A\left(\frac{a_jb_k+a_kb_j}{a_j^2}\right)\sum_n\frac{(-1)^{n+1}}{n+2}\left(\frac{a_k}{r_i}\right)^n$$

$$I_2'\left(\frac{z-z_i}{r^2}\right)=\frac{2\pi A}{a_j^2}\left[2A\sum_n\frac{1}{n+2}\left(\frac{a_{jk}}{r_j}\right)^n-2b_jr_i\sum_n\frac{1}{n+1}\left(\frac{a_{jk}}{r_j}\right)^n+a_{jk}b_j\right]$$

$$I_3'\left(\frac{z-z_i}{r^2}\right)=2\pi A\left(\frac{a_jb_k+a_kb_j}{a_k^2}\right)\sum_n\frac{(-1)^{n+1}}{n+2}\left(\frac{a_j}{r_i}\right)^n$$

$$I_4'\left(\frac{z-z_i}{r^2}\right)=\frac{2\pi A}{a_k^2}\left[2A\sum_n\frac{(-1)^{n+1}}{n+2}\left(\frac{a_{jk}}{r_k}\right)^n+2b_kr_i\sum_n\frac{(-1)^{n+1}}{n+1}\left(\frac{a_{jk}}{r_k}\right)^n-b_ka_{jk}\right]$$

$$I_1'\left(\frac{(z-z_i)^2}{r^2}\right)=4\pi A\left(\frac{a_j^2b_k^2+a_k^2b_j^2+a_ja_kb_jb_k}{a_j^3}\right)\sum_n\frac{(-1)^{n+1}}{n+3}\left(\frac{a_k}{r_i}\right)^n$$

If $b_j=0$,

$$I_2'\left(\frac{(z-z_i)^2}{r^2}\right)=\frac{4\pi Aa_j^2b_k^2}{3a_j^3}\sum_n\frac{1}{n+3}\left(\frac{a_{jk}}{r_j}\right)^n$$

If $b_k=0$,

$$I_2'\left(\frac{(z-z_i)^2}{r^2}\right)=\frac{4\pi Ab_j^2}{3a_j^3}\left[a_k^2\sum_n\frac{1}{n+3}\left(\frac{a_{jk}}{r_j}\right)^n-3a_jr_i\sum_n\left(\frac{1}{n+1}-\frac{1}{n+2}\right)\left(\frac{a_{jk}}{r_j}\right)^n+\frac{a_ja_{jk}}{2}\right]$$

$$I_3'\left(\frac{(z-z_i)^2}{r^2}\right)=4\pi A\left(\frac{a_j^2b_k^2+a_k^2b_j^2+a_ja_kb_jb_k}{3a_k^3}\right)\sum_n\frac{(-1)^{n+1}}{n+3}\left(\frac{a_j}{r_i}\right)^n$$

If $b_k=0$,

$$I'_4\left(\frac{(z-z_i)^2}{r^2}\right)=-\frac{4\pi Ab_j^2}{3a_k}\sum_n\frac{(-1)^{n+1}}{n+3}\left(\frac{a_{jk}}{r_k}\right)^n$$

If $b_j=0$,

$$I'_4\left(\frac{(z-z_i)^2}{r^2}\right)$$

$$=\frac{4\pi Ab_k^2}{3a_k^3}\left[3a_kr_i\sum_n(-1)^{n+1}\left(\frac{1}{n+1}-\frac{1}{n+2}\right)\left(\frac{a_{jk}}{r_k}\right)^n-a_j^2\sum_n\frac{(-1)^{n+1}}{n+3}\left(\frac{a_{jk}}{r_k}\right)^n-\frac{a_ka_{jk}}{2}\right].$$

Notice that use of the series forms of two of the integrals, $I'_2[(z-z_i)^2/r^2]$ and $I'_4[(z-z_i)^2/r^2]$, is limited to elements for which either b_j or b_k equals zero; that is, one side of the element must be oriented in the r direction. If an element has one side oriented at a small nonzero angle with respect to the z direction, no nodal point on the z axis, and no side oriented in the r direction, some other method is required to evaluate these two integrals. In such an event, the two integrals could be evaluated by the application of numerical integration to eqs (13) and (15) for the function $(z-z_i)^2/r^2$. Computational experience indicates that the series forms of the integrals are efficient for numerical computations within the bounds:

Case 1: $\frac{1}{2}>\frac{a_k}{a_j}>10^{-6}$ and $\frac{a_k}{r_i}<10^{-1}$

Case 2: $\frac{1}{2}>\frac{a_{jk}}{a_j}>10^{-6}$ and $\frac{a_{jk}}{r_j}<10^{-1}$

Case 3: $\frac{1}{2}>\frac{a_j}{a_k}>10^{-6}$ and $\frac{a_j}{r_i}<10^{-1}$

Case 4: $\frac{1}{2}>\frac{a_{jk}}{a_k}>10^{-6}$ and $\frac{a_{jk}}{r_k}<10^{-1}$.

For cases falling below the lower bound it is satisfactory to set the integrals equal to zero. For cases falling above either upper bound the general integrals containing the logarithmic terms can be used without difficulty.

The stiffness matrices of the various finite elements. $[k]$ in eqs (8) and (10), are superposed to form the stiffness matrix of the entire structure. This is done by adding the stiffness matrix elements that relate displacements to resulting forces for common or adjacent nodal points of adjacent elements. The resulting stiffness matrix of the entire structure $[K]$ relates the forces applied to the structure $\{F\}$ to the resulting nodal point displacements $\{w\}$ according to the equation

$$\{F\}=[K]\{w\}. \tag{16}$$

For problems involving large numbers of unknown displacements, eq (16) can be solved efficiently by iteration. For the work reported here, Gauss-Seidel iteration was used along with overrelaxation and group relaxation as described by Wilson [5]. For the analysis mesh shown in figure 1, 250 cycles of iteration resulted in convergence to a state having an absolute sum of unbalanced residual forces of one-half percent of the applied load. This iteration required about 48.8 s. running time on a UNIVAC 1108 computer. Evaluation of the stiffness integrals, eqs (12) through (15), and formation of the stiffness array for the entire structure required only about 6.1 s. computer running time.

3. Experimental Verification

To determine how well the finite-element analysis described the structural response of a load cell, a series of laboratory tests were conducted on the load-cell body dimensioned in figure 1. The load-cell body was made of 18 percent nickel 250 grade maraging steel. For the principal verification tests, an axisymmetric compressive load of 100,000 lbf (444,800 N) was applied through a small circular area on the top surface and through a circular ring-shaped area on the bottom surface. In a preliminary test, an axisymmetric compressive load of 800,000 lbf (3,558,400 N) was applied to the load-cell body through two solid cylindrical mild steel blocks. In all tests, the loads were applied by dead weight testing machines.

Strains on the surface of the load-cell body were monitored by fifty-four metal foil strain gages of 0.062 in (0.16 cm) gage length. Forty-six gages were oriented in the longitudinal direction and located on three lines defined by the intersections of the surface and three radial planes spaced 120 degrees apart. Eight gages were oriented in the circumferential direction and located beside longitudinal gages. Twenty-four longitudinal gages were located in sets of three at common heights and at the three angular locations to detect bending due to load eccentricity.

In the preliminary test, figure 4, the upper mild steel block was plastically indented by the spherical top surface of the load cell, giving a contact surface of about 1.41 in (3.58 cm) radius at 800,000 lbf (3,558,400 N) applied load. The lower mild steel block was used to permit plastic indentation by a small region that protruded about 0.002 in (0.005 cm) at the center of the bottom surface of the load-cell body. This resulted in continuous contact over the bottom surface upon application of the first 50,000 lbf (222,400 N) load increment. Recorded longitudinal surface strains due to a load of 800,000 lbf (3,558,400 N) are plotted in figure 5. The curves in figure 5 were obtained by finite-element analysis. One curve is for 800,000 lbf (3,558,400 N) load applied at the centers

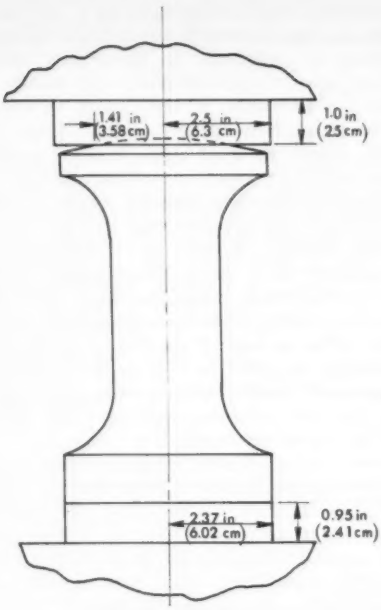

FIGURE 4. *Setup for applying 800,000 lbf (3,558,400 N) compressive load in a preliminary test.*

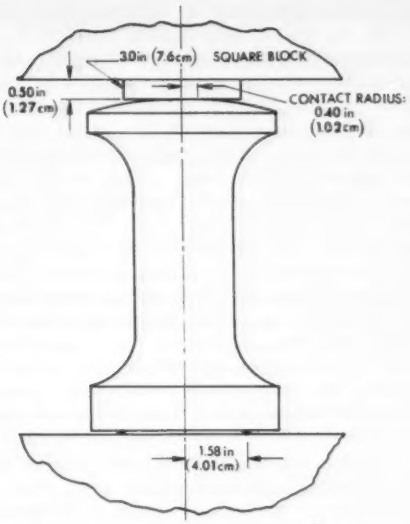

FIGURE 6. *Setup for applying 100,000 lbf (444,800 N) compressive load in one of the verification tests.*

of the top and bottom surface. The other curve is for 800,000 lbf (3,558,400 N) load applied at the radii of the edges of the contact surfaces in the laboratory test, figure 4. Although most of the test data points lie near or are bracketed by the analytical curves, this experiment is clearly insufficient for a precise verification of the analysis. Figure 5 shows that surface strains can be very sensitive to variations in the distribution of boundary loading.

Figure 6 shows the loading arrangement for one of the principal verification tests. Axisymmetric compressive loads of 100,000 lbf (444,800 N) were applied to the top surface of the load-cell body through a mild steel block and to the bottom surface through a 0.2 in (0.5 cm) wide by 0.035 in (0.088 cm) thick steel ring. Rings with mean radii of 0.40, 0.79, 1.58 and 2.27 in (1.02, 2.01, 4.01

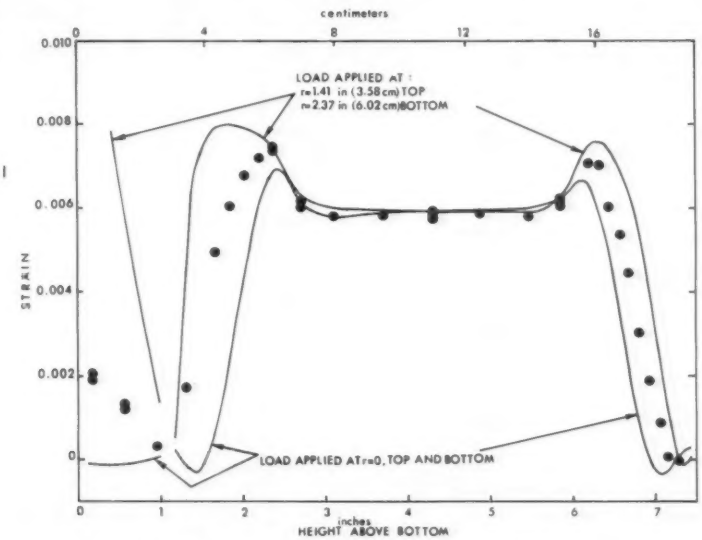

FIGURE 5. *Longitudinal surface strains for an applied load of 800,000 lbf (3,558,400 N).*

448-719 OL - 72 - 2

and 5.77 cm) were used in different tests. Figure 7 shows the recorded longitudinal surface strains for four of these tests (the plotted data points) along with corresponding curves obtained by finite-element analysis. For the finite-element analysis the bottom loading radius corresponds to the mean loading ring radius and the top loading radius corresponds to one-half the contact surface radius. Much of the scatter in the data is probably due to bending. The value of the modulus of elasticity used in the finite-element analysis was 26.8×10^6 lb/in^2 (1.85×10^{10} N/m^2). This value was computed by averaging, for several tests, the data obtained from the three strain gages located at $z = 4.31$ in (10.95 cm). This particular data was very repeatable and bending errors were essentially cancelled by the averaging. Admittedly, this procedure for determining the elastic modulus imposes good agreement between analysis and experiment in the region near $z = 4.31$ in (10.95 cm). A Poisson's ratio of 0.3, a value listed in the literature of steel producers for 18 percent nickel 250 grade maraging steel, was used in the finite-element analysis. The generally good agreement between the analysis and this test data for the entire length of the load-cell body (fig. 7) indicates that the analysis would be suitable for the study of such subjects as stress concentration and the optimum geometry of material test specimens and fixtures.

For use as a force transducer, a load-cell body of the type tested is ordinarily instrumented with strain gages over only a small region near mid-height. An important consideration in the design of such a load cell is the change in surface strain sensed by these strain gages due to a change in the distribution of boundary loading. A portion of the curves and test data in figure 7 that bear directly on this question are replotted to a much greater scale in figure 8. The test data points in figure 8 have been averaged from the strain readings of sets of three gages at different angular locations to minimize bending errors. Figure 9 is a plot of the differences between surface strain for a particular radius of load at the bottom surface and the corresponding strain for a 2.27 in (5.77 cm) radius of load. Figures 8 and 9 indicate very good agreement between the finite-element analysis and the test results at the three strain gage locations represented. The greatest difference between the analytical and averaged experimental values represented in figure 9 is 2×10^{-6}. This difference approaches the resolution of the digital indicator (1×10^{-6}) used in the laboratory tests. This data verifies the accuracy of the analysis in predicting the sensitivity of such a load cell to changes in the distribution of boundary loading.

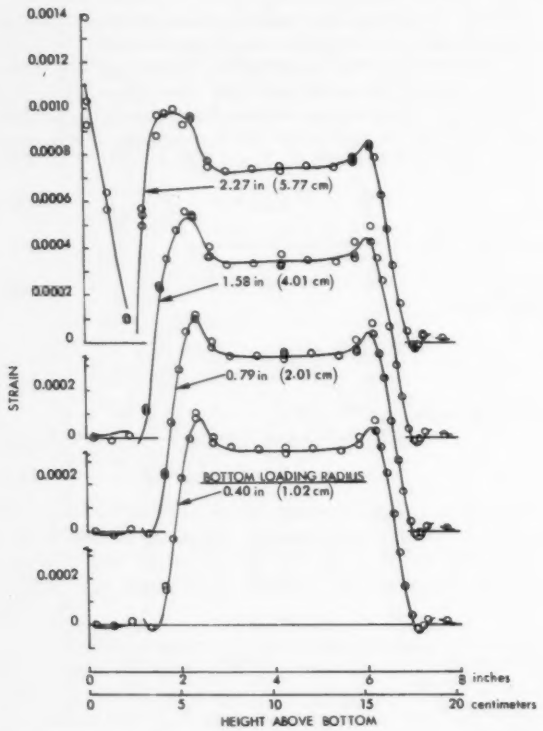

FIGURE 7. *Longitudinal surface strains for an applied load of 100,000 lbf (444,800 N).*

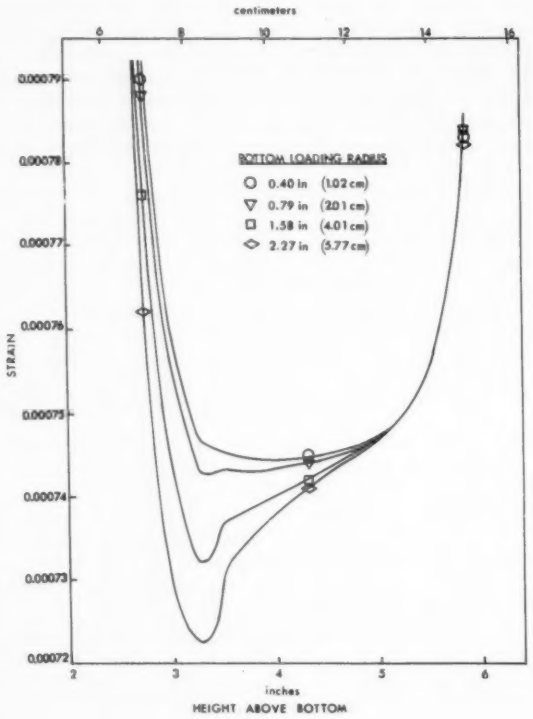

FIGURE 8. *Longitudinal surface strains averaged for sets of three gages at common heights and different angular locations.*

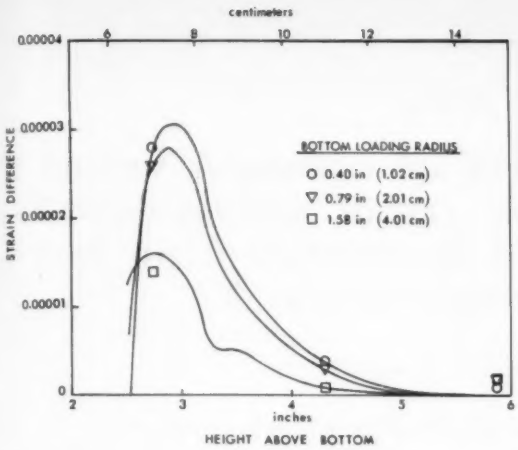

FIGURE 9. *Difference between surface strain for a particular loading radius and the corresponding strain for a loading radius of 2.27 in (5.77 cm).*

4. Conclusion

A finite-element structural analysis has been formulated for application to problems in which geometry and loading are axisymmetric and materials are isotropic elastic. An attempt to minimize restrictions imposed on the shape and orientation of the triangular elements employed has been largely successful. This facilitates use of the analysis, with automatic finite-element mesh generation, in parameter or optimization studies.

An experimental verification of the analysis has been obtained by a series of tests conducted on a load-cell body. In these tests the magnitude and distribution of boundary loading was known within narrow limits. Strains measured on the surface of the load-cell body were in good agreement with the finite-element analysis.

C. H. Melton was largely responsible for instrumenting the load cell for the measurement of surface strains.

5. References

[1] Clough, R. W., The finite element method in structural mechanics, chapter 7 of Stress Analysis, Eds. Zienkiewicz, O. C. and Holister, G. S. (Wiley, 1965).

[2] Clough, R. W., and Rashid, Y., Finite element analysis of axisymmetric solids, J. Engr. Mech. Div. ASCE **91**, No. EM 1 (Feb. 1965).

[3] Rashid, Y. R., Solution of elasto-static boundary value problems by the finite element method, Ph. D. Dissertation, U. of Cal. Berkely (1964).

[4] Rashid, Y. R., Finite element analysis of axisymmetric composite structures, AEC Res. and Dev. Report GA-6303 (June 4, 1965).

[5] Wilson, E. L., Finite element analysis of two-dimensional structures, Structures and Materials Research Report No. 63–2, U. of Cal. Berkeley (June 1963).

[6] Timoshenko, S. and Goodier, J. N., Theory of Elasticity (McGraw-Hill, 1951).

[7] Zienkiewicz, O. C., The Finite Element Method in Structural and Continuum Mechanics (McGraw-Hill, 1967).

[8] Peirce, B. O., A Short Table of Integrals (Ginn, 1929).

(Paper 75C3&4–322)

JOURNAL OF RESEARCH of the National Bureau of Standards—C. Engineering and Instrumentation
Vol. 75C, Nos. 3 and 4, July–December 1971

A Burnett Apparatus for the Accurate Determination of Gas Compressibility Factors and Second Virial Coefficients, and an Evaluation of Its Capability Based on Some Results for Argon and Carbon Dioxide

Meyer Waxman and John R. Hastings

Institute for Basic Standards, National Bureau of Standards, Washington, D.C. 20234

(June 2, 1971)

A Burnett apparatus has been developed for the determination of the compressibility factor of gases, including corrosive halogenic gases, to an accuracy of 0.1 percent to 0.01 percent at temperatures from 0 to 225 °C and for pressures up to 250 bars. The apparatus has been used throughout this temperature and pressure range and at temperatures within 15 °C of the critical temperature of the sample gas. The apparatus features a rugged yet highly sensitive and reproducible null-type pressure transducer to isolate the sample gas without introducing a pressure uncertainty greater than the precision of the pressure measurements, which is better than 1 part in 50,000. The pressure measurements are accurate to at least 1 part in 20,000. The reduction of the data is discussed extensively. The capability of the apparatus has been evaluated in terms of the compressibility factor represented by a finite pressure or density virial expansion and derived from argon data at 25 °C and pressures up to 250 bars and in terms of the second virial coefficient of carbon dioxide based on data at 50 °C and pressures below 35 bars. The value obtained for this second virial coefficient, -102.2 ± 0.2 cm³/mol, compares favorably with the value of -102.5 cm³/mol obtained from a recent correlation and is in substantial disagreement with the value of -100.7 ± 0.4 cm³/mol determined by Dadson and co-workers from the Burnett method and the piezometer method.

Key words: Adsorption, gas on metal; argon, compressibility factor of; Burnett data reduction; carbon dioxide, second virial coefficient of; compressibility factor; gas, compressibility factor of; gas, *PVT* properties of; measurements, gas; second virial coefficient.

1. Introduction

The accurate determination of the equation of state of a gas over a wide range of temperature and pressure provides important information about the gas both from a fundamental and an applied point of view. For example, the thermodynamic properties of a gas can be reliably extended beyond its ideal gas properties if its equation of state is known with sufficient accuracy. Equation of state data are conveniently represented by means of the compressibility factor. The compressibility factor Z is defined in terms of the gas constant R and the measurable gas variables pressure P, volume V, absolute temperature T, and quantity, expressed as the number of moles n, by the relationship

$$Z = PV/nRT. \tag{1}$$

The accuracy of Z obtained from a straightforward measurement of each variable is limited by the accuracy with which the difficult measurements of n and V can be made. The direct or indirect measurement of one (n) or both (n and V) of the difficult variables can be eliminated by the use of the virial expansions of Z as a function of P or of the density ρ and the fact that the dependence of Z on P is dominantly linear at sufficiently low pressures and approaches the ideal gas law

$$Z = PV/nRT = 1 \tag{2}$$

in the limit as P goes to zero [1,2].[1] The Burnett *PVT* method [3–7] is an experimentally simplified method in which neither n nor V is measured; instead, accurate isothermal pressure measurements are made before and after stepwise expansions between two volumes. The decrease in the overall measurement error achieved by the elimination of n and V measurements can in principle lead to more accurate values of Z than can be obtained from a method requiring the measurement of each variable in eq (1). For this reason we have developed a Burnett apparatus for the accurate determination of the compressibility factor of gases,

[1] Figures in brackets indicate the literature references at the end of this paper.

including corrosive halogenic gases [8], at temperatures from 0 to 225 °C and for pressures up to 250 bars (1 bar≡ 10^5 N · m^{-2}). The apparatus has been used by us throughout this temperature and pressure range including temperatures within 15 °C of the critical temperature of the sample gas. The apparatus is equally well-suited and has been used for the accurate determination of second virial coefficients.

This paper is concerned with both the apparatus for obtaining Burnett data and the methods for reducing the data. These subjects are described briefly in the remainder of this section. In the next section the apparatus is discussed in more detail, and its distinctive features are emphasized. Since the reduction of the data obtained with the apparatus is an essential element in the evaluation of its capability, the data reduction is discussed extensively in the following section. The discussion is illustrated with results for the compressibility factor of argon at 25 °C and pressures up to 250 bars and for the second virial coefficient of carbon dioxide at 50 °C.

The apparatus, shown schematically in figure 1, consists essentially of a sample volume V_I and an expansion volume V_{II} as well as components for (1) isolating, evacuating, or filling both volumes, (2) measuring the pressure in the sample volume, and (3) thermostating and measuring the temperature of the apparatus. The gas in the sample volume is isolated from the expansion volume by an expansion valve and from the external system by a metal diaphragm which is the pressure-responsive element of a null-type transducer. A counterbalancing gas acts on the other side of the diaphragm; the diaphragm is in its null position when the pressure on each side of the diaphragm is the same. The pressure of the sample gas is obtained indirectly from the measurement of the pressure of the counterbalancing gas with a piston gage and a barometer. The sample and the expansion volumes include the appropriate volumes of the transducer, expansion and filling-evacuation valves, and the interconnecting pressure lines; in our apparatus all these volumes are thermostated at a temperature which is regulated to about 0.001 °C and measured with a platinum resistance thermometer. Because no correction needs to be made for temperature differences among these volumes, a correction that is often a significant source of error in *PVT* measurements is thereby eliminated. The transducer produces negligible variations of the sample volume and has a negligible effect on the high precision and accuracy of the pressure measurements. This is due to the excellent reproducibility of the null position of the diaphragm and the high sensitivity of the transducer.

The experimental procedure is begun by filling the sample volume to the initial pressure, thermostating the apparatus at the isotherm temperature T_c, isolating the volumes from each other, and then measuring the gas pressure P_0 in the sample volume. The corresponding compressibility factor Z_0 is

$$Z_0 = P_0 V_I(P_0)/n_0 R T_c, \tag{3}$$

where n_0 represents the initial number of moles and $V_I(P_0)$ indicates that the sample volume is pressure dependent as a result of its distortion under pressure.

In the next step, which we call the expansion step, the expansion volume is evacuated and isolated, and the gas in the sample volume is allowed to expand

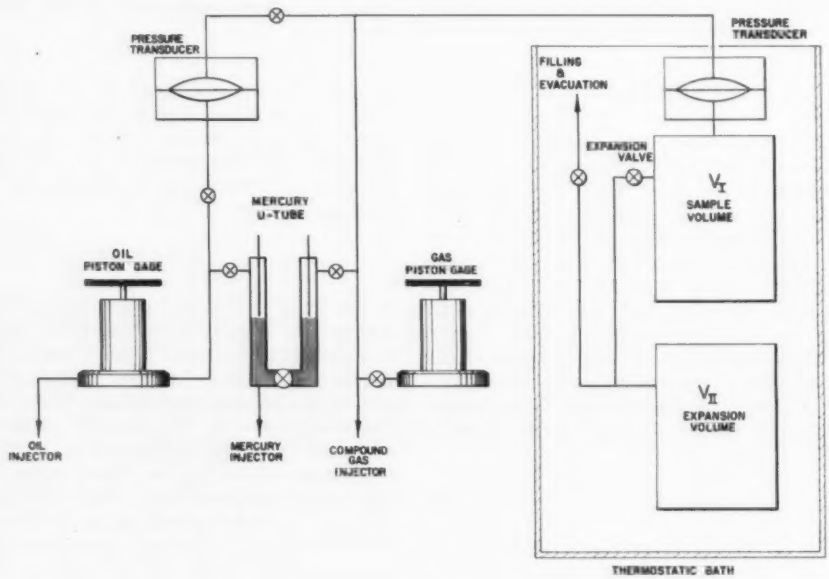

FIGURE 1. *Schematic diagram of the Burnett* PVT *apparatus.*

into it. After temperature and pressure equilibration has occurred, the pressure P_1 of the gas that now occupies both volumes is measured. For this first expansion step the compressibility factor Z_1 is

$$Z_1 = P_1[V_I(P_1) + V_{II}(P_1)]/n_0RT_c, \quad (4)$$

where n_0 and T_c are the same as in eq (3). By taking the ratio of eqs (3) and (4) and defining N_1 as the ratio of the combined sample and expansion volumes to the sample volume, i.e., $N_1 = [V_I(P_1) + V_{II}(P_1)]/V_I(P_0)$, one obtains

$$P_0/P_1 = N_1Z_0/Z_1, \quad (5)$$

in which N_1 depends slightly on both P_0 and P_1. The ratio of the volumes can be written as $N_1 = N[1 + \Delta N_1(P_0, P_1)]$, where N, known as the cell constant, is the value of the volume ratio in the limit as the pressure goes to zero and $\Delta N_1(P_0, P_1)$ is a cell constant correction for the dependence of the cell volumes on pressure.

Generally the sample volume is isolated again and the expansion step is repeated for the reduced quantity of gas n_1 that is now in the sample volume. This leads to a new pressure ratio, corresponding to eq (5),

$$P_1/P_2 = N_2Z_1/Z_2, \quad (6)$$

where $N_2 = N[1 + \Delta N_2(P_1, P_2)]$. This procedure is usually repeated to successively lower pressures with the successively smaller quantities of gas that remain in the sample volume after each expansion until the lowest pressures that can be measured both accurately and precisely are reached. The generalized form of eqs (5) and (6) for the rth expansion is

$$P_{r-1}/P_r = N_rZ_{r-1}/Z_r. \quad (7)$$

The combination of eq (7) and the relationship $P = \rho ZRT$, obtained from eq (1), leads to a corresponding Burnett equation in terms of the density

$$\rho_r = \rho_{r-1}/N_r. \quad (8)$$

Equations (7) and (8) are basic equations in the reduction of Burnett data and may be transformed into different relationships in which the compressibility factor is represented by a finite virial expansion in either pressure or density. Any one of the relationships may be applied to Burnett data to form an overdetermined set of equations for evaluating the virial coefficients and generally the cell constant by means of nonlinear statistics [9]. Regardless of the relationship used, the cell constant is not determined from volume measurements. In the data reduction the pressure corrections ΔN_1, ΔN_2, . . . are not considered as unknown quantities but are estimated from theoretical and empirical distortion equations for pressure vessels or are determined from a separate distortion experiment.

2. Apparatus and Experimental Procedure

2.1. Burnett Vessel and Gas Manifold System

An overall view of the apparatus is shown in figure 2. In the Burnett vessel, as shown in figure 3, the sample chamber, 0.022 m i.d. by 0.076 m long, and the expansion chamber, 0.022 m i.d. by 0.051 m long, are bored from opposite ends of 0.064 m o.d. nickel rod to within 0.051 m of each other. Nonrotating end closures are used for coupling to the transducer and to the filling-evacuation line. The top gland nut is split to accommodate the transducer coupling. The coupling to the expansion valve is made through 0.0032 m o.d. by 0.00080 m i.d. stainless steel capillary tubing silver-brazed into the sample chamber inlet. The coupling from the expansion chamber is made through similar capillary tubing silver-brazed into a T-connection which in turn is coupled to the expansion valve and to the filling-evacuation valve. A well for the platinum resistance thermometer is bored radially into the Burnett vessel between the sample and the expansion chambers.

Since halogenic gases react readily with most metals, particularly if a trace of moisture is present, the components exposed to the sample gas are fabricated from metals such as nickel and stainless steel that are resistant to corrosion. We have found that gold provides still better resistance to corrosion than nickel and stainless steel do, and have therefore gold-plated every surface exposed to the sample gas in the Burnett volumes except the surfaces in the Burnett valves. Extreme care is taken to keep the system free of moisture at all times. The sample gas is not reclaimed; if necessary, neutralizing columns are used for its disposal. Cold traps prevent corrosive gases from entering the vacuum system, which includes low and high vacuum pumps, a cold cathode vacuum gage, and several thermocouple vacuum gages. Commercial diaphragm compressors boost the gas pressure from the supply cylinder pressure to about 600 bars for storage in high pressure receivers.

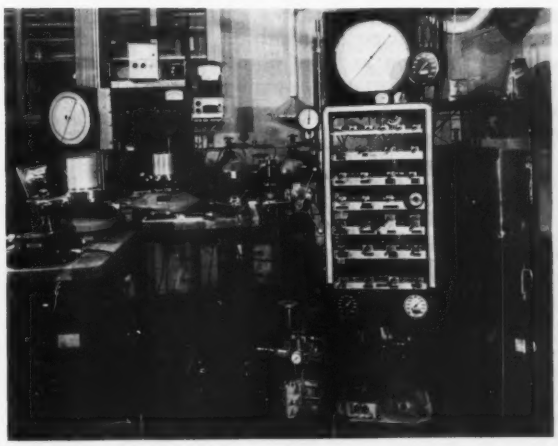

FIGURE 2. *Burnett* PVT *apparatus.*

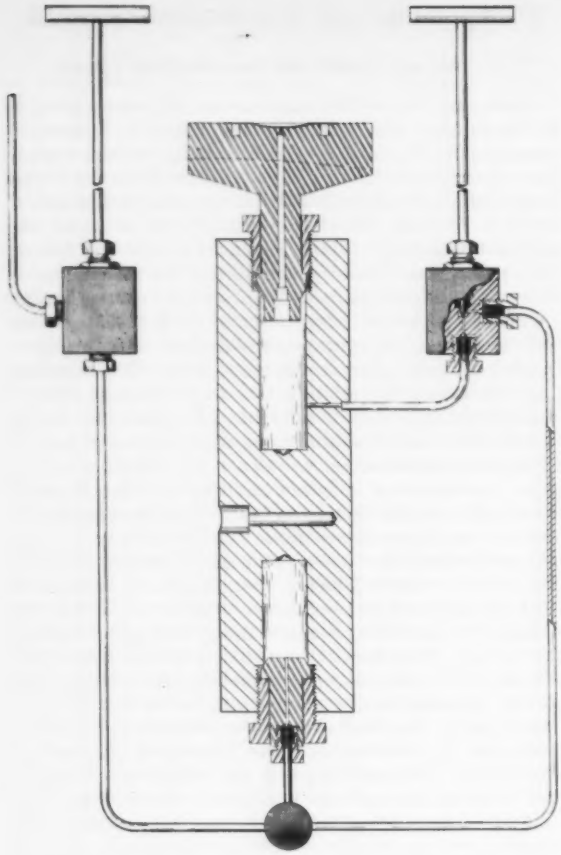

FIGURE 3. *Cross section of the Burnett volumes and valves.*

Carefully selected commercial nonrotating-stem valves are used; our experience shows that for a gas system the sealing surfaces of rotating-stem valves tend to gall and consequently to leak. The condition of the expansion and the filling-evacuation valves is particularly important; minimum deformation of the valve seat, long periods of trouble-free use, and certainty of valve closure are essential characteristics. A small valve with a block of 316 stainless steel, ports to accommodate 0.0032 m o.d. capillary tubing, and a stem of 17–4 stainless steel hardened to 40 R/C is used for each of these two valves. Valve blocks for all the valves are selected on the basis of the concentricity of the seat and the stem-packing section. The shoulder of the valve seat is beveled slightly and carefully lapped to the same angle as that of the conical end of the valve stem. The sealing surface is kept small to minimize the torque required for valve closure. To prolong valve life, all valves are closed with a torque wrench, and the required torque is recorded on each valve block.

2.2. Pressure Measurement System

a. Transducer

A rugged yet highly sensitive and reproducible null-type pressure transducer separates the sample gas from the pressure measurement system. The transducer is shown in figure 4; an earlier model has been described previously [10]. The transducer consists basically of a prestressed metal diaphragm as the pressure responsive element, a capacitance sensor for detecting deflections of the diaphragm as small as 0.025 μm or less, and diaphragm backing surfaces incorporated as part of both the base and the capacitance sensor.

The diaphragm is plane and circular, 25 μm thick, and prestressed to reduce inelastic behavior. The backing surfaces, spherically concave with a chord of 0.0238 m that determines the effective diameter of the diaphragm and a sagitta of 25 μm, are necessary because the stepwise expansions in the Burnett method result in temporary pressure imbalances across the diaphragm many times greater than the elastic range of a diaphragm with the required sensitivity.

The earlier model has been modified to improve its performance, especially above 125 °C. A metallized ceramic disk replaces the former metal-epoxy capacitance sensor assembly. This has enabled us to operate the apparatus at temperatures up to 225 °C, and the disk could even be used at temperatures as high as 500 or 600 °C. The diaphragm is now fabricated from rolled nickel, instead of Monel, sheet stock; its thermal expansion thus closely matches that of the nickel base, and the diaphragm tension does not depend significantly on the temperature. A polytetrafluoroethylene ring, prestressed by the clamping of the top and the base of the transducer and supported by inner and outer metal extrusion rings, replaces the former *V*-ring as the outer pressure seal. The diaphragm sealing ring has been redesigned so that it stretches the diaphragm radially as it forms a pressure seal and thus does not distort the diaphragm when the transducer is assembled. Consequently the sample volume is more precisely defined and the transducer behaves more reproducibly. An important source of error is thereby reduced significantly.

The transducer capacitance, consisting of the capacitance contributed by the capacitor plate, diaphragm, and intervening gas plus the residual capacitance, constitutes one arm of a capacitance bridge. For each temperature and pressure the bridge is initially adjusted so that it is balanced when the pressure on each side of the diaphragm is the same. A subsequent pressure imbalance deflects the diaphragm from its null position and causes a bridge imbalance. The corresponding signal is amplified, phase detected, and indicated on a 100–0–100 μA output meter. The counterbalancing gas pressure is then adjusted until the diaphragm returns to its null position as indicated by the bridge balance.

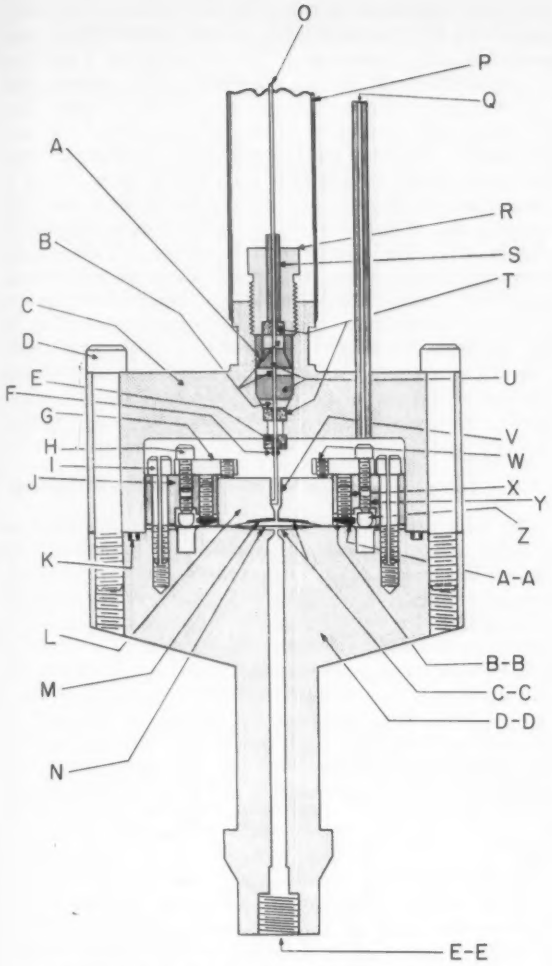

FIGURE 4. *Cross section of null-type pressure transducer.*

A. Follower, steel
B. Extrusion rings, lava stone
C. Top, nickel
D. Clamping bolts for pressure seal K
E. Ring, ceramic
F. Capacitor lead stop, silver-brazed bead
G. Clamping ring for capacitance disk
H. Inner clamping screws for clamping ring G
I. Outer clamping screws for clamping ring J
J. Clamping ring
K. Polytetrafluoroethylene ring with brass extrusion rings
L. Capacitance disk
M. Capacitor plate, metallized
N. Diaphragm, nickel
O. Capacitor lead, drill rod
P. Electrical and oil shield, Monel
Q. Counterbalancing gas inlet tube, nickel
R. Packing gland nut, steel
S. Electrical insulating sleeve, polytetrafluoroethylene
T. Extrusion rings, ceramic
U. Packing rings, polytetrafluoroethylene
V. Metallized surface to capacitor plate
W. Thrust screws for clamping capacitance disk
X. Thrust screws for diaphragm pressure seal A–A
Y. Thrust screws for stressing diaphragm N
Z. Stressing ring, nickel
A–A. Diaphragm seal
B–B. Diaphragm stressing-sealing ring
C–C. Diaphragm backing surfaces
D–D. Base
E–E. Sample gas port

The temperature dependence of the transducer null capacitance is negligible for temperature changes even two orders of magnitude greater than the fluctuations of 0.001 °C about the isotherm temperature that represent the resolution of the temperature control system. For each isotherm the transducer is calibrated before Burnett measurements are made: The counterbalancing gas, which has been argon in all of our work, is admitted to both sides of the diaphragm, and the null capacitance is measured as a function of pressure from atmospheric pressure up to the highest Burnett pressure to be measured. The pressure dependence found does not represent any significant change in the diaphragm null position but is caused primarily by the change in the dielectric constant of the counterbalancing gas. The pressure sensitivity of the transducer, as used by us in the Burnett apparatus for pressures up to 250 bars, exceeds the sensitivity of the piston gages and the barometer used to measure the pressure.

b. Piston Gages and Barometer

Although Bourdon gages are used, for convenience, as pressure indicators at various locations in the apparatus, the basic pressure measurements are made with piston gages and a standard barometer—instruments which are primary pressure standards. Two controlled-clearance piston gages with an accuracy of better than 1 part in 20,000 cover the range from about 2 to 3 bars gage pressure up to 250 bars and beyond. A gage with gas as the pressure fluid covers the lower part of the range, and a gage with oil as the pressure fluid covers the higher part. Both gages cover the region from about 30 to 45 bars and in this overlap region they agree with each other to within 1 part in 40,000 to 50,000 of the measured pressure.

The nominal effective area of the oil gage piston is 26×10^{-6} m^2 and of the gas gage piston, about 340×10^{-6} m^2. The pistons are fabricated from tungsten carbide; the cylinders, from stainless steel. The top of the oil gage piston is hemispherical and fits into a conical recess in the coupling that connects the piston to the weight holder on which the weights are loaded. In the gas gage a lubricated ball bearing fits into a conical recess in both the piston and the coupling. In each case the purpose of the spherical contact, which represents our modification of the gages, is to reduce the amount of side thrust applied to the piston. Similarly, the weight holders and the weights that nest on them are machined carefully to avoid eccentric loading. The prevention of side thrust is particularly important for the gas gage because its piston receives little lateral support. The gas gage piston and cylinder must also be kept scrupulously clean. For each gage the load applied to the piston is spun manually and continues to spin for up to an hour or more before it stops.

Even though the pistons and cylinders were carefully lapped and cleaned before they were delivered to us, we were able to improve the performance of the gages by using a simple motor drive assembly to rotate the piston and move it up and down within its cylinder

for several hours while the piston and cylinder were flooded with mineral spirits. The resultant burnishing increased the spin time, and the flooding helped to remove any fine particles that might have been present. The burnishing procedure can be used to improve performance at any time, particularly if the cylinder has become slightly scratched.

A simple piston gage without the controlled-clearance capability is used to make less accurate measurements over the range from 2 to 3 bars gage pressure down to 0.2 bars absolute pressure or less; the absolute measurements are made under an evacuated bell jar. The gage has three stainless steel piston and cylinder assemblies with nominal effective areas of 800×10^{-6} m², 80×10^{-6} m², and 8×10^{-6} m², and uses gas as the pressure fluid.

The atmospheric pressure is measured with a standard barometer of modified U-tube design consisting of a column and a cistern. The level of the mercury in the column is detected photoelectrically and is measured with a 31 in (0.79 m) scale and a vernier graduated to 0.001 in (25 μm); the level of the mercury in the cistern is detected electrically and is measured with a micrometer graduated to 0.0001 in (2.5 μm). The back pressure above the mercury in the column is measured with a McLeod gage and is generally about 4×10^{-6} bars or less. The accuracy of the barometer scale is easily checked with gage blocks. Repeated tests have shown that the barometric pressure measurements are accurate to 33×10^{-6} bars.

c. Other Components

Small adjustments in the counterbalancing gas pressure are made with a compound gas injector whose internal volume is changed by the manual displacement of a 0.013 m or 0.0032 m diam piston. The counterbalancing pressure acts directly on the gas gages but is separated from the oil gage either by a commercial diaphragm transducer or by a mercury U-tube. The U-tube is an adaptation of an earlier model by Keyes [11] and is shown in figure 5. To reduce capillary effects, the lower part of each bore containing the mercury is made large in diameter. The bore diameter is reduced slightly above the mercury to make the gas volume in the bore a small fraction of the total volume of the counterbalancing gas. As a result, the bore gas volume has only a small effect on the performance of the gas injector. The mercury level in each column is indicated by electrical contact between the mercury and a fine metal probe whose height is initially adjusted to within 25 μm of the reference height and is checked periodically. The modified design permits the valve at the base of the U-tube to be replaced conveniently.

2.3. Temperature Control and Measurement System

An oil bath and a servo heater system are used to control the temperature of the Burnett apparatus. As shown in figure 6, the Burnett vessel, the transducer, the expansion and the filling-evacuation valves, and the interconnecting lines are all immersed in oil in an inner chamber located in a thermally insulated bath. The inner chamber is double-walled, and the space between the walls can be evacuated to reduce radial heat flow. An oil-circulating pump at the bottom of the bath is coupled mechanically to a motor mounted on the top. Oil drawn into the manifold and the pump is ejected upward into the inner chamber and flows by the Burnett

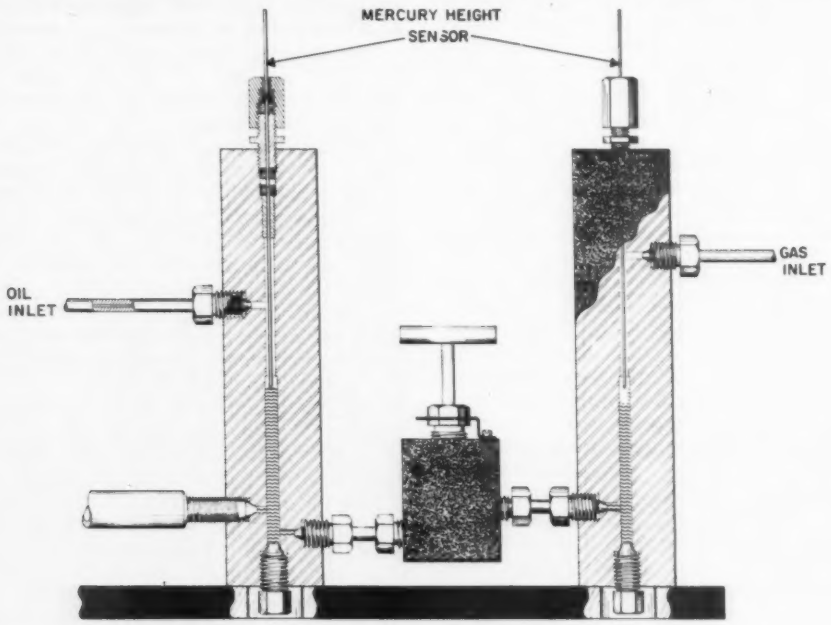

FIGURE 5. *Mercury U-tube.*

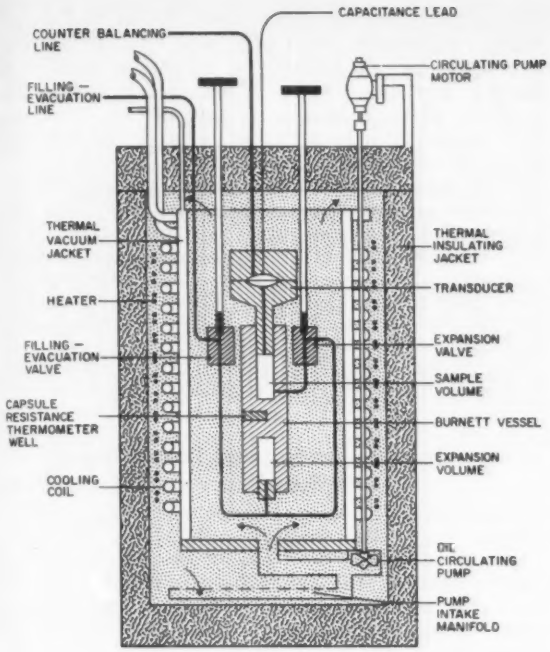

FIGURE 6. *Oil bath.*

apparatus, over the top of the inner chamber, and then downward past the heat exchanger to complete the cycle. Sufficient mixing of the oil occurs in the manifold and the pump to eliminate temperature gradients acquired during the flow of the oil past the heat exchanger.

The heat exchanger consists of a cooling coil and a series-parallel heater for low and high power output. A coolant is circulated through the coil and a refrigerated bath, which is thermostated to within 0.003 °C from −20 to 5 °C. The cooling system is used for oil bath temperatures from 0 °C to slightly above room temperature.

The servo heater system consists of an adjustable Wheatstone bridge with a resistance thermometer constituting one arm, a d-c amplifier and recorder, a three-mode controller for proportional, derivative, and integral response to the error signal, and a power amplifier connected to a heater circuit. The resolution of the temperature control is 0.001 °C; slight differences from the desired temperature are readily corrected by the use of a variable resistor in the bridge circuit.

The temperature as defined by the International Practical Temperature Scale of 1968 is measured with a capsule platinum resistance thermometer located in the well between the sample and the expansion chambers in the Burnett vessel. The thermometer leads are brought out through a protection tube filled with oil to ensure good thermal contact between the thermometer and the Burnett vessel. A Mueller bridge with a photoelectric galvanometer as the detector is used to measure the resistance.

Differential five-junction copper-constantan thermocouples are used to measure temperature differences over the Burnett vessel and transducer as well as near the top of the oil bath. A small temperature difference can exist between the Burnett vessel and the top of the bath due to heat loss through the apparatus supports and oil-vapor loss to the surroundings. This difference is limited to 0.01 °C by means of a manually-controlled auxiliary heater at the top of the bath. Temperature differences over the Burnett vessel are less than 0.002 °C. Electrical noise in the thermocouple circuits, which include the switching and measurement instrumentation, corresponds to a temperature uncertainty of less than 0.0001 °C.

2.4. Experimental Procedure

An experimental procedure has been evolved which ensures the reproducibility of the pressure measurements, the precise definition of the sample volume, and the detection of any sample gas leakage. A series of runs is made at each isotherm temperature. Each run may include up to approximately eight expansions; the initial pressure for each run is chosen so as to give a well-distributed set of pressures for the isotherm. Before any Burnett measurements are made, the oil bath is thermostated at the desired temperature and the transducer is calibrated over the desired pressure range. The transducer null capacitance at atmospheric pressure is checked before and after each day's measurements.

The first step in a run is to evacuate the sample gas part of the apparatus and flush it thoroughly with the sample gas. After this part of the apparatus has been reevacuated, the sample and the expansion volumes are filled with fresh sample gas to the highest pressure desired for the run. In the flushing and the filling process and throughout the run, any pressure imbalance across the transducer diaphragm greater than a few bars is directed toward the base, which is more rugged than the capacitance sensor and its clamping arrangement and hence provides better diaphragm support. This precaution helps to ensure the stability of the diaphragm null position and thus aids in the precise definition of the sample volume. Similarly, as a pressure measurement is made, the diaphragm is slightly overloaded toward the base prior to the final balancing of the counterbalancing and the sample gas pressures.

After the filling process is completed and the filling-evacuation valve closed, sufficient time is allowed for temperature and pressure equilibration. During the course of a run the temperature of the Burnett vessel may vary over a range of about 0.002 °C due to instabilities primarily in the temperature control bridge; equilibration times are chosen to keep short-term temperature changes well within this range and temperature differences within the ranges discussed earlier.

While the equilibration is taking place, preparations are made for the first set of Burnett measurements. The counterbalancing gas, which was maintained at a higher pressure than the sample gas during the filling

process, is gradually vented until the transducer null indicator returns to its zero position. The approximate counterbalancing gas pressure is then read from a Bourdon gage, and a variable capacitor in the capacitance bridge is adjusted in accordance with the transducer calibration so that the bridge balance will truly correspond to the diaphragm null position. The piston gage to be used for the precise pressure measurement is loaded with approximately the right combination of weights that will be needed.

When the resistance thermometer and the differential thermocouple readings show that the equilibration is essentially complete, the expansion valve is closed to isolate the sample and the expansion volumes. While the valve is slowly closed, the diaphragm is maintained in its null position by adjustment of the counterbalancing gas pressure with the compound gas injector. An amplifier and supplementary null indicator about ten times as sensitive as the transducer output meter are used in this process, partly because of their greater sensitivity and also because the location of the supplementary null indicator is more convenient to the person closing the valve and operating the compound gas injector.

After the expansion valve is closed, the first set of Burnett measurements can be made. In the operation of the piston gage a precise zeroing of the transducer output meter would require an unnecessarily long time to be achieved. Instead the gage operator calibrates the output meter over its central range by noting the difference in the scale readings that correspond to two nearly equal loads on the gage. The slight difference in the diaphragm position represented by the different scale readings changes the sample volume, which is bounded by the diaphragm, by a negligible amount—less than 2 ppm. The scale readings are made when the piston is at its reference height as shown by an electronic proximity sensor mounted underneath the weights loaded on the gage. The height of a gas gage piston is adjusted by means of the compound gas injector; the height of the oil gage piston is adjusted by means of a separate oil injector. For either type of gage the piston is raised above its reference height by means of the appropriate injector and is then allowed to fall slowly down to its reference height while the piston and its load are spinning steadily. The gage pressure and barometric pressure measurements are made almost simultaneously, and the resistance thermometer and differential thermocouple measurements are made immediately afterward. These measurements constitute the first set of Burnett measurements.

Next the expansion valve is opened and after about a minute is closed as before. A second set of Burnett measurements is made. Since the expansion step has not been performed, this second set of measurements should be in close agreement with the first set. If the second set, in fact, does not differ significantly from the first, the filling-evacuation valve is opened and the expansion volume is evacuated. After isothermal conditions are reestablished and a thermocouple vacuum gage, located as close to the expansion volume as is convenient, shows a pressure of about 4×10^{-6} bars, a third set of measurements is made. If this set does not differ significantly from the first two, the filling-evacuation valve is closed and the expansion valve is opened. The gas initially in the sample volume expands to fill the expansion volume as well. After this first expansion the measurement procedure is repeated to successively lower pressures.

To be considered satisfactory, the three sets of measurements corresponding to the initial filling or a subsequent expansion must show a pressure reproducibility of 1 part in 50,000 or better. Occasionally a set of measurements will be repeated if some temporary disturbance, such as a temperature or barometric fluctuation, has caused a poorer reproducibility. If a serious experimental failure, such as sample gas leakage, were to occur, the measurements for that run would not be used in the data reduction.

3. Data Reduction and Discussion of Results

3.1. Background

In contrast to the simplicity of the experimental measurements, the reduction of Burnett data involves rather formidable nonlinear statistical analysis of relationships containing the compressibility factor, defined by a pressure or a density virial expansion, and optional constants. The authors have previously presented a general discussion of the analysis of different Burnett relationships using two nonlinear statistical methods, due to Gauss and to Deming [9]. Related papers have also been published by others [12, 13].

Our experience indicates that compressibility factors and second virial coefficients calculated from Burnett data of high precision and accuracy are as accurate as those calculated from the best data obtained with any other *PVT* method. Various treatments of relationships, that is, various models, based on eqs (7) and (8) have been used in our analysis. In these models the cell constant, where it appears, is regarded as a single parameter common to all the experimental runs, as a separate parameter for each run, or as a constant to be determined from Burnett measurements for a nearly ideal gas. Meaningful comparisons of the results are difficult for at least two reasons: (1) the same systematic errors may propagate differently in each model and (2) the number of parameters to be evaluated varies from one model to another. The effect of the latter is subtle; it may introduce an analytical bias, as the magnitude of the correlation between the parameters, which is basically high, increases significantly with an increase in the number of parameters. It is not surprising, therefore, that slight discrepancies exist among the results of different models, even when applied to the same data. For example, a comparison of the compressibility factors derived from argon data taken with our Burnett apparatus shows discrepancies among the values of approximately 0.01 percent to 0.04 percent, which,

although small, are nevertheless greater than the estimated statistical uncertainties of less than 0.01 percent. For the six models considered, the results of four show comparative discrepancies of about 0.01 percent. Another example of this type of discrepancy occurred in an informal round-robin analysis of helium data by participants at a two-day Burnett conference held at the National Bureau of Standards in February 1969. Initial analyses indicated discrepancies of 0.04 percent among the results of the different models as compared to statistical uncertainties of 0.01 percent in the results themselves.

We shall not repeat our previous detailed presentation of the nonlinear statistical analysis of Burnett data [9], but shall present a brief discussion which emphasizes the important differences between the various models in order to help one choose the models that introduce the least bias. The fact that the data can be reduced in several ways is an attractive feature of the Burnett method and enables one to study the different effects of systematic errors.

The basic Burnett equations may be transformed into different relationships among the variables of interest. In terms of a finite virial expansion in pressure, $Z=1+\sum_{i=1}^{I} b_i P^i$, eq (7) may be expressed as

$$\frac{P_{r-1}}{P_r}=N_r\frac{\left(1+\sum_{i=1}^{I} b_i P_{r-1}^i\right)}{\left(1+\sum_{i=1}^{I} b_i P_r^i\right)}, \tag{9}$$

$$P_r(N_1N_2\ldots N_r)=\frac{P_0}{Z_0}\left(1+\sum_{i=1}^{I} b_i P_r^i\right), \tag{10}$$

$$\frac{P_{r-2}P_r}{P_{r-1}^2}=\frac{1+\Delta N_{r-1}(P_{r-2},P_{r-1})}{1+\Delta N_r(P_{r-1},P_r)} \times\frac{\left(1+\sum_{i=1}^{I} b_i P_{r-2}^i\right)\left(1+\sum_{i=1}^{I} b_i P_r^i\right)}{\left(1+\sum_{i=1}^{I} b_i P_{r-1}^i\right)^2}. \tag{11}$$

In terms of a finite virial expansion in density, $Z=1+\sum_{j=1}^{J} B_j\rho^j$, eq (8) may be expressed as

$$P_r=\frac{\rho_0}{N_1N_2\ldots N_r}RT_c\left[1+\sum_{j=1}^{J} B_j\left(\frac{\rho_0}{N_1N_2\ldots N_r}\right)^j\right]. \tag{12}$$

It should be noted that in these equations the second virial coefficient is represented by b_1 or B_1. For both the pressure and the density relationships

$$N_r=N[1+\Delta N_r(P_{r-1},P_r)]$$

and

$$N_1N_2\ldots N_r=N^r[1+\Delta N_1(P_0,P_1)] \times[1+\Delta N_2(P_1,P_2)]\ldots[1+\Delta N_r(P_{r-1},P_r)].$$

Any one of these relationships may be applied to Burnett data to form an overdetermined set of equations for evaluating the virial coefficients and the other parameters. The latter consist of the cell constant (except in eq (11) where the cell constant has been eliminated), the initial density ρ_0 in eq (12), and sometimes the quantity P_0/Z_0 in eq (10). The latter two parameters are characteristic of an individual run. As mentioned in the introduction, the pressure corrections (ΔN_1, ΔN_2, . . .) are not considered as parameters but are determined independently of the parameter evaluation.

3.2. Compressibility Factor of Argon at 25 °C

Compressibility factor results derived from the different relationships applied to our argon data are given in table 1 [9]. The models are designated briefly at the top of each column. For each model the parameters were evaluated simultaneously for all the data. Where a fixed cell constant was used, it was predetermined from eq (9) applied to helium data taken at the same temperature for pressures below 35 bars. For these conditions helium behaves nearly as an ideal gas, a characteristic which simplifies the data reduction.

The results at each pressure are essentially the same except for those derived from the density relationship with an adjustable cell constant included as either a separate parameter for each run or a single parameter common to all the runs. The discrepancies among the first four columns, which are about 0.01 percent, could be due to the presence of systematic error which propagates differently in each model. A likely source of such error is the correction for the volume distortion of the sample and expansion chambers with pressure. A study of simulated Burnett problems based on our argon data indicated that other probable sources of error had a negligible effect on the compressibility factor. In this study a simulated systematic error of 1 part in 30,000 was superimposed on the argon pressure data. The density reduction of these data, with the cell constant either fixed or regarded as a parameter, resulted in a change in the compressibility factor of less than 0.001 percent for all the pressures. An effect of less than 0.001 percent was also obtained when a simulated systematic error of 1 part in 20,000 was superimposed on the RT product in a density reduction of the data.

The volume distortion correction was determined from distortion equations and strain gage measurements of the external deformation of the Burnett

TABLE 1. *Comparison of results derived from Burnett argon data at 25 °C and to 250 bars*[a, b]

3 Runs (7, 7, & 6 expansions/run)

	Pressure series formulation			Density series formulation		
	Eq (9) Cell constant fixed	Eq (9) One cell constant adjusted	Eq (11) Cell constant eliminated	Eq (12) Cell constant fixed	Eq (12) One cell constant adjusted	Eq (12) All cell constants adjusted
N	1.74505	1.74502		1.74505	1.74511	1.74511 1.74509 1.74511
$Z_{10.133\ bars}$	0.99384	0.99387	0.99388	0.99380	0.99375	0.99376
$Z_{101.33\ bars}$	.95356	.95365	.95367	.95352	.95333	.95334
$Z_{202.65\ bars}$	.95202	.95209	.95212	.95194	.95169	.95173

[a] The compressibility factor is shown to five digits to indicate the differences in the numerical results and not to indicate the overall accuracy.

[b] 1 bar = 10^5 N · m^{-2}.

vessel due to internal pressure [14, 15]. The effect of the distortion correction and its estimated uncertainty on the compressibility factor is shown in figure 7 for argon data analyzed with the use of the pressure equation (10). The effect of the uncertainty is small, about 0.01 percent at the maximum pressure of 250 bars. The results of simulated problems indicate that the effect is the same in the density formulation. In the pressure series formulation the effect of the distortion correction uncertainty is consistent with the small differences between the results derived with the cell constant fixed and those derived with the cell constant evaluated or eliminated.

We now consider the basis for the differences, particularly at the higher pressures, which are significantly greater than 0.01 percent. These are between the results derived from the pressure series formulation and the results from the density series formulation, particularly with the cell constant included as either a separate parameter for each run or a single parameter common to all the runs. If the exact model were known, that is, if all the systematic errors were included in each equation, then the uncertainties in the values of the compressibility factor, the cell constant, and the initial densities would be consistent with the magnitude of any random errors in the pressure. This has been illustrated with a simulated Burnett problem for a particular model in which random errors were superimposed on the pressure data [16]. In the real world one cannot account exactly for all of the systematic errors. Consequently, a bias is introduced in the statistical analysis, and the results are not as reliable as the statistical uncertainties indicate. In addition, the number of parameters varies from one model to another. This variation adds to the bias since the absolute value of the correlation between the parameters increases significantly with an increase in the number of parameters.

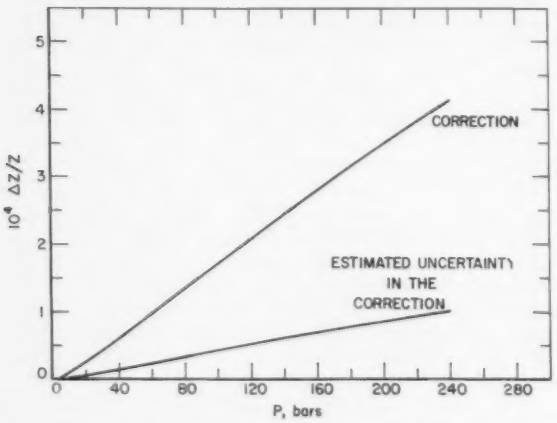

FIGURE 7. *Relative compressibility factor correction due to pressure distortion of Burnett cell volumes, argon run.*

In general the correlation between virial coefficients is high regardless of which *PVT* method is used to determine them. In the Burnett method additional highly correlated parameters are also present. In the density reduction of the argon data with a fixed cell constant, the absolute value of the computed correlation between each of the virial coefficients is about 0.85 on a normalized basis of 0 to 1, whereas it is about 0.6 between each of the initial densities and about 0.75 between any one of the virial coefficients and any one of the initial densities. In contrast, if the cell constant is included as a parameter, the statistical fit is improved over that for the fixed cell constant, in the sense that the sum of squares is reduced. However, the correlation between any two of the parameters increases significantly! The correlation between each of the virial coefficients becomes about 0.93; between each of the initial densities, about 0.994; and between any one of the virial coefficients and any one of the initial densities, about 0.87. The correlation between the cell constant and any one of the virial coefficients is about 0.88 and between the cell constant and any one of the initial densities, about 0.995. Exceptionally high correlations such as 0.994 and 0.995 indicate that these parameters are not truly independent and thus cannot be accurately evaluated [17].

Additional data, not highly correlated to the data already in the analysis, would reduce the high parameter correlation. As a result, the evaluation of the parameters would be enhanced and any analytical bias in the results would be reduced. In one approach the analysis would consist of data from the same apparatus for two or more sample gases with different compressibility characteristics. The data would be taken at the same temperature, and a single cell constant parameter, common to all the data, would be evaluated. Another approach would be to use a fixed cell constant obtained from helium data. This approach is less desirable because the cell constant would be entered without any statistical uncertainty, that is, as an exact quantity, and hence the computed statistical uncertainties would be too small. The significance of high parameter correlation should be considered carefully in estimating the reliability of results obtained from the density reduction methods. For the pressure reduction methods the situation is similar, although the parameter correlation is not as high.

Our values of the compressibility factor shown in table 2 represent the average of the results of the three pressure models and the density model with a fixed cell constant; the results of the density models with one or three separate cell constants were not included in the average because they were considered to be less reliable due to the high correlation between the parameters. For pressures up to 250 bars the overall accuracy of the averaged compressibility factor is estimated to be within ± 0.0002 on the basis of our error analysis. The statistical uncertainty of each value of the compressibility factor is no greater than one sixth of the overall accuracy of the averaged compressibility factor. Table 2 also includes comparative values of the argon compressibility factor derived from the piezometer results of Michels [18] for pressures up to 202.7 bars. The maximum difference is small, only 0.05 percent at 202.7 bars; *PVT* results are generally considered to be accurate if the overall error is less than 0.1 percent.

TABLE 2. *Comparative values of the compressibility factor for argon at 25°C*[a]

Pressure bars	This paper[b] Compressibility factor	Michels[c] Compressibility factor
10.133	0.9938	0.9938
101.33	.9536	.9534
202.65	.9520	.9515

[a] 1 bar = 10^5 N · m^{-2}.
[b] The overall accuracy is estimated to be ± 0.0002.
[c] [18].

3.3. Second Virial coefficient of Carbon Dioxide at 50 °C

In addition to accurate values of the compressibility factor, reliable second virial coefficients are also obtainable from the Burnett method. Our own experience with argon at 25 °C and with carbon dioxide at 50 °C, 19 degrees above its critical temperature, shows that this is true over a wide range of reduced temperatures greater than unity.[2] The argon results are for a reduced temperature of 1.98 and have been discussed previously [9]; the carbon dioxide results, which are discussed in the following paragraphs, are new and are for a reduced temperature of 1.06.

Two groups of carbon dioxide measurements were made: one group over the pressure range from 35 to 4.5 bars and another group over the range from 4.5 to 0.5 bars. The higher pressure data are the more accurate data and were reduced by the density model with a fixed cell constant determined from helium data at the same temperature. From the more accurate data a second virial coefficient for carbon dioxide of -102.25 ± 0.04 cm^3/mol was obtained, where the uncertainty is only the statistical uncertainty and is necessarily too small because it does not include the uncertainty in the cell constant. Our estimate of the overall systematic uncertainty, based on our error analysis, is 0.2 cm^3/mol. This value of the second virial coefficient was supported by a graphical evaluation which included the less accurate carbon dioxide data for the lower pressures. It compares favorably with the value of -102.5 cm^3/mol obtained from a recent correlation [19] which included an evaluation of all existing data but is in substantial disagreement with the value of -100.7 ± 0.4 cm^3/mol determined by Dadson and his co-workers [20, 21]. It should be noted that Dadson et al. carried out their measurements with both the Burnett method and the piezometer method. The fact that their results from both these methods agreed with each other and yet disagreed with the results of the correlation prompted our own measurements. Our results and more detailed comparisons will be the subject of a later publication.

Various potential sources of systematic error were investigated in our own work. In simulated problems based on the higher pressure data, superimposed systematic errors of ± 25 percent in the distortion correction and 1 part in 20,000 in the *RT* product had only a negligible effect on the second virial coefficient. The uncertainty in the distortion correction would be expected to have a negligible effect since the distortion correction itself is very small even at the highest pressures in the carbon dioxide data. A cell constant was computed for the carbon dioxide data in a separate calculation by treating it as an adjustable parameter in the density series formulation. The value obtained agreed with the predetermined value obtained from helium data to within 1 part in 20,000, which is excellent agreement in view of the large magnitude of the nonideality of carbon dioxide at 50 °C ($T/T_{\text{critical}} = 1.06$) and of the extremely high correlation between the parameters in the analysis.

The possibility of adsorption of carbon dioxide on the surfaces of the sample and the expansion volumes was investigated by means of a graph of the low pressure data in which the pressure ratio P_{r-1}/P_r was plotted

[2] The reduced temperature is the ratio of the sample gas temperature to its critical temperature, where both these temperatures are expressed on the absolute scale.

as a function of the pressure P_{r-1}. The significance of the graph is based on the equation

$$\frac{P_{r-1}}{P_r} = N + b_1(N-1)P_{r-1}, \tag{13}$$

which is the low pressure form of eq (9).[3] The extrapolation of the curve drawn through the points to the vertical axis yielded an intercept whose value, the cell constant, was essentially the same as the predetermined value obtained from the helium data. This agreement would not be expected if adsorption were present. For a nonpolar gas such as carbon dioxide and for our range of pressures, adsorption is expected to be saturated [22]; that is, above a relatively low pressure very little more adsorption occurs as the pressure is increased further. In the sample volume the adsorbed gas would remain essentially unchanged upon an expansion, whereas in the expansion volume gas would be desorbed in the evacuation process and adsorbed in the expansion process. As a result, the number of free molecules would be reduced upon an expansion, and the ratio P_{r-1}/P_r would therefore increase rapidly at low pressures. The extrapolation to zero pressure would yield a value for the cell constant that is greater than the value predetermined from helium data for which adsorption is not significant. Furthermore, the graph of this ratio versus pressure would show increasing nonlinearity at low pressures instead of the decreasing nonlinearity characteristic of real gases as the effect of the third and higher order virial coefficients not shown in eq (13) becomes insignificant. Neither of these signs of adsorption is present in our data. Hence we feel confident that any adsorption in our apparatus is so slight as to have an insignificant effect on our results.

We gratefully acknowledge the benefit we have received from general discussions with M. Klein and from comments regarding adsorption made by P. T. Eubank.

4. References

[1] Mason, E. A., and Spurling, T. H., The Virial Equation of State (Pergamon Press, Oxford, 1969).

[2] Levelt Sengers, J. M. H., The experimental determination of the equation-of-state of gases and liquids at low temperatures, Physics of High Pressures and the Condensed Phase, Ed. A. van Itterbeek, pp. 60–97 (North-Holland Publishing Co., Amsterdam, 1965).

[3] Burnett, E. S., Compressibility determinations without volume measurements, J. Appl. Mech. **3**, A136–A140 (1936).

[4] Pfefferle, W. C., Jr., Goff, J. A., and Miller, J. G., Compressibility of gases. I. The Burnett method. An improved method of treatment of the data. Extension of the method to gas mixtures, J. Chem. Phys. **23**, 509–513 (1955).

[5] Liley, P. E., Thermodynamic Properties of Steam/Carbon Dioxide Mixtures at High Temperature and Pressure, Thesis, University of London (1957).

[6] Silberberg, I. H., Kobe, K. A., and McKetta, J. J., Gas compressibilities with the Burnett apparatus, J. Chem. Eng. Data **4**, 314–330 (1959).

[7] Hoover, A. E., Canfield, F. B., Kobayashi, R., and Leland, T. W., Jr., Determination of virial coefficients by the Burnett method, J. Chem. Eng. Data **9**, 568-573 (1964).

[8] Waxman, M., Hilsenrath, J., and Chen, W. T., The compressibility factor and the second virial coefficient of boron trifluoride from 0 to 225 °C and for pressures up to 250 bars, (to be published).

[9] Waxman, M., Hastings, J. R., and Chen, W. T., Nonlinear statistical analysis of Burnett PVT data, Proceedings of the Fifth Symposium on Thermophysical Properties, Ed. C. F. Bonilla, pp. 248–261 (ASME, New York, 1970).

[10] Waxman, M., and Chen, W. T., A rugged null-type pressure transducer of high reproducibility for accurate gas phase PVT measurements, J. Res. Nat. Bur. Stand. (U.S.), **69C** (Eng. and Instr.), No. 1, 27–33 (1965).

[11] Keyes, F. G., Methods and procedures used in the Massachusetts Institute of Technology program of investigation of the pressures and volumes of water to 460 °C. Part I. Proc. Am. Acad. Arts Sci. **68**, 505–564 (1933).

[12] Barieau, R. E., and Dalton, B. J., A method for treating PVT data from a Burnett compressibility apparatus, Bureau of Mines Report of Investigations **7020** (1967).

[13] Hall, K. R., and Canfield, F. B., A least-squares method for reduction of Burnett data to compressibility factors and virial coefficients, Physica **47**, 99–108 (1970).

[14] Roark, R. J., Formulas for Stress and Strain (McGraw-Hill Book Company, Inc., New York, 1954).

[15] Kadkowski, P. P., Bluhm, J. I., and Bowie, O. L., Watertown Arsenal Laboratory, Thick-Walled Cylinder Handbook.

[16] Briggs, T. C., Dalton, B. J., and Barieau, R. E., Compressibility data for helium at 0 °C and pressures to 800 atmospheres, Bureau of Mines Report of Investigations **7287** (1969).

[17] Marquardt, D. W., An algorithm for least-squares estimation of nonlinear parameters, J. Soc. Indust. Appl. Math. **11**, 431–441 (1963).

[18] Michels, A., Wijker, Hub., and Wijker, Hk., Isotherms of argon between 0 °C and 150 °C and pressures up to 2900 atmospheres, Physica **15**, 627–633 (1949).

[19] Levelt Sengers, J. M. H., Klein, M., and Gallagher, J. S., Pressure-Volume-Temperature relationships of gases. Virial coefficients, American Institute of Physics Handbook, (to be published).

[20] Butcher, E. G., and Dadson, R. S., The virial coefficients of the carbon dioxide-ethylene system I. Pure gases, Proc. Roy. Soc. (London) **A277**, 448–467 (1964).

[21] Dadson, R. S., Evans, E. J., and King, J. H., The second virial coefficient of carbon dioxide, Proc. Phys. Soc. **92**, 1115–1121 (1967).

[22] Brunauer, S., The Adsorption of Gases and Vapors. Volume I Physical Adsorption (Princeton University Press, Princeton, 1943).

[3] Equation (13), together with the equation $B_1 = RTb_1$, was used in the graphical evaluation of the second virial coefficient.

(Paper 75C3&4-323)

JOURNAL OF RESEARCH of the National Bureau of Standards—C. Engineering and Instrumentation
Vol. 75C, Nos. 3 and 4, July–December 1971

An Extension to the Sliding Short Method of Connector and Adaptor Evaluation*

Glenn F. Engen*

Institute for Basic Standards, National Bureau of Standards, Boulder, Colorado 80302

(October 18, 1971)

Sliding short methods represent a measurement tool of substantial potential for the measurement of small losses such as are associated with waveguide connectors or adaptors. Until recently, however, the use of these methods has been inhibited by the uncertainty of the error contribution due to non-ideal short behavior.

A recent analysis by Almassy has shown that by the use of proper techniques, the error contribution from this source is usually negligible, provided that the adaptor (or connector) is "well matched."

It is the purpose of this paper to eliminate this latter restriction, develop additional measurement methods, and describe further applications.

Key words: Adaptor; connector; efficiency; sliding short.

1. Introduction

A measurement problem, of continuing interest in the microwave art, is that of adaptor evaluation. With the advent of the *power equation* [1][1] methods and use of *terminal invariant parameters* [2], the dependence upon impedance properties is suppressed, and the dissipative characteristic emerges as the parameter of major interest. A similar observation may be made with regard to connectors. Here the dissipation at the connector interface, or more specifically, the lack of loss repeatability, represents a basic limitation to the attainable accuracy in many microwave measurements.

The application of sliding short methods, to this measurement problem, has been known for some time [3, 4]. These techniques were generalized in conjunction with the development of the power equation methods [1, 2]. Despite this revival of interest, however, the technique has been subject to a major limitation: an ideal sliding short is assumed.

In practice, of course, no such device exists. Moreover, the losses in the short may be of the same order (or larger) than those in the joint or adaptor to be evaluated. In the absence of further information, this loss represents a potential source of substantial error.

A recent analysis by Almassy [5] has shown that, with proper techniques, the sliding short losses can be substantially reduced, provided that the adaptor (or joint) reflection is small (i.e., $|S_{11}| \ll 1$, $|S_{22}| \ll 1$).

It is the purpose of this paper to eliminate this restriction, develop additional measurement methods, and describe further applications.

2. Background

The major thrust of this paper will be directed towards the measurement of the *efficiency* of an arbitrary two-port. In particular this two-port may be a connector, waveguide-coax adaptor, etc. By definition, the efficiency is the ratio of the (net) power output, to the (net) power input, and is a function of the load (but not of the source) impedance. Throughout this paper, the efficiency is assumed to be large (small losses). (In general the accuracy of this method decreases rapidly with losses greater than 10 dB.)

It will prove convenient to briefly review the existing theory. The recommended instrumentation takes the form shown in figure 1. The basic configuration will

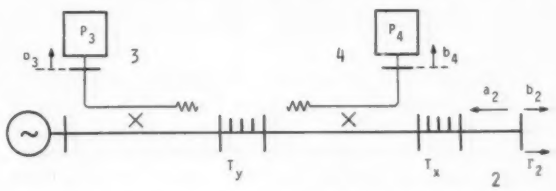

FIGURE 1. *Generalized reflectometer for use in efficiency measurement.*

*Senior Research Scientist, Electromagnetics Division, National Bureau of Standards, Boulder, Colo. 80302.

[1] Figures in brackets indicate the literature references at the end of this paper.

448-719 OL -72 - 3

be recognized as a generalized reflectometer (*g*-reflectometer), where the junction parameters are arbitrary except as subsequently noted. In particular, the tuning transformers T_x, T_y permit one to impose certain conditions on the measurement system. The device to be evaluated is connected to port 2, while arms 3 and 4 are terminated by power meters.

Although power meters have been specified for arms 3 and 4, it will prove convenient, momentarily, to assume an alternative detection scheme such that the complex ratio b_3/b_4 is measured, where b_3, b_4 are the emergent wave amplitudes. Let arm 2 be terminated by a moving short ($\Gamma_2 = e^{j\theta}$), and let the values $\left(\frac{b_3}{b_4}\right)$ be plotted in the complex plane as θ is permitted to vary. The resultant locus is a circle, an example of which is shown in figure 2. The parameters of this locus, in particular the radius of the circle, R, and the (absolute) distance, R_c, between its center and the origin, play a major role in the efficiency measurement.

Inspection of figure 2 indicates that [2]

$$\left|\frac{b_3}{b_4}\right|_{\max} = R + R_c, \tag{1}$$

$$\left|\frac{b_3}{b_4}\right|_{\min} = R - R_c. \tag{2}$$

and solving for R, R_c yields:

$$R = \frac{1}{2}\left(\left|\frac{b_3}{b_4}\right|_{\max} + \left|\frac{b_3}{b_4}\right|_{\min}\right), \tag{3}$$

$$R_c = \frac{1}{2}\left(\left|\frac{b_3}{b_4}\right|_{\max} - \left|\frac{b_3}{b_4}\right|_{\min}\right). \tag{4}$$

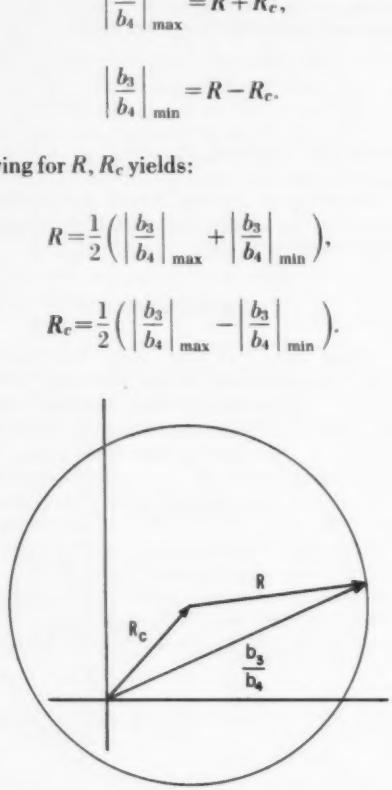

FIGURE 2. *Locus of* b_3/b_4 *as a function of* θ.

[2] It is assumed that the origin is within the circle. As long as the efficiency is high, this condition is assured. As the losses increase, however, it is possible that $R_c > R$. For a more complete discussion see [2].

The determination of R, R_c thus involves amplitudes only, the phase detection capability is not required. Finally, the power meters respond to the square of the amplitude such that $P_3 = |b_3|^2$ etc.

In order to make an efficiency measurement, the two-port is connected as shown in figure 3. Note that the designations have been chosen such that port 2 of the four arm junction mates with port 2 of the two-port. The "load" impedance, for which the efficiency is measured, is actually provided by the four arm junction.

To be more specific, it is convenient to postulate that P_4 is constant. (In practice this is often done by a "leveling" or feedback arrangement.) The source impedance, Γ_g, for the "equivalent" generator, which now obtains at port 2, depends upon T_x and the adjacent coupler [6], but is independent of T_y and the remaining coupler. The efficiency, which is obtained in the measurement described in the following paragraph, is that for an assumed power flow from terminal 1 to terminal 2, with the termination Γ_g. It will be denoted by $\eta_{21}(\Gamma_g)$.

The efficiency measurement calls for connecting a moving short to terminal 1 and determining the radius, R_1, of the resulting circular locus using (3). The two-port is then removed, and the operation repeated at terminal 2 to obtain R_2. It has been shown [2] that

$$\eta_{21}(\Gamma_g) = R_1/R_2. \tag{5}$$

In an alternative method, it is convenient (but not essential) to use the configuration shown in figure 4. Here the efficiency, $\eta_{12}(\Gamma_l)$, is measured for a power flow from terminal 2 to terminal 1, and for the terminating load Γ_l.

The measurement procedure now calls for the adjustment of T_x such that P_3 vanishes. The parameters, R, R_c, of the circular locus are then measured with the moving short connected to terminals 1 and 2. It will be shown (see appendix) that $\eta_{12}(\Gamma_l)$ is given by:

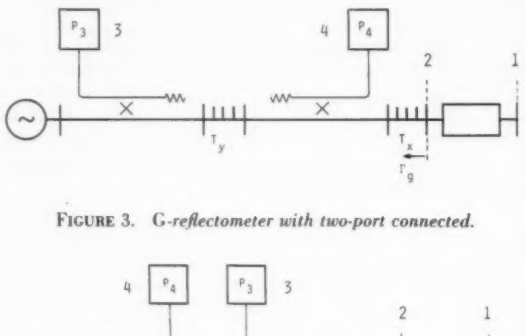

FIGURE 3. *G-reflectometer with two-port connected.*

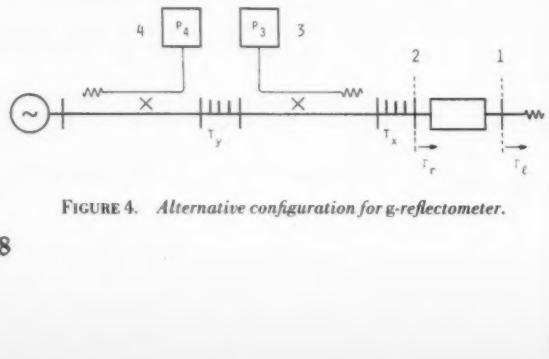

FIGURE 4. *Alternative configuration for* g*-reflectometer.*

$$\eta_{12}(\Gamma_l)=\frac{R_1}{R_2}\frac{\left(1-\left(\frac{R_{c1}}{R_1}\right)^2\right)}{\left(1-\left(\frac{R_c}{R_2}\right)^2\right)}. \tag{6}$$

It should be noted that the adjustment of T_x, in both cases, is dictated by the value of load impedance for which the efficiency is measured. Provided that the indicated configurations of couplers and tuners are used, the operation, in theory, is independent of the adjustment of T_y. Tuner T_y is useful, however, because of certain practical considerations which will be explained later. If the suggested coupler positions are interchanged, (i.e., the configuration of figure 4 is used to measure $\eta_{21}(\Gamma_g)$, or the configuration of figure 3 is used to measure $\eta_{12}(\Gamma_l)$) the indicated role of T_x is shared by T_y and the desired adjustments become interdependent and more difficult to realize.

3. Implementation

The application and implementation of these methods is perhaps best described in terms of a specific problem—an efficiency measurement of a waveguide joint or connector.

Referring to figure 5, it is convenient to first postulate a length of lossless waveguide lead, an ideal moving short, and an "ideal" reflectometer. (In terms of the description contained in (7), in the next section, an "ideal" reflectometer is one for which $b=c=0$.) The object is to measure the loss of the indicated waveguide joint. For reasons which will emerge, it is useful to record the reflectometer response as a function of short position. For the "ideal" system of figure 5 the expected response is that shown in the inset. This result is explained as follows.

As long as the short is to the left of the waveguide joint, the reflection coefficient presented to the reflectometer is of unit magnitude and variable phase. The system responds only to the magnitude; this accounts for the "straight" line section. With the short to the right, however, the joint losses will lead to reduced values for the reflection coefficient magnitude. In particular, this loss is determined by the longitudinal current component and thus will be a maximum when the short position is a multiple of a half-wavelength, and a minimum (zero[3]) when the position is an odd multiple of a quarter wavelength. In this case, the maximum and minimum values to the right of the joint are averaged, and the ratio of this average to the value left of the joint is the efficiency.

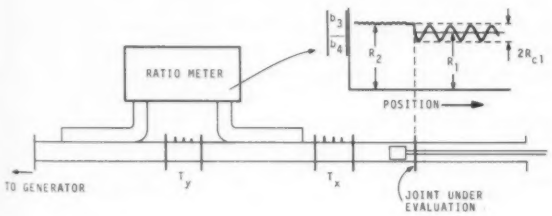

FIGURE 5. *An "ideal" measurement system and its response to the efficiency measurement of a waveguide joint.*

If this experiment is carried out in reality, a typical record is that shown in figure 6. The most obvious change is in the downward slope, this is caused by the waveguide loss. The measurement procedure now calls for a projection of the maxima and minima to the plane of the joint and the parameters R, R_c evaluated from these projections. The mathematical basis for this will be given in the following section.

Although an "ideal" reflectometer was assumed in figure 5, in principle it is possible to start with arbitrary couplers and provide only for the tuning adjustments specified in the preceding section. In general, depending upon the adjustment of T_y, the curve will show an oscillatory behavior on both sides of the joint. As a practical matter, it is generally desirable to adjust T_y such as to keep the amplitude of this oscillatory component within nominal limits. This point will be considered in greater detail in a following paragraph.

For an arbitrary two-port, it is not possible (in general) to make a continuous recording as shown here; in this case it is necessary to choose separate reference planes (usually coinciding with the waveguide flange) in the input and output arms; the determination of R, R_c follows from the projections of the maxima and minima to the reference planes as already described. At this point it is necessary to decide whether the associated joint losses are included as part of the two-port. In many cases the joint loss, or at least its reproducibility, limits the accuracy to which the two-port efficiency may be specified.

4. Analysis

The validity of the foregoing procedure was established by Almassy [5] under the condition that the two-port is "well-matched," (i.e., both $|S_{11}|$ and $|S_{22}|$ are much smaller than unity). The purpose of the present analysis is to demonstrate that the method loses very little of its accuracy, even when this condition is not satisfied.

In general the functional relationship between b_3/b_4, and a termination of reflection coefficient Γ, at either terminal 1 or terminal 2, is in the form:

$$\frac{b_3}{b_4}=\frac{a\Gamma+b}{c\Gamma+1}. \tag{7}$$

Here the complex parameters a, b, c depend upon both the reflectometer and the two-port when the termination is at terminal 1, but only on the former when the termination is at terminal 2. For an ideal short, $\Gamma=e^{j\theta}$ where θ is a function of short position.

[3] This assumes the equivalent circuit of the joint is that of a small series resistance.

In order to account for non-ideal behavior, the model here assumed is:

$$\Gamma = re^{j\psi}e^{-2(\alpha+j\beta)l} \tag{8}$$

where r, ψ are the magnitude and phase of the plunger reflection, α, β are the loss and phase constants of the line in which the "short" moves, and l is its position with respect to the reference flange.

If (8) is substituted in (7), the resulting relation can be written as follows:

$$\frac{b_3}{b_4} = \frac{b - ac^* r^2 e^{-4\alpha l}}{1 - |c|^2 r^2 e^{-4\alpha l}} + \frac{(a - bc) re^{j\psi} e^{-2(\alpha+j\beta)l} (1 + c^* re^{-j\psi} e^{-2(\alpha-j\beta)l})}{[1 - |c|^2 r^2 e^{-4\alpha l}](1 + cre^{j\psi} e^{-2(\alpha+j\beta)l})} \tag{9}$$

where (*) denotes the complex conjugate.

Although this expression is a complicated one, a great deal can be learned about the problem by inspection of this result. First, if the short is ideal, $r=1$, $\psi=\pi$, $\alpha=0$, and the expression becomes:

$$\frac{b_3}{b_4} = \frac{b - ac^*}{1 - |c|^2} - \frac{(a - bc) e^{-2j\beta l} (1 - c^* e^{2j\beta l})}{(1 - |c|^2)(1 - ce^{-2j\beta l})}. \tag{10}$$

Here it is noted that b_3/b_4 is the sum of two terms. The first is a constant (as l varies), while the second is of constant magnitude but variable phase. (Note that the last factors in the numerator and denominator of the second term are conjugates of each other.) This explicitly demonstrates the previously stated result: the locus of b_3/b_4 is a circle of radius

$$R = \left| \frac{a - bc}{1 - |c|^2} \right| \tag{11}$$

and distance to the center

$$R_c = \left| \frac{b - ac^*}{1 - |c|^2} \right| . \tag{12}$$

Next, it is desirable to return to the more general relationship contained in (9) and to consider the functional dependence of $|b_3/b_4|$ upon l. It is this relationship which is plotted in figure 6.

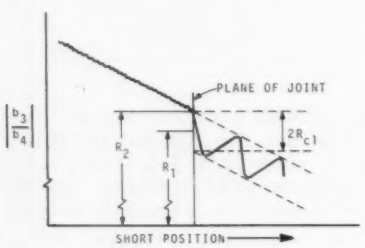

FIGURE 6. *"Typical" response in an actual measurement.*

In the discussion which follows, it will prove useful to consider not only the functional relationship of (9), but also the family of functions which is obtained from (9) for different values of ψ. Conceptually, one assumes the measurement is repeated a number of times, where the moving "shorts" have the same value for r, but differing values of ψ.

For a given l, the value of $|b_3/b_4|$ will depend upon ψ, and for some particular choice of ψ will have the maximum value:

$$\left|\frac{b_3}{b_4}\right|_{\max} = \frac{|a - bc| re^{-2\alpha l} + |b - ac^* r^2 e^{-4\alpha l}|}{1 - |c|^2 r^2 e^{-4\alpha l}}. \tag{13}$$

For some other choice of ψ, $|b_3/b_4|$ will have the minimum [4]:

$$\left|\frac{b_3}{b_4}\right|_{\min} = \frac{|a - bc| re^{-2\alpha l} - |b - ac^* r^2 e^{-4\alpha l}|}{1 - |c|^2 r^2 e^{-4\alpha l}} . \tag{14}$$

For each value of l, there will be some member of the family (value of ψ) for which these maximum and minimum values are realized, but these limits are never exceeded. Equations (13), (14) are evidently the envelope of the family. If this envelope is denoted by E, then:

$$E = \frac{|a - bc| re^{-2\alpha l} \pm |b - ac^* r^2 e^{-4\alpha l}|}{1 - |c|^2 r^2 e^{-4\alpha l}} . \tag{15}$$

Because of the oscillatory behavior of $|b_3/b_4|$, the envelope may be easily inferred from a single member of the family provided that several cycles, or more, have been recorded. From (15), the extrapolation of this envelope to the plane where $l=0$ yields:

$$E|_{l=0} = \frac{|a - bc| r \pm |b - ac^* r^2|}{1 - |c|^2 r^2} . \tag{16}$$

The use of this result to obtain approximate values for the efficiency will be evaluated in the following section. It is next instructive to consider the general behavior of E as l varies.

Returning to (15), the first term in the numerator tends to dominate the entire expression, and provides a simple exponential decay. The second term in the numerator determines the amplitude associated with the oscillatory behavior. If c vanishes, this amplitude is constant, while if b vanishes, the amplitude decays exponentially. If both these conditions obtain the oscillatory behavior is absent. The most distinctive situation occurs when b and ac^* are nominally equal. In this case there will be some value of l (which may or may not be physically realizable) for which this second term will be a minimum (possibly zero).

Finally, the second term in the denominator is usu-

[4] This assumes that the first term exceeds the second which, for the applications envisioned, is usually the case.

ally small[5] with respect to unity. As a whole the denominator increases as l increases, and the value of the complete expression decreases somewhat more rapidly than would otherwise be the case. As a rule, this effect is rather small. The most general form of the envelope is a distorted hyperbola as shown in figure 7.

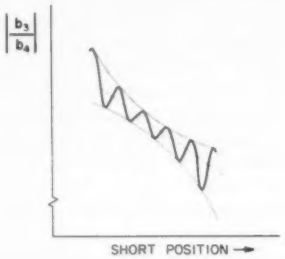

FIGURE 7. *General form of system response.*

5. Practical Considerations

As already noted, the measurement technique calls for recording $|b_3/b_4|$ as a function of l (short displacement). The envelope of this curve is then projected to the plane where $l=0$, and E_{max}, E_{min} substituted for $|b_3/b_4|$ in (3), (4). The resulting approximations to R, R_c are denoted by primes and given by:

$$R' = \frac{|a-bc|(1-\epsilon)}{1-|c|^2(1-\epsilon)^2} \tag{17}$$

$$R_c' = \frac{|b-ac^*(1-\epsilon)^2|}{1-|c|^2(1-\epsilon)^2}, \tag{18}$$

where $r=1-\epsilon$, and ϵ is usually a small quantity.

The evaluation of the error, e, due to nonzero ϵ, in an efficiency determination using (5), begins with the definition

$$e = \frac{\dfrac{R_1'}{R_2'} - \dfrac{R_1}{R_2}}{\dfrac{R_1}{R_2}}. \tag{19}$$

Substitution of (11), (17) into this result leads to

$$e \simeq 2\epsilon(|c_2|^2 - |c_1|^2) \tag{20}$$

where the subscripts 1, 2, differentiate between the g-reflectometer parameters which obtain at ports 1 and 2 respectively, and only the first order terms have been retained.

If $|c_1|$, $|c_2|$, ϵ were known, their values could be substituted into (20) and e would become a "correction factor" rather than error. As a rule, however, the potential accuracy improvement does not warrant the extra effort this requires. As a general guideline, in the configuration of figure 3, $|c| \simeq |\Gamma_u|$ where Γ_u is a reflection coefficient which is "representative" of the two-port (e.g., adaptor) and the load for which the efficiency is measured. In the configuration of figure 4, $|c|$ is determined by the adjustment of T_y; if this is such as to minimize the amplitude of the oscillatory behavior of $|b_3/b_4|$ in response to the short motion, the foregoing guideline ($|c| \simeq |\Gamma_u|$) is again satisfied.[6]

For an adaptor of VSWR of 1.5, a typical value of $|c|$ is 0.2, while ϵ will ordinarily be less than 0.01. The maximum expected error, due to the nonideal short is thus 0.1 percent over a wide range of practical operating conditions, and the typical error is probably 0.01 percent or less.

To complete this discussion, there will also be an error in the determination of R_{c1}, R_{c2} due to the nonideal short. Ordinarily the error contribution from this source will be one or more magnitudes smaller than that already described and thus negligible.

Thus far, the discussion has implicitly assumed that the same short is used at both terminals 1 and 2. In some applications, the evaluation of a waveguide-coax adaptor for example, this is obviously impossible. In this case, the generalization of (20) is

$$e \simeq (\epsilon_2 - \epsilon_1) + 2(\epsilon_2|c_2|^2 - \epsilon_1|c_1|^2). \tag{21}$$

Here ϵ_1, ϵ_2 are associated with the shorts used at ports 1 and 2 respectively.

It will be immediately recognized that the difference between ϵ_1 and ϵ_2 is now a potential source of substantial error. Fortunately, however, this error can be eliminated. The procedure is to make the measurement by each of the two described procedures (using (5) and (6)).[7] Assuming that the same pair of shorts are used for each of these measurements, it is easily shown that the geometric mean of the two efficiency determinations gives the desired result. Conversely, the square root of the ratio of these measurements gives the ratio between the reflection coefficient magnitudes of the respective plungers.

Returning to the expression for efficiency, it is convenient to write (5) in the form:

$$\eta_{21} = 1 - \frac{R_2 - R_1}{R_2}. \tag{22}$$

This shows that the vertical displacement between R_2 and R_1 (fig. 6) is a direct measure of the *difference* between η_{21} and unity. Typically, this difference is no more than a few percent, and the performance require-

[5] It is not within the scope of this paper to consider the many "pathological" situations which could be invented, e.g., couplers without directivity or reversed in direction, extreme departures from impedance match conditions, etc. Because the mathematical formulation is general enough to include these cases, these additional qualifying statements are required.

[6] Although this guideline should prove adequate for most practical purposes, an "exact" evaluation of c_1, c_2 is not difficult to obtain. In particular, the generator in figures 3 or 4 is replaced by a variable termination which is adjusted such that δ_4 vanishes when the system is excited via port 1 (or 2). The reflection coefficient observed at port 1 (or 2) is now $-c_1$ (or $-c_2$).

[7] This assumes that in the first of the described methods T_z has been adjusted such that "Γ_g" equals the load reflection coefficient for which η_{21} is desired. Moreover, it will be recognized that, during the second measurement, the two ports of the adaptor are reversed, in relation to the g-reflectometer, as compared with their positions during the first measurement.

ments on the associated measurement system are primarily for *resolution* and *stability* rather than "absolute" *accuracy*. For example, a 10% error in either R_2 or in (R_2-R_1) will cause an error of only a few tenths of a percent in η_{21}. Conversely, a system resolution of a part in 10^4 is required if (R_2-R_1) is to be observed with a resolution of one percent, etc.

The role of tuner T_y has been referred to a number of times. Although the operation is, in theory, independent of this adjustment, certain second order error considerations have been noted. In addition, however, is the practical requirement of matching the excursions of $|b_3/b_4|$ to the dynamic range limitations of the $x-y$ recorder. If these excursions are permitted to be large relative to R_2-R_1, the resolution, with which R_2-R_1 is measured, suffers. With a little experience this adjustment is not a difficult task.

Finally, it is of interest to note that the recording provides not only an indication of the joint or other losses, but also an indication of the loss of the transmission line in which the short moves. In many cases, this provides a useful confirmation of the system sensitivity and calibration. Indeed, it is possible to measure the loss in terms of the waveguide attenuation/wavelength without otherwise calibrating the system.

6. Applications

This technique represents a powerful tool for certain measurement problems. An immediate example, already alluded to, is the evaluation of connector loss. In order to gain some insight into the behavior of the Type N connector, a coaxial line was devised with a continuous outer conductor and a slip joint on the inner conductor such as is found in the Type N connector. This joint showed a loss of 0.006 dB at 9 GHz. In another test piece, the center conductor was continuous, while the outer conductor included a replica of the joint found in the Type N. This exhibited a loss of 0.05 dB.[8] The measured loss of a complete "Type N" joint, in which the slots had been deleted from the outer sleeve, was 0.01 dB.

This technique has also found application in the evaluation of certain parameters associated with a cryogenic noise source developed for the Comsat Corporation. In particular the corrected value of the temperature at the output port required both the loss per unit length in the output waveguide, and the loss in a waveguide window. Both of these quantities were easily measured via these methods.

Another use of these methods is in conjunction with the large antenna gain calibration project at the Jet Propulsion Laboratory [6]. Here a loss correction factor is obtained for the 30-40 foot waveguide run between the gain standard horn and the reference plane. The mismatch corrections are also explicitly accounted for with this technique.

7. Summary

The usefulness of the sliding short methods of "attenuation" measurement has been substantially enhanced by application of the first order correction theory, for nonideal short behavior, developed by Almassy [5], and the subsequent extension outlined in this paper.

The microwave art is rapidly approaching the place, if indeed it is not already there, where connector imperfections represent a major barrier to further advances in the accuracy of microwave measurements. Although a great deal of recent effort has been expended in the direction of improved VSWR specifications, the more important parameter, for many applications at least, is the dissipation characteristic. This method should prove a particularly valuable tool in assessing the magnitude of this problem.

The procedure may be implemented in a variety of ways, the major requirement is for a high degree of stability in the measuring system. One such system has been described in some detail by Almassy[9] [5]. At the Jet Propulsion Laboratory, a commercial version of the "precision insertion loss test set" developed at JPL [7] has been adapted for this use.

The existence of this first order correction theory also makes it possible to envision the extension of sliding short methods to much lower frequencies than has previously been feasible. In particular, because the theory explicitly takes account of line loss, it may prove useful to construct the inner and outer conductors in the form of a helix. Another possibility is that of immersing the line in a liquid dielectric.

Finally, the tuning adjustments, called out in this procedure, can be eliminated if a phase detection capability, such as is found in network analyzers, is assumed. Much of the detail for doing this has been worked out, but remains to be implemented.

8. Appendix

The purpose of this appendix is to derive (6).

Referring to figure 4, the relationship between b_3/b_4 and the reflection coefficient, Γ_r, presented at terminal 2 by the two-port and its load, Γ_l, may be written,[10]

$$\frac{b_3}{b_4}=\frac{A\Gamma_r+B}{C\Gamma_r+D} \tag{23}$$

where A, B, C, D are parameters of the g-reflectometer.

In a similar way, the relationship between Γ_r and Γ_l is given by,

$$\Gamma_r=\frac{a\Gamma_l+b}{c\Gamma_l+1} \tag{24}$$

[8] Although the purpose of these measurements was ostensibly that of evaluating the connector design, the real motivation was that of demonstrating the flexibility of the measurement technique. The above result is rather surprising, and may not be actually representative of the general design. In any case, it appears desirable to further pursue this subject.

[9] The "compensation" included in Almassy's system has not been found necessary in these measurements.

[10] The numerator and denominator could obviously be divided by D to obtain better agreement with the functional form of (7). The existing form, however, provides better continuity with earlier work in this area.

where for the moment, Γ_l is assumed to be arbitrary, and a, b, c are parameters of the two-port whose efficiency is required. (Note that this represents a change in terminology from (7).)

The required efficiency is given by [2],

$$\eta_{12}(\Gamma_l) = \frac{|a-bc|(1-|\Gamma_l|^2)}{|1+c\Gamma_l|^2-|a\Gamma_l+b|^2}. \tag{25}$$

By use of (11), (12), and a little algebra, it can be shown that

$$R_2\left(1-\left(\frac{R_{c2}}{R_2}\right)^2\right)=\frac{|A|^2-|B|^2}{|AD-BC|}. \tag{26}$$

To obtain the counterpart expression involving R_1, R_{c1} it is convenient to substitute (24) into (23) which (for an arbitrary Γ_l) yields,

$$\frac{b_3}{b_4}=\frac{(Aa+Bc)\Gamma_l+(Ab+B)}{(Ca+Dc)\Gamma_l+(Cb+D)}. \tag{27}$$

This is in the same form as (23) so,

$$R_1\left(1-\left(\frac{R_{c1}}{R_1}\right)^2\right)$$

$$=\frac{|Aa+Bc|^2-|Ab+B|^2}{|(Aa+Bc)(Cb+D)-(Ab+B)(Ca+Dc)|}. \tag{28}$$

By hypothesis, however, b_3 vanishes when Γ_l represents the load reflection for which the efficiency is desired. Therefore,

$$(Ab+B)=-(Aa+Bc)\Gamma_l, \tag{29}$$

from which,

$$\frac{B}{A}=-\frac{a\Gamma_l+b}{c\Gamma_l+1}. \tag{30}$$

Substitution of this result into (28), (26) leads to,

$$R_1\left(1-\left(\frac{R_{c1}}{R_1}\right)^2\right)$$

$$=\frac{|A|\cdot|a-bc|\cdot(1-|\Gamma_l|^2)}{|1+c\Gamma_l|\cdot|C(a\Gamma_l+b)+D(1+c\Gamma_l)|}, \tag{31}$$

$$R_2\left(1-\left(\frac{R_{c2}}{R_2}\right)^2\right)$$

$$=\frac{|A|\cdot(|1+c\Gamma_l|^2-|a\Gamma_l+b|^2)}{|1+c\Gamma_l|\cdot|C(a\Gamma_l+b)+D(1+c\Gamma_l)|}. \tag{32}$$

Finally, comparison of the ratio of (31) to (32) with (25) yields (6).

9. References

[1] Engen, G. F., Power equations: A new concept in the description and evaluation of microwave systems, IEEE Trans. Instr. Meas. **IM-20,** 49–57 (Feb. 1971).

[2] Engen, G. F., An introduction to the description and evaluation of microwave systems using terminal invariant parameters, Nat. Bur. Stand. (U.S.), Monogr. 112, 26 pages (Oct. 1969).

[3] Cullen, A. L., Measurement of microwave transmission efficiency, Wireless Engineer **26,** 255–258 (Aug. 1949).

[4] Beatty, R. W., Determination of attenuation from impedance measurements, Proc. IRE, **38,** 895–897 (Aug. 1950).

[5] Almassy, G., A first order correction to sliding short behavior with application to the problem of measuring small losses, IEEE Trans. Instr. Meas. **IM-20,** 162–169 (Aug. 1971).

[6] Batelaan, P. D., private communication.

[7] Stelzried, C. T., Reid, M. S., and Petty, S. M., A precision dc potentiometer microwave insertion loss test set, IEEE Trans. Instr. Meas. **IM-15,** 98–104 (Sept. 1966).

(Paper 75C3&4–324)

JOURNAL OF RESEARCH of the National Bureau of Standards—C. Engineering and Instrumentation
Vol. 75C, Nos. 3 and 4, July–December 1971

Accurate Microwave High Power Measurements Using a Cascaded Coupler Method

Kenneth E. Bramall*

Institute for Basic Standards, National Bureau of Standards, Boulder, Colorado 80302

The use of directional couplers to extend the range of low-level power meters is a well established technique. Calibration of bolometer-coupler units up to 20 dB is routine at NBS and other laboratories and allows power measurement to the 1 W level. For higher coupling ratios, however, the problems in calibration using conventional techniques becomes more difficult. This paper describes a cascade method which allows calibration of low power meter-coupler combinations for measurement up to the megawatt range.

The technique is based upon system linearity and the uncertainty limits are shown to be 1 percent to 1.5 percent using NBS low power standards. By using the NBS calibration services and commercially available equipment, the above power levels can be measured with uncertainty limits less than 2.7 percent. The method can also be adapted to measurement of large coupling ratios (20–80 dB).

Results are given for power (200 watts in WR–90 waveguide) and coupling ratio (40 dB coaxial coupler) measurements.

Key words: Accurate; calibration; directional coupler; high power; measurement; microwave.

1. Introduction

High level (above 1 W) microwave CW power measurements are commonly referenced to low-power standards by using a low-level power meter in combination with a power-reducing device such as a directional coupler or attenuator. Although better known and more economical than other methods for measuring high power, use of this method has been limited by uncertainties in relating the high power to the power indicated by the low-level power meter. An improved technique for determining this relationship is the main topic of this paper. The use of the directional coupler is emphasized, but the basic ideas presented will also apply to other attenuating or coupling devices.

2. Cascaded Feed-Through Power Meter Calibration Technique

The basic principles of the new calibration technique are described by discussing the calibration of a 40 dB coupler in combination with a low-level sidearm power meter having a dynamic range of 20 dB (0.1 to 10 mW).

It has been shown that the best accuracy is obtained by calibrating the sidearm power meter and the coupler as a unit [1].[1] This requires a measurement of the coupler output power while a reading is obtained on its sidearm power meter. If a standard power meter is available for measuring power in the range of 1 to 100 W (the power needed to obtain a reading within the range of the sidearm power meter) the calibration can be readily achieved. For the sake of explaining the technique, however, the calibration is to be achieved using a 10 mW standard power meter.

The calibration procedure employs an auxiliary 20 dB coupler and sidearm power meter with a dynamic range of 20 dB (0.1 to 10 mW) to transfer the calibration from the 10 mW standard power meter to the 40 dB coupler unit. Before starting the calibration, the 20 dB coupler is connected to the 40 dB coupler as shown in figure 1. At first glance, it appears that two coupler type, feed-through powermeters are in series. However, an alternate interpretation is also possible. In particular, the 40 dB coupler can be regarded as an extension of the main arm of the 20 dB coupler so that terminal

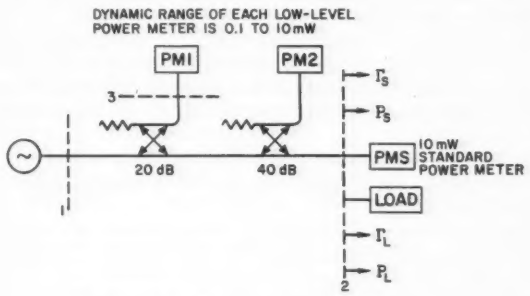

FIGURE 1. *Basic cascaded coupler system.*

*Electromagnetics Division, Power-Current-Voltage Standards, National Bureau of Standards, Boulder, Colo. 80302.

[1] Figures in brackets indicate the literature references at the end of this paper.

surface 2 serves a dual role; it is the output port of both the 20 and 40 dB couplers.

The 20 dB coupler unit (containing the 40 dB coupler unit) is calibrated by obtaining simultaneous readings on its sidearm power meter (PM1) and on the 10 mW standard power meter connected to terminal surface 2. If the standard power meter is now removed and replaced by a high power load (and for the present it will be assumed that their impedances are equal) the 20 dB coupler unit will permit measurements of the load power in the range of 10 mW to 1 W. The only requirement is that the component parameters be linear, i.e., independent of power level.

As the 1 W level is approached, the indicator on the 20 dB coupler reaches the upper limit of its dynamic range (10 mW) and the indicator on the 40 dB coupler comes into the lower region of its dynamic range (0.1 mW). Since the load power can be accurately predicted from the power meter on the sidearm of the 20 dB coupler, the 40 dB coupler unit is calibrated by obtaining simultaneous readings on the two sidearm power meters. The calibration is thus transferred from the 20 to the 40 dB coupler unit without introducing uncertainties associated with mismatch, with flange losses, or with losses occurring within the couplers. Following this calibration, the input power can be further increased another 20 dB and load powers in the range of 1 to 100 W determined by the 40 dB coupler-sidearm power meter unit. Again, the components must be linear.

As a practical matter, the power meter on the sidearm of the 20 dB coupler may be damaged by excessive power when the load power is increased beyond 1 W. This power meter overload problem is simply avoided by removing the 20 dB coupler after the 40 dB coupler unit is calibrated. The calibration of the 40 dB coupler unit is not affected by doing this because a directional coupler, like other three-port devices, has the property that the power split between the main and sidearms is independent of the source characteristics (see appendix).

The method described in the previous paragraphs can obviously be extended to systems employing any number of cascaded couplers. For example, figure 2 shows four coupler units where the calibration procedure is as follows:

1. Adjust power input so both PM1 and PMS are within their dynamic ranges.
2. Obtain simultaneous readings of PM1 and PMS.
3. Replace PMS with the high power load.
4. Increase power until PM2 is in its operating range (but upper limit of PM1 is not exceeded).
5. Obtain simultaneous readings of PM1 and PM2.
6. Remove PM1 and the 20 dB coupler from the system.
7. Increase power until PM3 is in its operating range (but upper limit of PM2 is not exceeded).[2]

[2] Since coupler 1 was removed from the system, PM1 may be transferred to coupler 3. Likewise PM2 may be transferred to coupler 4. Thus, only two power meters are required for any number of cascaded couplers. Although errors may be introduced by this procedure, they are negligible for couplers having large coupling coefficients. For couplers having small coupling coefficients, the error can be made negligibly small by using load isolators on their sidearms or by initially terminating the sidearms with loads having reflection coefficients approximately equal to the sidearm power meters.

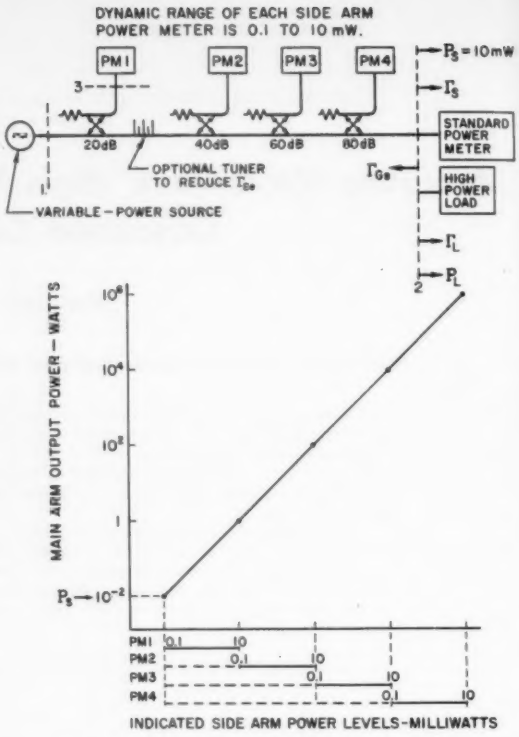

FIGURE 2. *Cascaded coupler system used to calibrate an 80 dB coupler-power meter combination.*

8. Obtain simultaneous readings of PM2 and PM3.
9. Remove PM2 and the 40 dB coupler from the system.
10. Increase power until PM4 is in its operating range (but upper limit of PM3 is not exceeded).
11. Obtain simultaneous readings of PM3 and PM4.
12. Remove PM3 and the 60 dB coupler from the system.
13. Measure power in the range 10^4 to 10^6 W.

By following the steps above, the 80 dB coupler and its sidearm power meter are calibrated as a unit and the load power is given by the expression

$$P_L = \frac{P_1'}{P_1}\frac{P_2'}{P_2}\frac{P_3'}{P_3}\frac{P_4'}{P_4}P_s \qquad (1)$$

where P_n is the reading of the nth side arm power meter when a calibration was effected and P_n' is the reading of this power meter when it measured the load power. The reading of the standard power meter is P_s. This expression for the load power, P_L, is exact when the standard power meter and the load impedances are equal. The effects of dissimilar impedances will be considered next.

When the standard meter and the load impedances are not equal, mismatch is introduced when the former is exchanged for the latter. This is the only impedance

mismatch introduced, however, because the same load is used for the remainder of the calibration procedure. The impedance mismatch introduced with the cascaded system is basically the same as for a single coupler unit and can be handled using existing techniques.

Engen [1] has shown that the load power determined by a single calibrated coupler unit is given by the expression

$$P_L = \frac{P_1'}{P_1} P_s \frac{1-|\Gamma_L|^2}{1-|\Gamma_s|^2} \left|\frac{1-\Gamma_{GE}\Gamma_s}{1-\Gamma_{GE}\Gamma_L}\right|^2 \qquad (2)$$

where P_1 is the reading of the side arm power meter when the unit was calibrated with a standard power meter whose reading was P_s. The reading P_1' of the side arm power meter determines the power delivered to the load after it replaces the standard meter. The reflection coefficients of the standard meter and the load are given, respectively, by Γ_s and Γ_L. The factor Γ_{GE} is defined by Engen [2] as the equivalent generator reflection coefficient which the coupler provides, and its measurement is discussed in the referenced paper. This coefficient is given in terms of the coupler's scattering coefficients as

$$\Gamma_{GE} = S_{22} - \frac{S_{21}S_{32}}{S_{31}} \qquad (3)$$

when the reference planes are chosen so that the source is connected to port 1, the output of the coupler main arm is port 2 and the sidearm is port 3.

Similarly, an equivalent generator reflection coefficient Γ_{GE} can be defined for the first feed-through power meter in the cascaded coupler system with reference planes as indicated in figure 2. By doing this and comparing the expression for the load power given in eq (1) with eq (2), eq (1) can be modified to include the effects of impedance mismatch. The results are:

$$P_L = \frac{P_1'}{P_1}\frac{P_2'}{P_2}\frac{P_3'}{P_3}\frac{P_4'}{P_4} P_S \frac{1-|\Gamma_L|^2}{1-|\Gamma_S|^2}\left|\frac{1-\Gamma_{GE}\Gamma_S}{1-\Gamma_{GE}\Gamma_L}\right|^2. \qquad (4)$$

Only the Γ_{GE} of the first feed-through power meter appears in eq (4), although an equivalent generator reflection coefficient can also be defined for each of the other feed-through power meters in the cascaded system. Unlike the first feed-through power meter, the others measure the power delivered to the same load that terminates their output when they are calibrated. As a result the power measurement is not affected by their equivalent generator reflection coefficients. They need not be known unless, as discussed below, the load is exchanged for another after the calibration is complete. The Γ_{GE} of the first feed-through power meter must be known, however, in order to evaluate the mismatch error in eq (4). This requires that Γ_{GE} be measured before the calibration begins and the system is disassembled.

In addition to giving a method for measuring Γ_{GE} in the above reference, Engen showed that it is possible to reduce the value of Γ_{GE} for a single coupler by using a tuner in the output arm. A tuner can also be incorporated into the cascaded system and used to reduce the value of Γ_{GE} that exists when the load replaces the standard meter. The tuner can be added anywhere between the first coupler and the output port. There is an advantage, however, in locating it between the first and second couplers. After the calibration is transferred to the second coupler, the tuner becomes part of the source for this coupler. Thus the tuner can be removed with the first coupler, eliminating the need for a tuner that will operate at high power levels.

An alternative method for measuring and reducing Γ_{GE} is provided by employing the first coupler as part of a reflectometer [3, 4]. When this reflectometer is tuned with respect to the output port, Γ_{GE} is made small and a method is provided for measuring the reflection coefficient magnitudes of the standard meter and the load. Again, as with the single tuner, the added reflectometer components can be removed with the first coupler. More details about this method are given later with the experimental results.

The high power load can be exchanged for another after the calibration is complete. However, another mismatch error will be introduced. Specifically, if after the last coupler has been calibrated using a particular load, another load with a reflection coefficient Γ_{L2} is substituted, the expression for the power delivered to this second load is

$$P_{L2} = \frac{P_1'}{P_1}\frac{P_2'}{P_2}\frac{P_3'}{P_3}\frac{P_4'}{P_4} P_s \frac{1-|\Gamma_{L2}|^2}{1-|\Gamma_s|^2}\left|\frac{1-\Gamma_{GE}\Gamma_s}{1-\Gamma_{GE}\Gamma_L}\right|^2 \left|\frac{1-\Gamma_{GE}'\Gamma_L}{1-\Gamma_{GE}'\Gamma_{L2}}\right|^2 \qquad (5)$$

where Γ_{GE}' is the equivalent generator reflection coefficient associated with the last coupler, and the other terms are as previously defined. Evaluation of the additional mismatch error in eq (5) requires additional measurements to determine Γ_{GE}' and Γ_{L2}.

3. Application to Attenuation Measurements

The calibration technique as described provides a method for accurately determining the power delivered to a particular high power load. The technique does this by using several power meters with limited dynamic ranges to produce the same results as would be obtained using one power meter with a large dynamic range. This characteristic also makes the technique useful for other applications such as evaluating the linearity of detectors with large dynamic ranges or for measuring attenuation using the power ratio method of measurement.

The power ratio method for measuring attenuation requires measurements of the input and output powers of a two-port device. This method has been shown to be capable of high accuracy when using bolometric power meters for attenuation measurements up to 20 or 30 dB [5]. A wider range of attenuation can now be measured using a cascaded coupler system, since it permits a wider range of input power levels

to be measured. For best accuracy, the output power can be measured with the same standard power meter used to calibrate the cascaded coupler system. The maximum attenuation that can be measured is limited, of course, by the component's ability to withstand the high power. This limitation, for several measurements, is not as severe as it may seen. For example, by using power meters with dynamic ranges of 0.1 to 10 mW, 40 dB of attenuation can be measured with a source of 1 W, 50 dB with a source of 10 W, and 60 dB with a source of 100 W. Several components including directional couplers can tolerate these (and higher) power levels.

The measurement of a coupler coupling coefficient is an attenuation measurement between the input and the side arm when the output is terminated in a nonreflecting load. An 80 dB coupler, for example, requires an input power level of 10 kw in order to obtain a reading of 0.1 milliwatt at the side arm. A measurement of this input power is provided by using a cascaded system of 20, 40, and 60 dB coupler units. Using this system and computing the coupling coefficient yields

$$K = 10 \operatorname{Log}_{10} \frac{P_1'}{P_1}\frac{P_2'}{P_2}\frac{P_3'}{P_3}\frac{P_s}{P_{s2}}\left|\frac{1-\Gamma_{GE}\Gamma_s}{1-\Gamma_{GE}\Gamma_C}\right|^2 \frac{1}{|1-S_{33}\Gamma_s|^2} \quad (6)$$

where S_{mn} are the scattering coefficients of the coupler and Γ_C is the reflection coefficient at the input to the coupler with the nonreflecting high power load and standard power meter connected. The expression for this reflection coefficient is

$$\Gamma_c = S_{11} + \frac{S_{13}S_{31}\Gamma_s}{1-S_{33}\Gamma_s} \quad (7)$$

Note that since the ratio of P_s/P_{s2} is taken, where P_{s2} is the side arm power reading obtained with the standard meter, a calibrated standard power meter is not required for these measurements. Consequently, this meter can be incorporated with a tuner to obtain $\Gamma_s \simeq 0$ and reduce the mismatch error introduced. The advantage of tuning $\Gamma_{GE} \simeq 0$ at the low power level is apparent.

4. Alternate Calibration Method

The system shown in figure 3, is an alternate calibration method which uses attenuators between the coupler sidearms and the power meters. Compared with the purely cascaded system, it is physically shorter and the power ratio calibration steps can have any value if the attenuators (A_1 and A_2) are continuously variable. The utility of this method is that it allows couplers having relatively low coupling ratios to be transformed into ones having the equivalent of high coupling ratios. For example, a 40 dB coupler can be transformed to the equivalent of a 60 or 80 dB coupler.

The calibration procedure for this system is similar to that for the purely cascaded system, the difference being that the calibration is transferred back and forth between power meters 1 and 2 as the power level

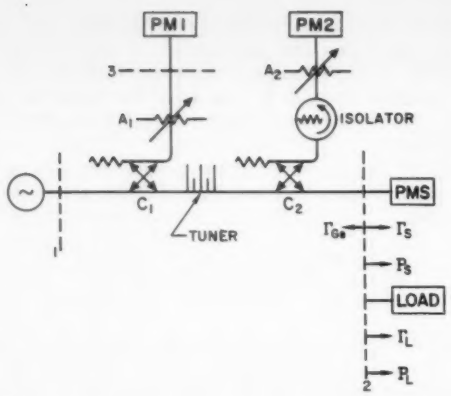

FIGURE 3. *Variation of the cascaded coupler calibration technique.* The attenuators are alternately used to reduce the coupling to one power meter while the other retains the calibration.

is increased. The attenuators are alternately used to reduce the coupling to one power meter while the other retains the calibration.

The first coupler unit can be considered as part of the source for the second unit and the setting of attenuator A_1 can be changed without introducing an error when the calibration is referenced to power meter 2. When the calibration is referred to power meter 1, however, a change in the setting of attenuator A_2 can introduce an error, because the amount of power reflected back into the system may change which in turn can change the relation between the first sidearm power meter reading and the load power. This error can be made negligibly small by using an isolator as shown in figure 3. The other errors associated with this calibration scheme are the same as for the strictly cascaded coupler system.

A tuner for reducing Γ_{GE} can be inserted between the couplers. It can be removed after the calibration is first transferred to power meter 2 and an error will not be introduced when the calibration is transferred back to power meter 1. Similarly, a reflectometer can be used to reduce and evaluate the mismatch error introduced at arm 2.

5. Experimental Systems and Results

A WR–90 waveguide coupler system was assembled in the laboratory to obtain experimental data. The system incorporated a reflectometer and provided the capability of obtaining two separate calibrations of the last low power meter-coupler unit. This system is shown in figure 4. One calibration for the 40 dB coupler unit was obtained by using couplers 1 through 4 to provide 10 dB power ratio calibration steps. The other calibration was obtained by using couplers 2 and 4 to provide power ratios of 20 dB. The two calibrations disagreed by no more than 0.11 percent which indicates the precision of the method.

No unusual problems were encountered or unpredicted results obtained in performing the double

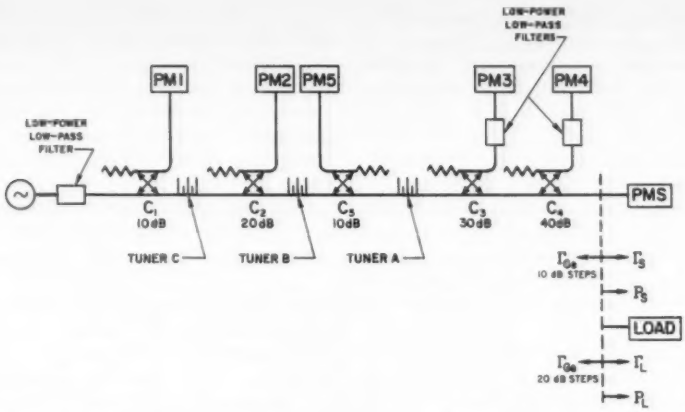

FIGURE 4. *A coupler system that incorporates a reflectometer and provides the capability of obtaining two separate calibrations of the 40 dB coupler.*

calibration. Intercomparison power measurements were made at the 70 to 200 W level between the 40 dB coupler unit and a stirred-water calorimeter [6]. The disagreement was around 1 percent, well within the combined error limit for the two meters.

In the tuning procedure for this system, tuner A was first adjusted so that the coupler sampling the reflected power (coupler 5) would have near infinite directivity. Tuner B was then adjusted to obtain $\Gamma_{GE} \simeq 0$ for the system using power ratios of 20 dB. Finally, tuner C was adjusted to obtain $\Gamma_{GE} \simeq 0$ for the system using power ratios of 10 dB. All of the tuning was done with respect to the output of the system by using well known tuning procedures [3, 4]. The tuning operation was performed by sliding high and low calibrated reflecting loads within a waveguide section attached as part of the coupler system. The low reflection load was used as the reflection coefficient standard. By using this approach, the reflectometer measured the combined reflection coefficient of the load and flange at the output of the system.

The reflectometer, the first two couplers, the three tuners, and the low-power low-pass filter in the main line were removed when the calibration was transferred to couplers 3 and 4.

A second system using coaxial components was assembled to measure the output to sidearm power ratios of a set of 5 coaxial couplers having nominal coupling values of 12, 20, 23, 30, and 40 dB. These are slot type, quarter wave precision couplers as described by Hudson [7] and have 50 dB directivity and maximum VSWR of 1.02 at all ports. Their center frequency is 1.45 GHz and measurements were made at frequencies in the range 1 to 2 GHz. For the lower value couplers (up to 20 dB), the output-to-sidearm power ratio was measured directly using standard bolometric power meters (VSWR < 1.03). The cascade system was used to measure the higher value couplers, and because VSWR of the ports is low, tuners were not required to reduce the value of Γ_{GE}. The limit of uncertainty in the measurement of the 40 dB coupler was computed to be 0.8 percent (0.035 dB) which includes the effects of impedance mismatch, repeatability, etc. The 40 dB coupler was also measured using the NBS coaxial calorimeter [8] and a standard bolometric power meter. The two measured power ratio values differed less than 1 percent.

6. Errors

The limit of uncertainty in a high power measurement, using the cascade system, depends primarily upon the uncertainties introduced by the reflection coefficients and by the low level standard and side arm power meters. Since bolometric power meters conveniently yield accurate measurements in the 0.1 to 10 mW range, they are used in the following discussion to demonstrate the accuracy obtainable.

There are at least two methods available for obtaining less than 0.1 percent for the uncertainty introduced by the reflection coefficients. In one, the uncertainty is eliminated, in principle, by adjusting the reflection coefficients of the standard meter and the high power load to be equal. In the other method, the uncertainty is reduced by using a tuner to obtain a small, near zero, equivalent generator reflection coefficient and then correcting the measured power using the measured reflection coefficient magnitudes of the standard meter and the load.

The limit of uncertainty associated with the measurement of P_s results primarily from the uncertainty in the bolometer mount effective efficiency and from the uncertainty in the measurement of the bolometrically substituted dc power. The National Bureau of Standards presently provides routine effective efficiency calibrations with limit of uncertainty of 1 percent for waveguide bolometer units [9]. The uncertainty can be as low as 0.2 percent, however, for a WR–90 waveguide mount calibrated against the NBS microcalorimeter [10].

Self-balancing bolometer bridges have been developed that enable a measurement of the substituted dc power to be made with an uncertainty of 0.09 percent $+0.1\ \mu$W [11]. This corresponds to uncertainties

of 0.09, 0.1, and 0.19 percent in measurements of 10, 1 and 0.1 mW, respectively.

In a power ratio measurement, some of the systematic errors, such as those resulting from the bolometer mount reflection coefficient and its effective efficiency, cancel. The only uncertainties that need to be evaluated are those associated with the measurements of the bolometrically substituted dc powers. By using the bolometer bridge mentioned above, power ratios of 10 and 100 can be measured with uncertainties of 0.19 and 0.28 percent, respectively.

The uncertainty in a high power measurement is the sum of the uncertainties introduced by the standard power measurement, by the mismatch error, and by the uncertainties introduced in the power ratio measurements. Table 1 shows an example breakdown of these uncertainties.

The power ratio uncertainties in table 1 can be re-

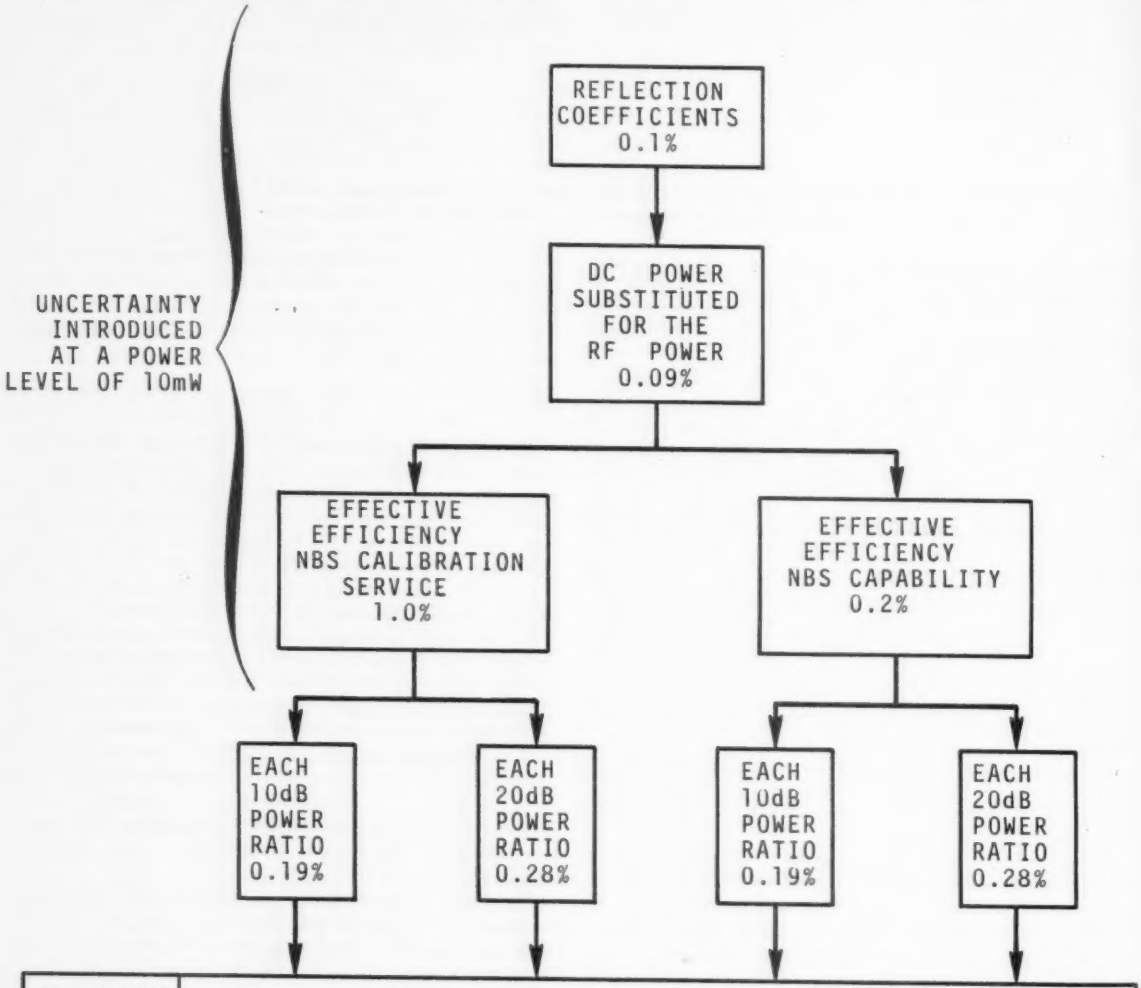
UNCERTAINTY INTRODUCED AT A POWER LEVEL OF 10mW
REFLECTION COEFFICIENTS 0.1%
DC POWER SUBSTITUTED FOR THE RF POWER 0.09%
EFFECTIVE EFFICIENCY NBS CALIBRATION SERVICE 1.0%
EFFECTIVE EFFICIENCY NBS CAPABILITY 0.2%
EACH 10dB POWER RATIO 0.19%
EACH 20dB POWER RATIO 0.28%
EACH 10dB POWER RATIO 0.19%
EACH 20dB POWER RATIO 0.28%

RF POWER LEVEL	TOTAL UNCERTAINTY IN A HIGH POWER MEASUREMENT (%)			
100W	1.95	1.75	1.15	0.95
10kW	2.33	2.03	1.53	1.23
1MW	2.71	2.31	1.91	1.51

TABLE 1. *Examples showing the uncertainty limit obtainable in a high power measurement by using the cascaded coupler calibration technique and equipment that is available commercially.*

duced by the use of the same bolometer bridge and accessory instrumentation in measuring the numerator and denominator powers. The amount of reduction will, in part, depend upon the systematic error common to both measurements.

Other sources of error that need to be considered in practice include rf power instability and the effects of bolometer mount temperature changes. Because the calibration is performed by making simultaneous power measurements, only short term stabilities are important, and the exacting power and temperature stability requirements are reduced.

The output from some high-power sources may contain large harmonic components. Since the coupling for the harmonic power is generally not the same as for the fundamental power, this can be a source of error. This error is easily reduced by incorporating low-power, low-pass filters with the power meters, as shown, for example, in figure 4.

In general, the calibration technique is based upon the assumption that the system is linear. The parameters of all the components used in the system must be independent of the rf power level and any other variable, such as environmental temperature, that may affect the linearity. The linearity of all the components except the directional couplers can be easily measured, since they operate at low power levels. The linearity of a coupler unit, however, must be measured at high power levels. Since this measurement requires a high power meter, another coupler unit can be used. In this way the power linearity of different types of couplers can be compared by comparing the side arm power readings as the power level is changed. With several comparisons any nonlinear components can be detected.

7. Summary

Accurate measurements of microwave power at high CW levels can be accomplished using the cascaded feed-through power meter calibration technique. The accuracy is based upon existing low-level standards, system linearity, and the ability to accurately measure power ratios. The technique can be used at any frequency in the rf spectrum where directional couplers (or other suitable 3-port devices), low-level power meters, and low-level power standards are available. (See fig. 5.)

Alternative systems, which employ directional couplers and attenuators, provide an additional flexibility in the calibration of coupler-low-power-meter units. The use of feed-through devices other than directional couplers may be advantageous, especially at the lower frequencies where the waveguide components are large. Since absolute power measurements are not required for measuring power ratios, detectors other than power meters, such as a precision variable attenuator and detector combination or an IF detector, are possible alternatives. Both of these detectors, however, may be subject to additional errors cuased by impedance changes.

Large values of attenuation or coupling ratio can be accurately measured using the cascade technique, provided the components can withstand the high power required.

The author expresses his appreciation to Lyman Elwell for his encouragement and suggestions in this work and to Glenn Engen for his valuable criticism in the preparation of this report. Credit is due to Lloyd Hendricks and Edward Andrusko for their efforts in obtaining the calorimeter-coupler intercomparison measurements.

The development of this technique was supported by the Advanced Research Projects Agency under Project DEFENDER and was monitored by M. I. Witow under ARPA Order No. 515.

8. Appendix

The calibration technique uses one calibrated feed-through power meter to calibrate another, and since a feed-through power meter has an input and two outputs, the theory for 3-port junctions is applicable. The ratio of the powers at ports 2 and 3 of any linear 3-port junction, with a source connected to port 1 as shown in figure 5, is given by [12]

$$\frac{P_2}{P_3}=\left|\frac{S_{21}}{S_{31}}\right|^2\frac{1-|\Gamma_2|^2}{1-|\Gamma_3|^2}\left|\frac{1-\left(S_{33}-\frac{S_{31}S_{23}}{S_{21}}\right)\Gamma_3}{1-\left(S_{22}-\frac{S_{21}S_{32}}{S_{31}}\right)\Gamma_2}\right|^2 \quad (8)$$

where S_{MN} are the scattering coefficients of the junction, and Γ_2 and Γ_3 are the reflection coefficients of the loads at ports 2 and 3.

The expression shows that the ratio of P_2 to P_3 is independent of the source reflection coefficient, Γ_G. For a linear system, the reflection and scattering coefficients are not a function of the power level and the ratio is independent of the source amplitude. In general, the ratio, or the calibration of a feed-through power meter, is independent of the source characteristics, and an error is not introduced by changing the source at port 1.

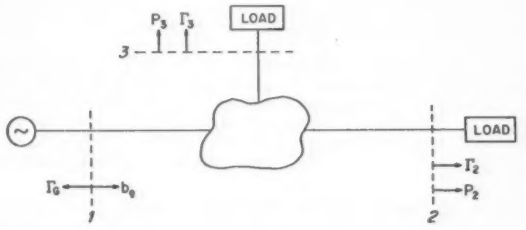

FIGURE 5. *A generalized 3-port junction.*

9. References

[1] Engen, G. F., Recent developments in the field of microwave power measurements at the National Bureau of Standards, IRE Trans. on Instrumentation, vol. **I-7**, pp. 304–306, December 1958.

[2] Engen, G. F., Amplitude stabilization of a microwave signal source, IRE Trans. on Microwave Theory and Techniques, vol. **MTT-6**, pp. 202–206, April 1958.

[3] Engen, G. F., and Beatty, R. W., Microwave reflectometer techniques, IRE Trans. on Microwave Theory and Techniques, vol. **MTT-7**, pp. 351–355, July 1959.

[4] Anson, W. J., A guide to the use of the modified reflectometer technique of VSWR measurement, J. Research NBS, vol. **65C**, pp. 217–223, October–December 1961.

[5] Engen, G. F., and Beatty, R. W., Microwave attenuation measurements with accuracies from 0.0001 to 0.06 decibels over a range of 0.01 to 50 decibels, J. Res. NBS, **64C**, pp. 139–145, April–June 1960.

[6] Hendricks, L. J., A stirred-water calorimeter for the measurement of microwave power, to be published.

[7] Hudson, P. A., A high directivity, broadband coaxial coupler, IEEE Trans. on Microwave Theory and Techniques, vol. **MTT-14**, pp. 293–294, 1966.

[8] Crawford, M. L., and Hudson, P. A., A dual-load flow calorimeter for RF power measurements to 4 GHz, J. Research NBS, vol. **71C**, no. 2, pp. 111–117, April–June 1967.

[9] Rumfelt, A. Y., and Elwell, L. B., Radio frequency power measurements, Proc. IEEE, vol. **55**, no. 6, pp. 837–850, June 1967.

[10] Engen, G. F., A refined X-band microwave microcalorimeter, J. Research NBS, vol. **63C**, pp. 77–82, July–September 1959.

[11] Engen, G. F., A self-balancing direct-current bridge for accurate bolometric power measurements, J. Research NBS, vol. **59**, pp. 101–105, August 1957.

[12] Beatty, R. W., and Macpherson, A. C., Mismatch errors in microwave power measurements, Proc. IRE, vol. **41**, pp. 1112–1119, September 1953.

[13] Kerns, D. M., and Beatty, R. W., Basic theory of waveguide junctions and introductory microwave network analysis, New York: Pergamon, 1967.

(Paper 75C3&4–325)

JOURNAL OF RESEARCH of the National Bureau of Standards—C. Engineering and Instrumentation
Vol. 75C, Nos. 3 and 4, July–December 1971

Publications of the National Bureau of Standards*

Selected Abstracts

Ahearn, A. J., **Quantitative analysis of solids by spark source mass spectrometry,** *(Proc. Intern. Conf. on Mass Spectroscopy, Kyoto, Japan, Sept. 6–13, 1969), Chapter in Recent Development in Mass Spectroscopy, K. Ogata and T. Hayakawa, Ed., pp. 150–157 (University of Tokyo Press, Tokyo, Japan, 1970).*

Key words: Fluctuations; homogeneity; ion sensitive emulsion; mass spectrometry; precision; quantitative analysis; solids; spark source; trace elements.

In spark source mass spectrometry, the ion sample generally misrepresents the solid sample. Consequently, standard reference materials are needed for direct comparison with the unknown or for the determination of correction factors. The precision in measurement of matrix element ions, trace element ions and their ratio is dependent on the homogeneity of the ion sensitive emulsion used. Methods for testing emulsion uniformity and results on Q2 plates are presented. In some the nonuniformity is less than 5%; in others up to a 60% change in 8 cm has been detected. Under optimum conditions, matrix ions are measured with an RSD $\leq 5\%$ but with trace ions this precision is usually poorer. This means that the trace element contents of the recorded ion sample fluctuate. The trace ions in a spark source ion sample from NBS SRM Platinum 681 fluctuate but not independently. Ion microprobe and other tests should indicate whether the observed fluctuations arise in solid sample inhomogeneities or in fluctuations in the production and/or transmission of trace ions in SSMS.

Almer, H. E., **Methods of calibrating weights for piston gages,** *Nat. Bur. Stand. (U.S.), Tech. Note 577, 54 pages (May 1971) 55 cents, SD Catalog No. C13.46:577.*

Key words: Balance; buoyancy; calibration; standards; substitution weighing; transposition weighing; true mass; uncertainty; value.

Generally weights for piston gages have odd denominations that are often not readily calibrated by intercomparison methods. Therefore, these weights are frequently calibrated by direct comparison methods. This paper presents direct comparison methods for calibrating piston gage weights for use with both equal-arm balances and single-pan balances. Methods of estimating the uncertainty of the values obtained are given. Also included are methods of checking for blunders or gross errors.

Baker, M. A., **Study of the adherence of porcelain enamel to aluminum-use of the electron microscope and electron microprobe,** *Proc. Porcelain Enamel Institute Technical Forum, University of Illinois, Urbana, Ill., Oct. 7–9, 1970, 32, 48–51 (Porcelain Enamel Institute, Washington, D.C., 1971).*

Key words: Adherence; aluminum; electron microprobe; electron microscope; interaction zone.

The interfacial zone between porcelain enamel and aluminum has been examined with the electron microprobe and the electron microscope to gain insight into the mechanism of adherence of the porcelain enamel to aluminum. The results obtained indicate that good adherence may be associated with an interaction between the enamel and the aluminum.

Ballard, D. B., Yakowitz, H., Goldstein, J. I., **Study of metal in the lunar soil,** *Proc. 4th Annual Scanning Electron Microscope Symp., ITT Research Institute, Chicago, Ill., April 29, 1971 Part 1, 169–176 (April 29, 1971).*

Key words: (U) Lunar soil; (U) metal inclusions; (U) meteorite; (U) microstructure; (U) SEM.

Metal particles and metallic inclusions in lunar (Apollo 11 and 12) soil particles were investigated using a SEM with a solid state detector. Many of the Metallic particles were coated with lunar material and had impact craters on the surface. The SEM was used specifically to identify the type of lunar material in the craters and the exposed dendrites on the surface. In several metal particles slip bands indicating plastic deformation were observed.
Several glassy spherules in the Apollo 11 soil were studied because the surfaces contained metal particles. Metal (Fe-Ni-Co), as identified with the solid state detector, was spread on the surface presumably as a result of the same impact event which produced the spherule. Other impacts may have formed the craters on the surface. Several nonmetallic soil particles were sectioned and metallographically polished. Metallic inclusions in these soil particles are small, $< 100\ \mu m$ in their largest dimension. The SEM was employed to study the microstructure of these inclusions. Evidence of various degrees of shock damage in the metal was obtained. Most of these inclusions were also analyzed chemically using the electron probe microanalyzer.

Beaker, D. A., LaFleur, P. D., **Production and certification of NBS biological standard reference Materials,** *Proc. 4th Annual Conf. on Trace Substances in Environmental Health, June 1970, pp. 433–435 (University of Missouri, Columbia, Mo., March 1971).*

Kew words: Biological standards; blood standard; botanical standards; environmental samples; standard reference material; tissue standard; trace analysis.

The use of adequate standards is important in the trace element analyses of complex biological materials comprising many environmental and biomedical samples. Available biological materials for interlaboratory comparisons are almost exclusively "round-robin" type samples, and have failed to provide a well-characterized widely distributed and easily available standard. The NBS Office of Standard Reference Materials is in the process of acquiring, analyzing and certifying a series of biological standards. These standards, when issued, will include six botanical standards, a blood standard and a tissue standard.

Bell, F. C., Wollin, H. F., Editors, **Report of the 55th National Conference on Weights and Measures 1970,** *Nat. Bur. Stand. (U.S.), Spec. Publ. 342, 315 pages (April 1971) $1.75, SD Catalog No. C13.6/3:342.*

Key words: Conference, weights and measures—laws; weights and measures—regulations; weights and measures—technical requirements; weights and measures—history; weights and measures.

This is a report of the proceedings (edited) of the Fifty-fifth National Conference on Weights and Measures, sponsored by the National Bureau of Standards, held in Salt Lake City, Utah, July 13–17, 1970, and attended by state, county, and city weights and measures officials and representatives of the Federal Government, business, industry, railroads, and associations.

Bennett, H. S., **Absorbing centers in laser materials,** *J. Appl. Phys.* **42,** *No. 2, 619–630 (Feb. 1971).*

Key words: Antimony; heat conduction; laser materials; Nd-doped glass; platinum; stress components; and thermoelastic theory.

448-719 OL - 72 - 4

One of the severe problems encountered in high-power-solid-state laser systems is the thermal damage to laser rods and optical elements arising from metallic or dielectric inclusions; i.e., impurities with physical and optical properties which differ substantially from those of the host material. Such inclusions may absorb an appreciable amount of the incident radiation and thereby may produce major stresses within the host material. In this paper, the dependence of the maximum value of the tensile stress upon the size of the inclusion and upon the physical properties of the host is examined. The feasibility of using optical techniques to detect metallic and dielectric inclusions in laser materials before they cause damage also is studied. The computations suggest that the use of laser pulse widths of the order of microseconds or longer may be more promising for the detection of small incipient absorbing centers than the use of nanosecond pulse widths.

Bennett, L. H., Swartzendruber, L. J., **Interactions between small magnetic clusters in copper-rich Cu-Ni-Fe alloys,** *J. Appl. Phys.* **42,** *No. 4, 1547–1548 (March 15, 1971).*

Key words: Alloys; clustering; copper; iron; local moments; Mössbauer effect; nickel.

Traces of iron in "nonmagnetic" Cu-rich Cu-Ni alloys produce small magnetic clusters largely limited to an Fe site and its Ni nearest neighbors, as observed in Mössbauer *source* experiments. The present work concerns ^{57} Fe Mössbauer *absorber* data for higher Fe concentrations (¼%–3%), in the 10%–30% Ni range, which demonstrates the existence of a magnetic-moment distribution centered about *two* distinct moment values. For the lower Fe concentrations, the smaller and more abundant of these moments is identical to that observed in the source experiments and is associated with isolated small Fe-Ni clusters. The other moment is about twice as large and can be ascribed to coupled pairs of these small clusters. These results are almost free of effects of metallurgical clustering. By appropriate heat treatment, clustered samples are obtained with different moment distributions and higher Curie temperatures.

Boyd, M. E., Mountain, R. D., **Methods for determining the second virial coefficient of a gas from speed-of-sound data,** *Phys. Rev. A.* **2,** *No. 5, 2164–2167 (November 1970).*

Key words: Acoustic thermometry; equation of state; equilibrium gas properties; helium; second virial coefficient; speed of sound in gases.

Two methods of analyzing data on speed of sound in gases to obtain the second virial coefficient $B(T)$ are compared. The older method, which assumes a form for the temperature dependence of B, is shown to correspond to finding an exact solution to an approximate differential equation for B, while a method recently proposed by Bruch solves the exact equation, but in an approximate manner. Examination of the errors in each method indicates that the first method is preferable.

Boyne, H. S., **Laser frequency stabilization techniques and applications,** *Proc. 24th Annual Frequency Control Symp., on Frequency Control, Atlantic City, N.J., April 27–29, 1970, pp. 233–339 (U.S. Army Electronics Command, Fort Monmouth, N.J., 1970), IEEE Trans. Instr. Meas.* **IM–20,** *No. 1, 19–22 (Feb. 1971).*

Key words: Frequency; laser; laser frequency measurement; stabilization; techniques; time standard.

A review of progress in laser stabilization techniques and laser frequency measurement is given. Methods for relating laser frequencies to the time standard and methods for absolute laser frequency stabilization are described. Experimental information on reproducibility and noise characteristics is reported. Application to frequency and wavelength standards is discussed.

Boyne, H. S., Hall, J. L., Barger, R. L., Bender, P. L., Ward, J., Levine, J., Faller, J., **Absolute strain measurements with a 30 meter vacuum interferometer,** *Proc. Conf. Laser Applications in the Geoscience, Huntington Beach, Calif., June 1969, pp. 215–225 (1970).*

Key words: Earth strain; earth tide; geophysics; laser strainmeter; seismograph.

We present details on the design and performance of a 30 meter interferometric strain gauge. We also discuss a practical method for recording absolute earth strain measurements by comparing length changes in the interferometer with an absolute wavelength standard.

Breden, L. H., **Technical Standards Coordinator, Fluorinated ethylene-propylene (FEP) plastic lined steel pipe and fittings,** *Nat. Bur. Stand. (U.S.), Prod. Stand. 34–70, 12 pages (Mar. 1971) 10 cents, SD Catalog No. C13.20/2:34–70.*

Key words: FEP lined pipe; fluorinated ethylene-propylene plastic lined pipe; pipe and fittings, steel, plastic lined; plastic lined steel pipe; steel pipe and fittings, plastic lined.

This Voluntary Product Standard covers requirements and methods of test for the material, dimensions, construction, and performance of commercially available steel pipe and fittings lined with fluorinated ethylene-propylene (FEP) plastic intended to be used for conveying acids, gases, solvents, and other corrosive materials.

Breden, L. H., **Technical Standards Coordinator, Poly(vinyl-shrinkable film,** *Nat. Bur. Stand. (U.S.), Prod. Stand. 29–70, 16 pages (Jan. 1971) 15 cents, SD Catalog No. C13.20/2:29–70.*

Key words: Balanced and unbalanced film; film, plastic; orientation release stress; plastic heat-shrinkable film; retraction ratio; shrink film, plastic.

This Voluntary Product Standard covers plastic film which, within its useful temperature range, will shrink at least 20 percent in either or both the machine and the transverse directions. Included are requirements and methods of test for shrink properties, dimensions, yield, weight, and slip.

Breden, L. H., **Technical Standards Coordinator, Poly(vinylidene fluoride) (PVF_2) plastic lined steel pipe and fittings,** *Nat. Bur. Stand. (U.S.), Prod. Stand. 35–70, 12 pages (Mar. 1971) 10 cents, SD Catalog No. C13.20/2:35–70.*

Key words: Pipe and fittings, steel, plastic lined; plastic lined steel pipe; poly(vinylidene fluoride) plastic lined pipe; PVF_2 lined pipe; steel pipe and fittings, plastic lined.

This Voluntary Product Standard covers requirements and methods of test for the material, dimensions, construction, and performance of commercially available steel pipe and fittings lined with poly(vinylidene fluoride) (PVF_2) plastic intended to be used for conveying acids, gases, solvents, and other corrosive materials.

Breden, L. H., **Technical Standards Coordinator, Polystyrene plastic sheet,** *Nat. Bur. Stand. (U.S.), Prod. Stand. 31–70, 14 pages (January 1971) 15 cents, SD Catalog No. C13.20/2:31–70.*

Key words: Impact resistance, plastic sheet; oriented sheet; plastic sheet; polystyrene plastic sheet; sheet, plastic.

This Voluntary Product Standard covers requirements and methods of test for dimensions, and mechanical and physical properties of hot-melt extruded polystyrene plastic sheet. The standard does not cover polystyrene foam or biaxially oriented sheet.

Breden, L. H., **Technical Standards Coordinator, Polytetrafluoroethylene (PTFE) plastic lined steel pipe and fittings,** *Nat. Bur. Stand. (U.S.), Prod. Stand. 33–70, 12 pages (Mar. 1971) 10 cents, SD Catalog No. C13.20/2:33–70.*

Key words: Pipe and fittings, steel, plastic lined; plastic lined steel pipe; polytetrafluoroethylene plastic lined pipe; PTFE lined pipe; steel pipe and fittings, plastic lined.

This Voluntary Product Standard covers requirements and methods of test for the material, dimensions, construction, and performance of commercially available steel pipe and fittings lined with poly-

tetrafluoroethylene (PTFE) plastic intended to be used for conveying acids, gases, solvents, and other corrosive materials.

Brenner, A., **Note on an organic-electrolyte cell with a high voltage,** *J. Electrochem. Soc.* **118,** *No. 3, 461–462 (March 1971).*

Key words: Graphite electrode; high energy density cell; lithium deposition; organic electrolyte.

An unusually high back EMF of 5.2 volts was obtained after electrolysis of a 10% solution of lithium fluoborate in sulfolane with a graphite anode.

Brenner, A., **Note on the electrodeposition of magnesium from an organic solution of a magnesium-boron complex,** *J. Electrochem. Soc.* **118,** *No. 1, 99–100 (January 1971).*

Key words: Decaborane; electrodeposition of magnesium; lithium deposition; nonaqueous electroplating; organometallic compound.

A magnesium electroplating bath which yields smooth, white deposits, has been prepared from lithium methyl, decaborane, and magnesium chloride. The solvent consisted mostly of tetrahydrofuran.

Brenner, F. C., Kondo, A., **Research for a uniform quality grading system for tires. IV. Tread wear,** *Rubber Chem. Technol.* **44,** *No. 1, 106–121 (March 1971).*

Key words: Automobile tires; grading; rating; test method; tread wear.

This research had as its objective the development of a test procedure for rating tires for tread wear. The results of preliminary experiments on roads of different composition and severity are discussed. The authors conclude that the course on which tires are to be rated should include several different pavements and a variety of maneuvers of unequal severity.
Two courses, one near Bryan, Texas, and the other near San Antonio, Texas, were designed on this principle. Eighteen brands of tires including bias, radial, and G78 belted bias tires were run on each course. The tires ranked in order of decreasing projected mileage on each course were highly correlated, although the mileages were not equal.

Brown, D. W., Lowry, R. E., Wall, L. A., **The radiation-induced polymerization of 3,3,4,4,5,5,5-heptafluoropentene-1 at high pressure,** *J. Poly. Sci.* **8,** *Part A–1, 3483–3493 (1970).*

Key words: 3,3,4,4,5,5,5-Heptafluoropentene-1; irradiation; polymerization; pressure.

A study was made of the radiation-induced polymerization under pressure of 3,3,4,4,5,5,5-heptafluoropentene-1. Polymerization rates increase with pressure (activation volume equals −11 cm^3/mol) and temperature (activation enthalpy equals 6.5 kcal/mol) in liquid phase. At 13800 atm and 25 °C freezing occurs; the polymerization rate in the solid is very small. In liquid phase polymerization can continue for many hours after the irradiation is terminated. An active species is formed by radiation which initiates polymerization in the dark period.

Brown, R. L., **Diffusion of a trace gas into a flowing carrier,** *Intern. J. Chem. Kinetics* **2,** *475–477 (1970).*

Key words: Diffusion equation; diffusion of gases; flow reactor; gas mixing; mixing by diffusion; relaxation methods.

Numerical methods are used to solve the differential equation for diffusion of a trace gas into a flowing carrier gas having a parabolic velocity profile in a cylindrical tube. Steady state solutions are given in the form of contour diagrams of constant trace gas concentration.

Bullis, W. M., Baroody, A. J., Jr., Editors, **Methods of measurement for semiconductor materials, process control, and devices,** *Quarterly Report, April 1 to June 30, 1970, Nat. Bur. Stand. (U.S.), Tech. Note 560, 58 pages (Nov. 1970) 60 cents, SD Catalog No. C13.46:560.*

Key words: Alpha-particle detectors; aluminum wire; carrier lifetime; die attachment; electrical properties; epitaxial silicon; gamma-ray detectors; germanium; gold-doped silicon; metallization; methods of measurement; microelectronics; microwave devices; nuclear radiation detectors; resistivity; semiconductor devices; semiconductor materials; semiconductor process control; silicon; thermal resistance; thermographic measurements; ultrasonic bonder; wire bonds.

This quarterly progress report, eighth of a series, describes NBS activities directed toward the development of methods of measurement for semiconductor materials, process control, and devices. Principal emphasis is placed on measurement of resistivity, carrier lifetime, and electrical inhomogeneities in semiconductor crystals; evaluation of wire bonds, metallization adhesion, and die attachment; and measurement of thermal properties of semiconductor devices and electrical properties of microwave devices. Work on related projects on silicon nuclear radiation detectors and specification of germanium for gamma-ray detectors is also described. Supplementary data concerning staff, standards committee activities, technical services, and publications are included as appendixes.

Bullis, W. M., Editor, **Methods of measurement for semiconductor materials. process control, and devices,** *Quarterly Report, July 1 to September 30, 1970, Nat. Bur. Stand. (U.S.), Tech. Note 571, 58 pages (Apr. 1971) 60 cents, SD Catalog No. C13.46:571.*

Key words: Alpha-particle detectors; aluminum wire; base transit time; carrier lifetime; die attachment; electrical properties; epitaxial silicon; gamma-ray detectors; germanium; gold-doped silicon; metallization; methods of measurement; microelectronics; microwave devices; nuclear radiation detectors; probe techniques (a-c); resistivity; semiconductor devices; semiconductor materials; semiconductor process control; silicon; thermal resistance; thermographic measurements; ultrasonic bonder; wire bonds.

This quarterly progress report, ninth of a series, describes NBS activities directed toward the development of methods of measurement for semiconductor materials, process control, and devices. Work is continuing on measurement of resistivity, carrier lifetime, and electrical inhomogeneities in semiconductor crystals; specification of germanium for gamma-ray detectors; evaluation of wire bonds, metallization adhesion, and die attachment; measurement of thermal properties of semiconductor devices and electrical properties of microwave devices; and characterization of silicon nuclear radiation detectors. New effort is being started on the measurement of transit-time and related carrier transport properties in junction devices. Supplementary data concerning staff, standards committee activities, technical services, and publications are included as appendixes.

Burdick, M. D., **An instrumental procedure for evaluating adherance of porcelain enamel cover coats direct-to-steel,** *Proc. Porcelain Enamel Institute Technical Forum, University of Illinois, Urbana, Ill., Oct. 7–9, 1970, 32, 160–167 (Porcelain Enamel Institute, Washington, D.C., 1971).*

Key words: Adherence; instrumental evaluation; porcelain enamel direct-to-steel.

An instrumental method for rating the quality of direct-on adherence is described. The method is appropriate, either for monitoring day-to-day production or for making interlaboratory comparisons. The rating method is firmly based on present practice, is rapid and does not require the somewhat subjectuve judgement of trained observers.

Carter, G. C., Kahan, D. J., Bennett, L. H., Cuthill, J. R., Dobbyn, R. C., **The NBS alloy data center: permuted materials index,** *Nat. Bur. Stand. (U.S.), Spec. Publ. 324, 683 pages (Mar. 1971) $7.00, SD Catalog No. C13.10:324.*

Key words: Alloy data; bibliography; index; information; Knight shifts; NMR; soft x-ray.

This Index contains literature references to ~10,000 research papers on physical properties of metals and alloys. The Index

contains all NMR Knight shift papers and soft x-ray emission papers. It also contains many soft x-ray absorption papers and a number of papers on generally related topics such as susceptibilities, specific heats, hyperfine fields, and band structures. The papers are annotated in depth and the coded information put onto a magnetic tape. The Permuted Materials Index was created from this tape, listing alloys under each of their constituent components (i.e., CuNi appears under CuNi and under NiCu alloys).

Cassidy, M. D., **Calibration and test services of the National Bureau of Standards,** *Nat. Bur. Stand. (U.S.), Spec. Publ. 250—1970 Edition, 209 pages (Dec. 1970) $2.00, SD Catalog No. C13.10:250. Supersedes NBS Miscellaneous Publication 250—1968 Edition.*

Key words: Calibration services; fees for testing; test fee schedule; test procedures.

This publication contains a descriptive listing, item by item, of most of the test and calibration work done at the National Bureau of Standards with the respective fees. The content is fully indexed providing easy access to data on specific measurement services. Included also is information about the Bureau's organization and statutory functions, the procedures for requesting tests, and the reports issued thereon. Throughout the text are mentioned various other publications which form a bibliography in measurement techniques. This publication supersedes Special Publication 250—1968 Edition and the supplementary material in Measurement Users Bulletins Numbers 1 through 11.

Cezairliyan, A., **A high speed method of measuring thermal expansion of electrical conductors,** *Rev. Sci. Instr.* **42,** *No. 4, 540–541 (April 1971).*

Key words: High-speed measurements; high temperature; platinum; thermal expansion.

A transient method for the measurement of thermal expansion of electrical conductors is described. The method is based on detecting the change in radiance coming from a constant radiation source as a result of the expansion of the specimen placed between the radiation source and a radiation detecting system. The specimen can be pulse heated from room temperature to near its melting point in less than one second and pertinent experimental quantities can be measured with a time resolution of 0.4 ms and a full-scale signal resolution of one part in 8000. To check the method, preliminary experiments were performed on platinum in the temperature range 300 to 700 K. The estimated inaccuracy of the results is within 5 percent. The agreement of the results with those in the literature is within 3 percent.

Cezairliyan, A., **High-speed methods of measuring thermophysical properties at high temperatures** *(Proc. Conf. Thermophysical Properties, Manchester, England, April 7–10, 1970), Rev. Inst. Hautes Temper. Refract T.7, 215–229 (1970).*

Key words: High-speed measurement methods; high temperatures; thermodynamics; thermophysical properties.

In this paper, "high-speed" refers to experiments which are of subsecond duration. However, in some cases quasi-dynamic experiments with durations greater than one second are also included. Advantages of high-speed measurement of thermophysical properties of substances at high temperatures (above 2000 K) are presented. Requirements of high-speed measurements are given. Methods used for the generation and measurement of thermal energy in short times are described. Various techniques (photoelectric, photographic, and others) used for the measurement of the temperature of rapidly heating or cooling specimen are presented. Techniques for high-speed recording of quantities are described. Particular attention is given to millisecond-resolution digital data acquisition systems. Application of the high-speed techniques to the measurement of specific heat, electrical resistivity, thermal radiation properties, melting point, thermal diffusivity and others are described. Accuracy of high-speed measurements are discussed and are compared with those of conventional methods. Potential applications of high-speed methods are presented.

Cezairliyan, A., **Short-time (ms) fluctuations of radiance temperature of graphite arc,** *Appl. Opt.* **10,** *No. 5, 1178 (May 1971).*

Key words: Graphite arc; high-speed measurements; high temperatures; pyrometry; radiance standards.

Short-time fluctuations of the radiance temperature graphite arcs are investigated with a millisecond resolution photoelectric pyrometer. Standard deviation of the fluctuations around their mean is found to be 4 K. The range of low and high temperatures for four experiments extended from 3799 K to 3808 K, with an average of 3804 K on IPTS-68.

Chamberlain, G. E., Mielczarek, S. R., Kuyatt, C. E., **Absolute measurement of differential cross sections for electron scattering in helium,** *Phys. Rev.* **A2,** *No. 5, 1905–1922 (November 1970).*

Key words: Absolute differential cross section; Born; elastic; electron impact; helium; inelastic.

Absolute measurements of cross sections for electron-impact scattering in helium at 5° angle have been made for elastic scattering and excitation of the 2^1P and 2^1S states and for incident energies of 50–400 eV. Cross section values of $\sigma(2^1P,5°)$ are found to be lower than theoretical Born values by 10% at 400 eV, 30% at 100 eV, and 60% at 50 eV. Deduced values of total 2^1P excitation cross sections ($E \geq 100$ eV) are in agreement with other experimental values. Our measurements for elastic scattering agree well with recent theoretical calculations.

Chandler, H. H., Rupp, N. W., Paffenbarger, G. C., **Poor mercury hygiene from ultrasonic amalgam condensation,** *J. Am. Dental Assoc.* **82,** *553–557 (March 1971).*

Key words: Amalgam condensation; mercury; mercury vapor levels; threshold limit.

There is a potential hazard of mercury poisoning in using an ultrasonic device for amalgam condensation. A cloud of mercury droplets and alloy particles was emitted from the soft amalgam at the working tip of the instrument. Mercury vapor levels as recorded by a vapor detector held 30 cm from the working tip were 20% of the allowable threshold limit value (0.1 mg Hg/m^3 of air) and probably do not represent unsafe levels. The continued long-time use of the ultrasonic instrument would result in the deposition of a great many mercury droplets throughout a dental operatory and could thereby cause higher mercury vapor levels especially in poorly ventilated spaces. In addition, the inhalation of the emitted material by the patient and the dental health personnel cannot be considered good hygiene. Therefore, the use of this instrument for amalgam condensation is contra-indicated until such time as the safety of the instrument for this purpose is firmly established.

Chappell, S. E., Humphreys, J. C., **Silicon detector measurements of energy deposition in aluminum by monoenergetic electrons** *(Proc. Annual Conf. Nuclear Space Radiation, La Jolla, Calif., July 1970), IEEE Trans. Nuclear Science* **NS–17,** *No. 6, 272–277 (Dec. 1970).*

Key words: Absorbed energy vs depth; absorbed-energy distributions; incident monoenergetic electrons; Monte Carlo calculations; semi-infinite aluminum medium; silicon detector.

The energy deposited at various depths in aluminum by incident monoenergetic electrons has been measured with a silicon semiconductor, transmission detector. Beams of monoenergetic electrons with incident energies of 0.50, 0.75, and 1.0 MeV were directed normally on a semi-infinite slab of aluminum in which a 0.196-mm silicon detector was positioned at various depths. The pulse-height distributions recorded with the detector were converted to absorbed-energy distributions from which the probability of energy absorption per incident electron in the specific layer, as well as the absorbed energy as a function of depth in the material, could be determined. The curves of absorbed energy as a function of depth obtained for aluminum at each energy were compared to those calculated by Berger and Seltzer, employing a Monte Carlo method. Good agreement is shown between calculations and measurements.

Cohen, J., Edelman, S., **Direct piezoelectric effect in polyvinylchloride films,** *J. Appl. Phys.* **42,** *No. 2, 893–894 (February 1971).*

Key words: g Modulus; piezoelectricity; polymers; polyvinylchloride films.

The piezoelectric modulus, g_{31}, of polyvinylchloride films has been measured at 20 Hz. Values are in the range of approximately 0.4 to 3 Vm^{-1}/Nm^{-2}, which are larger than the g values of conventional piezoelectric materials.

DeVoe, J. R., Spijkerman, J. J., **Mössbauer spectrometry,** *Anal. Chem. Annual Reviews* **42,** *No. 5, 366R–388R (April 1970).*

Key words: Chemical applications: literature; Mössbauer spectroscopy; review.

A review of the literature on chemical applications of Mössbauer Spectrometry for 1968 and 1969 are presented. This is done primarily with a table of pertinent information on compounds and techniques. New developments in the field are also presented.

Dikkers, R. D., Marshall, R. D., Thom, H. C. S., **Hurricane Camille—August 1969,** *Nat. Bur. Stand. (U.S.), Tech. Note 569, 71 pages (Mar. 1971) 70 cents, SD Catalog No. C.13.46:569.*

Key words: Buildings; failure; hurricanes; mobile homes; roofs; structural engineering; tides; wind.

One week after Hurricane Camille devastated the Mississippi-Louisiana Gulf Coast with 125 mph winds and 20-ft tides on August 17, 1969, a four-man NBS team investigated the damage to buildings and other structures. This report presents photographic survey data from this investigation along with additional data on wind speeds and storm surge. Based on these data, suggestions are made pertaining to the improvement of building design and construction practices.

DiMarzio, E. A., Guttman, D. M., **Separation by flow and its application to gel permeation chromatography,** *J. Chromatog.* **55,** *83–97 (1971).*

Key words: Chromatography; elution volume; flow; gel permeation chromatography; hydrodynamic volume; polymer; polymer separation.

When dilute solutions of finite size particles undergoing Brownian motion flow through a capillary, the larger particles have higher average velocities than the smaller particles. Thus one can obtain a separation of particles of different sizes due to fluid flow. The elution volumes of suspended particles or polymer molecules are derived for various tube geometries. Following Taylor, the effects of diffusional broadening of the volume elution peak for finite size particles are discussed and the process is shown to be chromatographic.
Models of a GPC column are proposed in which there is fluid and particle flow through each of the beads as well as around them. Diffusion is allowed within and outside of the beads. Equations for the location of the volume elution peaks are computed for such models and shown to yield functional dependence on the polymer radius and column geometry very much like equations derived by previous workers for models of GPC columns in which there was no flow allowed within the beads. Explicit formulae are given for the second and third moments for the above models. It is shown that for a monodisperse species the volume elution peak is always a gaussian of a finite width. It is shown that beads with open pores that allow for flow always have better separation capabilities than beads with pores that do not allow for flow.

Dziuba, R. F., Dunfee, B. L., **Resistive voltage-ratio standard and measuring circuit,** *IEEE Trans. Instr. Meas.* **IM–19,** *No. 4, 266–277 (Nov. 1970).*

Key words: Divider; measurement system; ratio; ratio standard; resistive divider; voltage ratio.

This paper describes a highly stable, guarded d-c voltage ratio standard and the measuring network and techniques used to establish the values of its ratios to an accuracy of 0.2 ppm. The entire system is housed within a dry air enclosure whose temperature is maintained at 23 ± 0.05 °C. Discrete ratios from 1/1, to 1000/1, are provided with maximum rated voltage set at 1000 volts. The design of the standard was chosen so that a redundancy of measurment could be incorporated in the system. Thus it is possible to measure each *successive* ratio by a substitution or "boot-strap" method, and, by satisfying the conditions of the series-parallel principle, to measure the 10/1, 100/1, and 1000/1 ratios by a second independent method. The design also admits additional checks on the validity of the measurements. An analysis of measurement errors and a discussion of their possible origin are included. Since the intent also was to design the ratio standard for low frequency operation some preliminary data is included on its ac performance.

Edgerly, D. E., **Weights and Measures Labeling Handbook,** *Nat. Bur. Stand. (U.S.), Handb. 108, 406 pages (May 1971) $3.25, SD Catalog No. C13.11:108.*

Key words: Consumer package; exemption; fluid measure; labeling; net quantity; principal display panel; regulations; weights and measures.

The Weights and Measures Labeling Handbook has been prepared for use by State weights and measures officials in the enforcement of State laws and regulations pertaining to the packaging and labeling of commodities. The Handbook provides a cross indexed compilation of the requirements of the Model State Packaging and Labeling Regulation, U.S. Department of Agriculture regulations, and regulations of the Food and Drug Administration and Federal Trade Commission issued pursuant to the Fair Packaging and Labeling Act.

Engen, G. F., **A new method of characterizing amplifier noise performance,** *IEEE Trans. Instr. Meas.* **IM–19,** *No. 4, 344–349 (Nov. 1970).*

Key words: Amplifier noise; noise; noise factor; noise temperature; Y-factor.

Although the use of noise figure or noise temperature to characterize amplifier performance is a well-established practice, it is also recognized that this parameter provides only a partial description of the amplifier noise properties. In general, the noise figure (or temperature) depends upon the generator inpedance and is thus a function of the signal-source and amplifier combination.
Typically, the noise figure is measured by the Y-factor method using hot and cold noise sources that are nominally matched (reflectionless). The result of this measurement is of value as a figure of merit; however, if optimum performance is to be realized, the applications engineer must know whether to adjust the signal source impedance for maximum power transfer, minimum noise figure, or some other criterion, and he must know the deterioration in performance that results if this is not done. It is the purpose of this paper to present an alternative method of characterizing amplifier noise performance in terms of parameters that provide ready answers to these questions. In addition, the measurement of these parameters via a simple extension of the Y-factor method will be described.

Evenson, K. M., Radford, H. E., Moran, M. M., Jr., **CH free radicals detected by infrared lasermagnetic resonance,** *Appl. Phys. Letters,* **18,** *No. 10, 426–429 (May 15, 1971).*

Key words: CH; far infrared; free radical; laser; laser magnetic resonance.

CH radicals in an oxyacetylene flame have been detected by a magnetic resonance absorption method, with a water-vapor laser as the source oscillator at a frequency of 2.5 THz. The absorption spectrum is identified with the pure rotational transition, J, $K=(5/2,2)\rightarrow(7/2,3)$ at a wavelength of 118.6 μm.

Evenson, K. M., Wells, J. S., Matarrese, L. M., Jennings, D. A., **Variable output-coupling far-infrared Michelson laser,** *J. Appl. Phys.* **42,** *No. 3, 1233–1234 (March 1, 1971).*

Key words: HCN lasers; H_2O lasers; infrared lasers; variable laser coupling.

A method for varying the output coupling of far-infrared gas lasers is described. It is based on the Michelson interferometer principle and has the advantages of increasing the power available from the laser and providing a smooth variation of the output coupling.

Farabaugh, E. N., Mauer, F. A., **Application of a modified technique for x-ray topography of large crystals,** *J. Crystal Growth* **7**, *282–284 (1970).*

Key words: Laser rod; orientation; ruby; single crystal; topography x-ray.

A transmission x-ray topography technique has been developed which is suitable for examining large, uncut crystals. A relatively large volume is represented in each photograph, and regions that are misoriented by more than 0.3° can be detected. Examination of single crystal ruby laser rods is used to illustrate the capabilities and limitations of the method.

Fatiadi, A. J., **Determination of inososes with an alkaline solution of copper (II) oxalate-tartrate complex (the Somogyi reagent) and reaction mechanisms involved,** *Carbohydrate Res. 17, 419–430 (March 1971).*

Key words: Determination; electron-transfer; inosose; oxidation; quantitative; radical; reagent.

Four inososes have been analyzed with the Somogyi reagent and empirical equations for their quantitative determination were derived because reaction of the Somogyi reagent with inososes affords non-stoichiometric quantities of cuprous oxide, and each inosose has a different reducing power.
Results from spectrophotometric and e.s.r. studies of the mechanism of oxidation of inososes with the Somogyi reagent at 25 to 55° are in agreement with a one-electron transfer process; however, at 90 to 100°, extensive degradation of inososes by the Somogyi reagent occurs, doubtless caused by generation of transient radicals during the oxidation, as evidenced by results of a radical-scavenging experiment.

Fickett, F. R., **Resistivity of polycrystalline aluminum and copper in high magnetic fields: The effect of temperature and purity,** *Appl. Phys. Letters* **17**, *No. 12, 525–527 (Dec. 15, 1970).*

Key words: Aluminum; copper; magnetoresistance.

Data are presented on the resistivity of polycrystalline aluminum and copper at 40 kOe and at temperatures from 4 K to 30 K. Specimen purity varies over three decades of residual resistance ratio. For either metal, the actual resistivity measured in the field at a given temperature decreases with increasing specimen purity. This result is important for proposed high magnetic field applications of these metals.

Franklin, A. D., Bennett, H. S., Editors, **ARPA–NBS Program of research on high temperature materials and laser materials,** *January 1 to June 30, 1970, Nat. Bur. Stand. (U.S.), Tech. Note 565, 84 pages (Jan. 1971) 75 cents, SD Catalog No. C13.46:565.*

Key words: Aluminum oxide; band structure; borides; bulk optical properties; chemical analysis; chromium ions; corundum; crystal defects; crystal growth; density of states; diffusion; glass; high temperature materials; laser damage; laser degradation; laser glass; laser materials; mass transport; neodymium glass; optical properties; opto-elastic properties; oxides; ruby; rutile; titanium; titanium dioxide; transition metal.

Brief reviews are given of work performed during this reporting period on several problems in the areas of High Temperature Materials and Laser Materials. Under the High Temperature Materials extremely pure Al_2O_3 crystals have been prepared and analysed chemically with the aim of providing specimens for research on mass transport, electronic, and similar properties. Oxygen diffusion data on TiO_2, obtained by the gas uptake method, agree with literature values, and work is now proceeding on developing a sectioning technique for oxygen diffusion. The optical constants of titanium have been determined over the visible portion of the spectrum. Soft x-ray spectra, nmr data, Mössbauer spectra, magnetic susceptibility, and other probes of the electronic density of states have been determined for a group of diborides of the first-series transition metals (Sc, Ti, V, Cr, and Mn) and interpreted in terms of the d-electron contribution to the density of states near the Fermi level. Both this project and the previous one on the optical properties of titanium have been completed. Under Laser Materials, the measurement of bulk optical properties and chemical analyses of ruby and Nd-glass are complete. Several techniques for determining the Cr^{3+} content in laser ruby have been developed and shown to agree; with these, it has been shown that very little loss of Cr^{3+} occurs when ruby turns orange under optical (x-ray or γ-ray) irradiation. A theory of laser pulse-induced damage at foreign particles in Nd-glass has been worked out; it suggests that detection before damage might be easiest with pulses of microsecond or longer duration. A high-power Nd-glass laser, Q-switched, has been purchased for damage studies. The beam characteristics, which must be properly controlled for meaningful damage threshold measurements, are currently being studied.

Furcolow, W. H., **Technical Standards Coordinator, Clinical thermometers (Maximum-self-registering, mercury-in-glass),** *Nat. Bur. Stand. (U.S.), Prod. Stand. 39–70, 12 pages (May 1971) 15 cents, SD Catalog No. C13.20/2:39–70.*

Key words: Clinical thermometers; glass thermometers, clinical; mercury-in-glass thermometers; thermometers, self-registering, clinical.

This Voluntary Product Standard covers the requirements and methods of testing maximum-self-registering, mercury-in-glass thermometers of the types commonly used for measuring body temperatures, such as oral and rectal types in both regular and basal temperature scales. It is intended to serve as a nationally recognized basis for certification of compliance by manufacturers and for procurement purposes by consumers. The standard includes requirements for bulb and stem glasses, mercury, dimensions, temperature scale ranges, and graduations, and performance criteria for thermometer aging, hard shaking determination, and accuracy of scale reading.

Furcolow, W. H., **Technical Standards Coordinator, Hinged interior wood door units,** *Nat. Bur. Stand. (U.S.), Prod. Stand. 32–70, 15 pages (Mar. 1971) 30 cents, SD Catalog No. C13.20/2:32–70.*

Key words: Door units, wood; hinged door units, interior; prefabricated door units; wood door units.

This Voluntary Product Standard covers the designs, grades, sizes, materials (including hardware), and construction of prefabricated wood door units, as well as a means of identifying units represented as conforming to the standard, and definitions of terms used in the standard.

Gadzuk, J. W., Plummer, E. W., **Energy distributions for thermal field emission,** *Phys. Rev.* **B. 3**, *No. 7, 2125–2129 (April 1, 1971).*

Key words: Field emission; surfaces and tunneling.

A sequence of total energy distribution curves for field emission was experimentally obtained for a tungsten emitter heated to 1570 K. Theoretical curves using the Miller-Good WKB-type approximation for tunneling probabilities are in good agreement with the experimental measurements. A significant feature of both sets of curves is a change in slope corresponding to electron emission near the top of the surface where the emission mechanism changes from tunneling to thermionic emission. This feature is in accord with the classical-image force model for the surface potential which appears to be valid for distances approaching 3–4 Å to the metal surface.

Garner, E. L. Machlan, L. A., Shields, W. R., **Standard Reference Materials: Uranium isotopic standard reference materials,** *(Certification of uranium isotopic standard reference materials),*

Nat. Bur. Stand. (U.S.), Spec. Publ. 260–27, 162 pages (April 1971) $1.25, SD Catalog No. C13.10:260–27.

Key words: Absolute isotopic abundance; ignition procedure; isotopic standards, mass spectrometry; stoichiometry; uranium.

An ignition procedure has been developed that will yield reproducible stoichiometry for U_3O_8. The effects of temperature, length of ignition, rate of cooling, pressure and type of atmosphere were investigated. This ignition procedure has been used for the blending of high purity ^{235}U and ^{238}U separated isotopes to prepare calibration standards for the determination of bias effects in the thermal emission mass spectrometry of uranium. Weight aliquoting was used to prepare calibration mixes with $^{235}U/^{238}U$ ratios of more than 10 and less than 0.1 and to add a ^{233}U spike for the determination of minor isotope abundances in the uranium isotopic standards by the isotope dilution technique.
A description of the unique features of the mass spectrometer instrumentation including the source, NBS collector and expanded scale recorder are given. Two specific analytical procedures were used for the isotopic analysis of uranium and are adaptable, within a general framework, to fit the particular ion current intensity requirements of a wide range of isotopic distributions. Mass discrimination due to evaporation and ionization on the filaments, and other parameters such as temperature, time, sample size, sample mounting, total sample composition, acidity, filament material, pressure, non-ohmic response, R-C response and source memory were studied as part of the development effort to establish sound analytical procedures.
The absolute isotopic abundances of 18 uranium SRMs were determined by thermal emission mass spectrometry. The general approach was to determine absolute $^{235}U/^{238}U$ ratios by using calibration mixes to correct for filament bias. Then the absolute ^{234}U and ^{236}U were determined by ^{233}U isotope dilution. For SRM U–0002, isotope dilution was the only practical means of determining the low abundance of ^{235}U as well as the ^{234}U. The limits given for the isotopic composition of the uranium SRMs are at least as large as the 95 percent confidence limits for a single determination and include terms for inhomogeneities of the material as well as analytical error.

Hahn, T. A., **Thermal expansion of copper from 20 to 800 K—*Standard reference material 736*, *J. Appl. Phys.* 41, *No. 13, 5096–5101 (December 1970).***

Key words: Components of error (within and between samples); copper; interferometer; standard reference material; thermal expansion.

Copper is the first of a series of materials that will be certified as thermal expansion standards by the National Bureau of Standards. The results of tests on five specimens indicate the stock is of consistent quality so that it may be certified as Standard Reference Material 736. A Fizeau interferometer was used for the expansion measurements. Above room temperature a controlled atmosphere furnace using a calibrated Pt vs. Pt-10% Rh thermocouple was used. Below room temperature a cryostat capable of operation with both liquid nitrogen and helium was used with a calibrated platinum resistance thermometer. Values of expansivity were calculated between equilibrium temperatures. The expansivity was used in the analysis of the data. Third order polynomials were fit to the data for each of the five specimens in the overlapping temperature ranges from 0 to 70 K, 50 to 270 K, and 210 to 800 K to test for variations between the specimens. The deviations between the five equations were well within the standard deviations of the data for each of the specimens in the respective temperature intervals. All the expansivity data was then pooled and used to obtain an equation for each of the temperature ranges given above. These equations and their integrals were used to calculate the final values of expansivity and expansion respectively. The results of the statistical analysis of the expansion and expansivity data is presented. A comparison is made with the data in the literature.

Hamer, W. J., **Standard cells, the primary battery,** *George W. Heise and N. Corey Cahoon, Ed.*, **1,** *No. 12, 433–477 (John Wiley & Sons, Inc., New York, N.Y., January 1971).*

Key words: Electromotive force; saturated standard cells; standard cells; unsaturated standard cells.

This paper gives a survey of saturated and unsaturated standard cells including descriptions of their construction and their behavior under diversified conditions. The survey also includes a discussion of the role standard cells play in the maintenance of the unit of electromotive force. A discussion of the Hulett standard battery is also included.

Harman, G. G., Kessler, H. K., **Application of capacitor microphones and magnetic pickups to the tuning and trouble shooting of microelectronic ultrasonic bonding equipment,** *Nat. Bur. Stand. (U.S.), Tech. Note 573, 24 pages (May 1971) 35 cents, SD Catalog No. C13.46:573.*

Key words: Capacitor microphone; flip-chip; magnetic pickup; microelectronic interconnections; spider bonding; ultrasonic bonding; wire bonding.

Microelectronic ultrasonic wire bonding equipment typically welds wires to integrated circuits at frequencies between 50 and 65 kHz. Mechanical vibrations at these frequencies are difficult to measure directly and malfunctions of the system may not be recognized. Two different methods of measuring these vibrations are described. The first method involves use of a capacitor microphone and a tapered tip, and the second method use of a small magnetic pickup. Procedures are given for establishing a specific ultrasonic vibration amplitude, tuning the ultrasonic system to resonance, and diagnosing both mechanical and electrical problems in wire bonding equipment. Although these techniques and procedures were developed for ultrasonic wire bonding equipment, they are applicable to other ultrasonic welding systems of lead attachment, such as flip-chip, beam lead and spider bonding.

Harris, F. K., Fowler, H. A., Olsen, P. T., **Accurate Hamon-pair potentiometer for Josephson frequency-to-voltage measurements,** *Metrologia* **6,** *No. 4, 134–142 (October 1970).*

Key words: Frequency-to-voltage ratio; Josephson effect; potentiometer; voltage standard.

Accuracy and precision of parts in 10^7 have been demonstrated in a potentiometer which compares two- to ten-millivolt dc signals from Josephson junctions against the U.S. "legal volt" secondary standard cells. The circuit comprises two (10 × 100 ohm) Hamon boxes in series-to-parallel interchange, linked by a calibrated Kelvin-Varley current divider. The critical Hamon-circuit contacts are all made through mercury-wetted amalgams; the entire circuit operates in smoothly stirred oil. Observations indicate the pair of Hamon boxes to be initially balanced within 0.2 ppm at the operating temperature. Typical standard deviation in the day-to-day, run-to-run scatter of Josephson frequency-to-voltage ratio, measured with this instrument, is 0.3 ppm or less. Preliminary values for the observed ratio are in general accord with the quoted values of Parker et al., Petley and Morris, and Finnegan et al.

Harvey, J. L., Milliken, L. T., Forthofer, R. J., **Trends in motor vehicle brake fluids and their standards,** *Proc. Society of Automotive Engineering Conf., Paper No. 710253, pp. 1–17 (January 11–15, 1971).*

Key words: Brake fluids; brake fluid standards; motor vehicle brake fluid; passenger car braking systems.

The development of motor vehicle brake fluids (MVBF's) and of their specification requirements is reviewed and discussed with emphasis on the major problems encountered in service. Those factors held to be of major importance in establishing performance requirements for MVBF's are considered also, and applied to the major changes that have recently been proposed for revision of Federal Motor Vehicle Safety Standard No. 116. The needs and possibilities for further revision in the MVBF safety standard are examined. Finally, potential effects of some current trends in the design of passenger car braking systems are considered.

Hellwig, H., **Areas of promise for the development of future primary frequency standards,** *Proc. 24th Annual Symp. on Frequency Control, Atlantic City, N.J., April 27–29, 1970, pp.*

246–258 (Electronic Industries Assn., Washington, D.C., 1970); Metrologia **6**, *No. 4, 118–126 (October 1970).*

Key words: Accurate frequency standards; accurate length standards; accurate time standards; accurate voltage standards; ion storage; laser stabilization; maser oscillator; metrology; quantum electronics; saturated absorption; slave oscillators.

In this paper possibilities are discussed which may lead to the development of future primary frequency standards of superior accuracy capability. A review is given of the various methods and techniques which are currently employed in quantum electronic frequency standards or which have a potential usefulness. Various effects which influence the output frequency of a primary standard are associated with these methods. A classification is given: (a) Effects associated with the interrogation of particles (atoms or molecules); (b) effects related to the method of confining the particles; and (c) effects associated with the particles themselves and the way in which they are treated for an effective interrogation by electromagnetic radiation. These three classes of effects are discussed in detail, and expectation values for the related uncertainties are given. For selected particles certain methods of interrogation, confinement, and particle preparation can be combined such as to minimize the net uncertainty due to all applicable effects. Different technical solutions are the result. A review of existing and proposed devices is given, including quantitative data on the stability and accuracy capability. Aspects of the most promising devices are discussed, and it is concluded that accuracy capabilities of 10^{-14} should be within reach of today's research and development.

Heydemann, P. L. M., **A simple and dependable electrical feedthrough for high pressures,** *Rev. Sci. Instr.* **41**, *No. 12, 1896 (December 1970).*

Key words: Closure; feedthrough; high pressure; leads.

This note describes a novel type of high pressure feedthrough capable of withstanding more than 25 kbar repeatedly. It can be used for measurements with DC requiring very high insulation resistance as well as for RF up to 30 MHz.

Hicho, G. E., Yakowitz, H., Rasberry, S. D., Michaelis, R. E., **Standard reference materials: A standard reference material containing, nominally four percent austenite,** *Nat. Bur. Stand. (U.S.), Spec. Publ. 260–25, 22 pages (Feb. 1971) 30 cents, SD Catalog No. C13.10:260–25.*

Key words: Austenite in ferrite; electron microprobe; powder metallurgy; quantitative microscopy; SRM; x-ray fluorescence analysis.

This standard was produced by powder metallurgical techniques using known amounts of austenite. Using these techniques, 134 specimens were prepared. Because these standards are expected to be used primarily for the calibration of x-ray diffraction equipment, only one surface of each standard is certified, and these surfaces range from 3.1 percent to 5.2 percent in austenite content. To make the specimens, 310 stainless steel powder (austenitic) was blended with 430 stainless steel powder (ferritic) to make a mixture of 5 percent austenite in ferrite. The material was compacted, sintered, polished and etched so the austenite appears white and the ferrite, a deep brown. Then quantitative microscopy methods were used to determine the percentage of austenite near the surface. Furthermore, the 310 powder contains 20 percent of nickel while the 430 powder contains virtually no nickel. Therefore, after establishing a meaningful calibration curve, x-ray fluorescence analysis for the nickel content was also used as a direct measurement of the amount of austenite on the surface of the compact. Both procedures were carried out on fifteen specimens statistically selected from the total number of compacts produced. Agreement, within experimental error limits, was obtained between the x-ray fluorescence results and quantitative microscopy results. The x-ray fluorescence method was used to characterize all additional compacts. X-ray diffraction determinations of austenite content are in good agreement with the x-ray fluorescence and quantitative microscopy results. The compacts may be used as x-ray diffraction standards for austenite or in special cases as x-ray fluorescence standards for nickel content.

Hoer, C. A., Agy, D. L., **Broad-band resistive-divider-type directional coupler,** *IEEE Trans. Instr. Meas.* **IM–19**, *No. 4, 336–343 (November 1970).*

Key words: Coupler; directional coupler; directivity; impedance measurements; power measurements.

A new lumped circuit directional coupler is described for the 1 to 30 MHz frequency range. Directivity greater than 50 dB is achieved over this frequency range for coupling ratios of 30, 40, and 50 dB. Greater directivity can be achieved over a narrower frequency range, and the coupler can be tuned for essentially infinite directivity at a fixed frequency. The couplers, although resistive, can pass 100, 300, or 1000 Watts for the coupling ratios of 30, 40, and 50 dB respectively with less than 0.01 dB change in coupling ratio. The coupling ratios are constant with frequency to ± 0.25 dB. Equations and curves are given for obtaining component values needed to design a resistive divider type coupler with any coupling from 3 to 60 dB.

Hord, J., Voth, R. O., **Tabulated values of cavitation *B*-factor for helium, H_2, N_2, F_2, O_2, refrigerant 114, and H_2O,** *Nat. Bur. Stand. (U.S.), Tech. Note 397, 116 pages (Feb. 1971) $1.00, SD Catalog No. C13.46:397.*

Key words: Cavitation; cryogenics; pumps.

A brief history is given on the development of the *B*-factor concept and its application to the design of liquid pumps. Adaptation of the "quasi-static" vaporization model to the cavitation process is discussed; previous methods of computing *B*-factor are reviewed and a simplified, more precise computation, consistent with the "quasi-static" model, is established. Merits of the different computational techniques are discussed and two of the methods are graphically compared. The best available property data are used to compute *B*-factors for several fluids over a wide range of temperatures. The results are tabulated as reference data; they are useful in the application of the *B*-factor concept to the prediction of performance in cavitating liquid pumps.

Hudson, R. D., Kieffer, L. J., **Compilation of atomic ultraviolet photoabsorption cross sections for wavelengths between 3000 and 10 Å,** *Atomic Data* **2**, *No. 3, 205–262 (May 1971).*

Key words: Atoms; compilation; cross section data; photoabsorption; photoionization; photon.

Graphical displays of selected experimental data on atomic photoabsorption cross sections as functions of wavelength are presented for 24 atoms. Criteria used in the data selection are discussed. References for all data chosen and an author index are included. The literature has been covered through October 1969.

Ives, L. K., Ruff, A. W., Jr., **Extended dislocation configurations in HCP silver-tin alloys of low stacking-fault energy,** *Metal Sci. J.* **4**, 201–*209 (May 1970).*

Key words: Dislocation multipoles; dislocation networks; dislocation nodes; dislocations; electron microscopy; hexagonal alloys; silver-tin alloys.

Configurations resulting from the interaction of extended dislocations in low stacking fault energy hcp silver-tin alloys are studied by means of transmission electron microscopy. The interactions of all possible sets of two different extended dislocations are considered. Since there are two different modes by which dislocations extend in the hcp structure, these interactions fall into two classes: Class I interactions occur between two dislocations extended in the same way, and Class II interactions involve two dislocations extended in different ways. The resulting configurations consist of several different kinds of nodes, node pairs, double ribbons, and dipoles. Interactions between arrays of extended dislocations lead to the formation of networks of these configurations and to multipoles. Many of the observed configurations are similar to those reported in hexagonal graphite. The Class I configurations are similar to those found in low stacking fault energy fcc metals.

Jennings, D. A., **Power and energy measurement of repetitively pulsed lasers,** *Nat. Bur. Stand. (U.S.), Tech. Note 398, 10 pages (March 1971) 25 cents, SD Catalog No. C13.46:398.*

Key words: Average power; energy per pulse; laser; peak power; repetitively pulsed lasers.

The problem of measuring average power, energy per pulse, and peak power of some of the more common repetitively pulsed lasers is discussed. The techniques which have been used at the National Bureau of Standards are mentioned along with some of the accuracies obtained. Accuracies of 3 to 10 percent can be achieved depending on the laser source and the parameter of interest.

Kamas, G., Hanson, D. W., **Recent VHF/UHF satellite timing experiments at the National Bureau of Standards,** *Proc. Precise Time and Time Interval (PTTI) Strategic Planning Meeting (U), Washington, D.C., December 10–11, 1970,* **1,** *79–82 (1970).*

Key words: ATS satellite; LES–6 satellite; NBS satellite timing; satellites; TA CSAT satellite; time; timing accuracy.

A summary discussion is presented of the current work accomplished by NBS in the field of time dissemination by geostationary satellites. The results of that program and its implication for the future are given.

Kamper, R. A., Zimmerman, J. E., **Noise thermometry with the Josephson effect,** *J. Appl. Phys.* **42,** *No. 1, 132–136 (Jan. 1971).*

Key words: Josephson effect; noise; superconductivity; thermometry.

Thermal noise causes a random frequency modulation of the self-oscillation of a Josephson junction, and the temperature of the noise source can be determined by analysis of the generated signal. We discuss the theoretical limitations of thermometry with this principle, and describe a prototype thermometer which has recorded noise temperatures down to 0.075 K.

Keysar, B. C., **Specifications and tolerances for reference standards and field standard weights and measures. 2. Specifications and tolerances for field standard measuring flasks,** *Nat. Bur. Stand. (U.S.), Handb. 105–2, 6 pages (Jan. 1971) 25 cents, SD Catalog No. C13.11:105–2.*

Key words: Accurate measurements of volume of liquids; field standard measuring flasks; specifications; tolerances; weights and measures inspection.

These specifications and tolerances are recommended as minimum requirements for standards used in the field by State and local weights and measures officials in quantity determinations of liquid commodities.

Keysar, B. C., **Specifications and tolerances for Reference Standards and Field Standard Weights and Measures—3. Specifications and tolerances for Metal Volumetric Field Standards,** *Nat. Bur. Stand. (U.S.), Handb. 105–3, 8 pages (May 1971) 25 cents, SD Catalog No. C13.11:105–3.*

Key words: Accurate measurement of volumes; field standard; metal volumetric field standards; provers; specifications; test measures; tolerances; weights and measures inspection.

These specifications and tolerances are recommended as minimum requirements for standards used in the field by State and local weights and measures officials in quantity determinations of liquid commodities.

Kruger, J., Frankenthal, R. P., B. **Corrosion of metals,** *Chapter in Volume* **IV,** *Techniques in Metals Research, Chapter 10B oxidation and corrosion,* R. A. Rapp, Ed., R. F. Bunshah, Series Ed., **14,** *Part 2, 571–667 (John Wiley and Sons Inc., New York, N.Y. 1970).*

Key words: Corrosion; electron diffraction; electron microscopy; research techniques.

The application of non-electrochemical techniques to corrosion research are discussed. These include optical techniques, x-ray techniques, electron microscopy and diffraction, tracer techniques and mechanical techniques.

Kulin, G. Surewitz, P. H., Editors, **Hydraulic Research in the United States 1970--Including Contributions from Canadian Laboratories,** *Nat. Bur. Stand. (U.S.), Spec. Publ. 346, 354 pages (Mar. 1971) $2.50, SD Catalog No. C13.10:346.*

Key words: Fluid mechanics; hydraulic engineering; hydraulic research; hydraulics; hydrodynamics; model studies; research summaries.

Current and recently concluded research projects in hydraulics and hydrodynamics for the years 1969–1970 are summarized. Projects from more than 250 university, industrial, state and federal government laboratories in the United States and Canada are reported.

Kurylo, M. J., Peterson, N. C., Braun, W., **Temperature and pressure effects in the addition of H atoms to propylene,** *J. Chem. Phys.* **54,** *No. 11, 4662–4666 (June 1, 1971).*

Key words: Absolute rate constant; activation energy; fluorescence; H atom; propylene; reaction kinetics.

The effect of He pressure on the rate of addition of hydrogen atoms to propylene was measured at 298 °K. H atom signal was recorded by the method of resonance of Lyman α radiation at 121.6 nm. The results are consistent with the $1/p^1{}_2$ dependence of k_{bi} recently observed in the H atom-ethylene system. The limiting high pressure rate constant obtained in this work is $H + C_3H_6 \rightarrow C_3H_7$ $k_1 = 1.61 \pm 0.04 \times 10^{-12}$ cm^3 mol c^{-1} s^{-1}.
The temperature dependence of the H atom addition was investigated at 50 torr total pressure over the temperature range 177–473 °K. Analysis of the data below room temperature gives the following Arrhenius parameters for addition to the terminal olefinic position: $K_{\delta 1}^{50} = (10.18 \pm 0.26) \times 10^{13} \exp[-(1211 \pm 11)/1.987T]$ cm^3 mol c^{-1} s^{-1}. Deviations from this dependence above 298 °K can be assigned to non-terminal addition, H atom abstraction, and increased decomposition of the excited propyl radicals.

Lamb, V. A., Johnson, C. E., Valentine, D. R., **Physical and mechanical properties of electrodeposited copper, III. Deposits from sulfate, fluoborate, pyrophosphate, cyanide, and amine baths.** *J. Electrochem. Soc.* **117,** *Nos. 9, 10, 11, 291C–318C, 341C–352C, 381C–404C (Sept., Oct., Nov. 1970).*

Key words: Annealing-electroylic copper; electrodeposited copper; impurity content; properties of mechanical structure.

This paper is the third published report on the results of a broad program on properties of electrodeposited copper, sponsored jointly by the American Electroplaters' Society, The International Copper Research Association, Inc., The Copper Development Association, and the National Bureau of Standards. The first paper is a comprehensive review of the literature to 1965. The second paper is an interim report on experimental results. The present and final paper, which incorporates the data in the second, includes data from the baths designated in the title, for deposits prepared under a wide range of operating conditions and with use of a variety of addition agents. Properties measured include tensile strength, yield strength, elongation, modulus of elasticity, fatigue limit, hardness, internal stress, density, electrical resistivity, and thermal expansivity. Properties were measured for as-plated deposits, deposits after annealing at several temperatures, after cold-working, and at low and high ambient temperatures. Structure of deposits was examined by optical, electron micrograph, and x-ray methods. Content of impurities in deposits was determined. Correlations are developed among properties, structure, impurity content, type of bath, and operating conditions.

Larsen, N. T., Clague, F. R., **The NBS type II power measurement system,** *Proc. 25th Annual 1970 Instrument Society of America Conf. and Exhibit, Philadelphia, Pa., October 26–29, 1970, 11 pages.*

Key words: Bridge; leveler; microwave; power; self balancing; stabilizer.

The design, construction, and performance of a new solid state microwave power measuring system are described. The instrument consists of two modules—a self-balancing bolometer bridge and a reference generator. The reference generator is a multi-function module which may be used as either a 0.01 percent differential voltmeter with a 0 to 10 volt range, a 0 to 10 volt reference voltage source of 0.01 percent absolute accuracy, or a precision microwave power leveler. A six decade divider provides high precision in all three functions.

Laufer, A. H., **Low-temperature chromatographic determination of ketene and methyl ketene,** *J. Chromatogr. Sci.* **8,** *677–678 (Nov. 1970).*

Key words: Analysis; gas chromatography; ketene; methyl ketene.

This note describes the rapid, simultaneous analysis by conventional gas chromatography of both ketenes in small quantities.

Liu, Y. M., Coleman, J. A., **Electron radiation damage effects in silicon surface-barrier detectors,** *IEEE Trans. Nucl. Sci.* **NS–18,** *No. 1, 192–199 (February 1971).*

Key words: Alpha particles counting response; capacitance; detector noise; electron fluence; electrons radiation damage; front and rear contact; leakage current; silicon surface-barrier detector.

Silicon surface-barrier detectors have been irradiated at room temperature with monoenergetic electrons in the energy range of 200 keV to 1 MeV. The changes of detector reverse leakage current, noise, capacitance and alpha-particle counting response were determined. In general, detector current and noise increased with electron fluence and energy for electron energies of 400 keV and above. Detector capacitances tended to decrease slightly for electron fluences up to 10^{13} cm^{-2} and increase at higher fluences. No significant degradation of detector performance was observed as a result of irradiation with 200-keV electrons for fluences up to $10^{16}/cm^2$. The effects of damage on detector performance were reduced when the rear, aluminum contact was irradiated rather than the front, gold contact.

Lloyd, E. C., Editor, **Accurate characterization of the high-pressure environment,** *Proceedings of a Symposium held at the National Bureau of Standards, Gaithersburg, Maryland, October 14–18, 1968, Nat. Bur. Stand. (U.S.,), Spec. Publ. 326, 343 pages (March 1971) $4.50, SD Catalog No. C13.10:326.*

Key words: Accurate measurement; equation-of-state; fixed points; high pressure; high-pressure equipment; instrumentation; pressure scale; shock wave technique; temperature.

The volume contains 38 papers prepared for the Symposium on Accurate Characterization of the High-Pressure Environment held on October 14–18, 1968, at Gaithersburg, Maryland, under the sponsorship of the National Bureau of Standards and the Geophysical Laboratory of the Carnegie Institution of Washington. The papers are presented with the discussions that occurred during the sessions. The book also includes reports of several informal committees of the conferees on choices of reference pressure materials and on other matters relevant to improved measurement and calibration. The Symposium was intended to provide an authoritative survey of problems and techniques presently in use or proposed for precise high-pressure measurement and for temperature measurement at high pressure.

Lutz, G. J., **Photon activation analysis—A Review,** *Anal. Chem.* **43,** *No. 1, 93–104 (January 1971).*

Key words: Bremsstrahlung; carbon; electron accelerators; nitrogen; oxygen; photon activation analysis; review; sensitivities.

Prior to the availability of high energy electron accelerators, photon activation analysis was limited to the determination of deuterium and beryllium with isotope sources. During the past fifteen years, however, the development of high current cyclic and linear electron accelerators has made possible many analyses not readily accomplished by other methods. These include the determination of beryllium and deuterium with isotope sources, accelerator produced photons and nuclear considerations in photon activation analysis, determination of carbon, nitrogen and oxygen, determination of the heavier elements with emphasis on biological, geochemical, oceanographic and forensic matrices, and errors and corrections in photon activation analysis.

McCaa, W. D., Jr., Nahman, N. S., **Generation of reference waveforms by uniform lossy transmission lines,** *IEEE Trans. Instr. Meas.* **IM–19,** *No. 4, 382–390 (November 1970).*

Key words: Lossy uniform transmission lines; oscilloscope errors; pulse generators; standard waveforms.

This paper describes a method for generating fractional nanosecond pulse waveforms of known shape thereby providing an a priori means for establishing reference waveform generators or standards to be used in pulse measurements and other applications. The method employs the bandlimiting properties of a lossy uniform transmission line to produce a known waveform and generator impedance. A theory for generator characterization and application is presented which defines a given generator in terms of time domain or frequency domain functions. A new term called the "available" waveform is defined. RMS error is employed as the error criteria.
An example of generator design is given which employes planar skin effect loss and provides an output response having 0.2% RMS error over the interval $0 \leq t \leq 600$ picoseconds referred to the inherent step response of the waveshaping line. The input transition generator is assumed to be a 30 picosecond unit ramp generator. Also, an application example is given which employs a reference waveform generator to evaluate a sampling oscilloscope. The reference waveform generator uses a Debye Dielectric lossy transmission line.

McConnell, P. M., Daney, D. E., Kirgis, J. B., **Thermoelastic expansion and creep of polyethylene terephthalate and polypyromelitimide film and polyethylene terephthalate fibers from 20 to 295 K,** *J. Appl. Phys.* **41,** *No. 13, 5066–5070 (Dec. 1970).*

Key words: Longitudinal; polyethylene terephthalate; polypyromelitimide; relative creep; thermoelastic; transverse.

A quartz tube dilatometer was used to measure the lineal thermal expansion and creep of single lengths of polyethylene terephthalate (PETP) film, Mylar, polypyromelitimide (PPMI) film, Kapton, and PETP multi-fiber yarn, Dacron, while stressed under constant tension. Tensions below and above the conventionally defined yield strength were used and the sample temperature ranged from 20 to 295 K. Relative creep strain measurements, taken at the constant temperatures 77, 195 and 295 K, were found to obey the equation

$$\epsilon = \exp\left[-2.3 \exp\left(A' y\right)\right]$$

where y is a function of stress, time, and temperature and A' is a constant depending on the material. This equation was used to correct the thermoelastic expansion measurements for creep at the higher stresses. PETP multi-fiber yarn subjected to a slight tension was found to elongate during cooldown from 293 to 20 K. Higher stresses caused less elongation; i.e., the coefficient of expansion increased with stress. This result is believed to be due to changes in crystallanity at the higher stresses. A similar stress effect was found with PETP film but not with PPMI film. The thermoelastic expansivity of the film samples was also found to be sensitive to the thickness.

McDonald, D. G., Evenson, K. M., Wells, J. S., Cupp, J. D., **High-frequency limit of the Josephson effect,** *J. Appl. Phys.* **42,** *No. 1, 179–181 (Jan. 1971).*

Key words: Detectors; infrared; Josephson effect; lasers; superconductivity.

Coherent detection of applied radiation via a Josephson current-step has been achieved with an applied frequency approximately a factor of 3 higher than reported heretofore. The detected signal is at

2.5 THz (118 μm). The inadequacy of existing theory to predict the frequency dependence of the Josephson effect is discussed.

McLaughlin, W. L., Hussmann, E. K., Eisenlohr, H. H., Chalkley, L., **A chemical dosimeter for monitoring gamma-radiation doses of 1–100 krad,** *Intern. J. Appl. Radiation Isotopes* **22,** *135–140 (1971).*

Key words: Chemical dosimeter; disinfestation; dosimeter; dyes; gamma rays; insect sterilization; shelf-life extension: sprouting inhibition.

A simple chemical dosimeter is described for measuring gamma-ray doses useful for insect sterilization, seed-sprouting inhibition, and food shelf-life extension. The solutions, colorless before irradiation, assume a stable blue-violet color when irradiated to absorbed doses from 1 to 100 kilorads. The readout may be made either visually, colorimetrically, or spectrophotometrically. The optical density is linear with dose, and the response does not vary with dose rate.

Mackay, D. R., **Technical Standards Coordinator, Editorial format for Voluntary Product Standards. Part I. Contents of a Voluntary Product Standard,** *Nat. Bur. Stand. (U.S.), Prod. Stand. 0–70, 13 pages (March 1971) 15 cents, SD Catalog No. C13.20/2:0–70. Supersedes PS 0–67.*

Key words: Editorial format; format; product standards; standard; voluntary product standards.

This publication is intended to assist individuals, organizations, and agencies which are concerned with the writing of standards. It establishes and describes the material to be contained in a standard and provides specific instructions for writing standards. It is primarily intended for those developing initial drafts of standards to be submitted to the Bureau under the *Procedures for the Development of Voluntary Product Standards* published by the Department of Commerce.

Mandel, J., **A new analysis of variance model for non-additive data.** *Technometrics* **13,** *No. 1, 1–18 (February 1971).*

Key words: Factorial experiments; interaction; non-additivity; principal components; surface fitting; two-way arrays.

A method is presented for the analysis of data representing functions of two variables, when the response can be tabulated in a rectangular array. The procedure is based on a partitioning of the row by column interaction effects into a sum of terms, each of which is the product of a row factor by a column factor. The factors in each term are estimated by a method involving the extraction of characteristic roots.
The method contains as special cases a number of procedures used for the handling of non-additivity in two-way arrays. It is very useful for the fitting of empirical surfaces, but is also applicable to cases in which the data depend on qualitative rather than quantitative factors.
Comparisons with other techniques are made and an illustrative example is given.

Mangum, B. W., Thornton, D. D., **Vibrating sample magnetometer for use at very low temperatures and in high magnetic fields,** *Rev. Sci. Instr.* **41,** *No. 12, 1764–1766 (December 1970).*

Key words: Bimorph; cryogenic; low-temperature; magnetometer; piezoelectric; vibrating-sample magnetometer.

A high-sensitivity vibrating-sample magnetometer, for use at the very low temperatures produced by a ^{3}He refrigerator or by a ^{3}He-^{4}He dilution refrigerator is described. It can be made extremely compact by the use of a piezoelectric element as the vibrator. The complete magnetometer can be placed in the cryostat between the poles of an electromagnet, and can be operated at high applied magnetic fields.

Manning, J. R., **Correlation effects and activation energies for diffusion in alloys** *(Proc. Conf. Atomic Transport in Solids and Liquids, Marstand, Sweden, June 1970), Z. Naturforsch.* **26A,** *No. 1, 69–76 (Jan. 1971).*

Key words: Activation analysis; concentrated alloys; correlation factor; diffusion; random alloy; vacancies.

The problems involved in calculating correlation factors for diffusion in dilute alloys can be contrasted to those arising in concentrated solid solutions. As one moves from the pure element to the dilute alloy to the concentrated alloy, the calculation becomes progressively more difficult. Because of the complex atom configurations which can occur in concentrated alloys, it usually is not possible to calculate correlation factors in these alloys exactly.
Several important simplifications are available in nondilute random alloys. A large reduction in complexity can be secured by using a random alloy model where each atom is treated as diffusing in a uniform matrix, with the matrix properties being determined by the composition and jump frequencies in the alloy. Resulting equations in this random alloy model can be expressed directly in terms of the experimentally measurable tracer diffusion coefficients with no unknown vacancy jump frequencies appearing. Also these equations have the advantage of being in simple analytic form and not requiring numerical methods to evaluate the correlation factors. These two features make possible the direct expression of the temperature dependence of the correlation factor in terms of the experimental activation energies.
Equations are found for $\Delta H/\Delta Q$ in random binary cubic alloys, where ΔH is the difference between the activation enthalpies for diffusion of the two species and ΔQ is the difference between the experimentally measured activation energies of the two species. This ratio is never less than unity and can be much larger than unity. Values are plotted for diamond, body-centered cubic and face-centered cubic structures. From the magnitude and composition dependence of $\Delta H/\Delta Q$, it is concluded that the temperature dependence of the correlation factor cannot by itself explain the difference between the activation energies measured from tracer diffusion and from internal friction in the non-dilute range.

Marsden, C. P., Editor, **Silicon device processing.** *Proceedings of a Symposium held at Gaithersburg, Maryland, June 2–3, 1970, Nat. Bur. Stand. (U.S.), Spec. Publ. 337, 467 pages (Nov. 1970) $5.50, SD Catalog No. C13.10:337.*

Key words: Analysis; device processing; diffusion; epitaxy; junctions; resistivity; surface preparation.

This Proceedings contains the information presented at the Symposium on Silicon Device Processing held at the National Bureau of Standards on June 2–3, 1970.
This Symposium covered the measurement field and was purposefully restricted to the generic topics of diffusion, epitaxy, surface preparation and interdependence of unit processing operations. This emphasis on measurement during the processing operation or on the characteristics of the processed material, showed the necessity and more important, the ambiguities of current methods of measurement. The application of some new techniques to measurement were also discussed.

Marshak, H., Dove, R. B., **A right angle ^{3}He cryostat incorporating a high field superconducting solenoid,** *Nat. Bur. Stand. (U.S.), Tech. Note. 562, 22 pages (Dec. 1970) 30 cents, SD Catalog No. C13.46:562.*

Key words: ^{3}He cryostat; ^{3}He refrigerator; nuclear orientation; superconducting solenoid.

Construction and operation of a novel ^{3}He cryostat, incorporating a large superconducting solenoid mounted at right angles to the cryostat's vertical axis, is described. This new cryostat which is part of the transportable National Bureau of Standards ^{3}He refrigerator, has been used successfully for nuclear orientation studies at the Atomic Energy Research Establishment, Harwell, England.

Martin, J. F., **Standard Reference Materials: National Bureau of Standards-U.S. Steel corporation joint program for determining oxygen and nitrogen in steel,** *Nat. Bur. Stand. (U.S.), Spec. Publ. 260–26, 40 pages (February 1971) 50 cents, SD Catalog No. C13.10:260–26.*

Key words: Inert gas fusion; one ppm of oxygen and nitrogen in steel; research associate program; simultaneous determination of oxygen and nitrogen; standard reference material for oxygen.

Because of a need for a method for the rapid, simultaneous determination of small concentrations of oxygen and nitrogen in steel, a joint project under the Industrial Fellowship Program of U.S. Steel and the Research Associate Program of the National Bureau of Standards (NBS) was established. After investigation of various techniques, an analytical apparatus was constructed with excellent sensitivity for both elements. This apparatus consists of an inert gas fusion system coupled to a gas chromatograph. Recommended modifications have been completed on this equipment, and simultaneous determinations of oxygen and nitrogen in steel are presently being made. The detection limit is < 1 ppm for both oxygen and nitrogen, and the analysis time is about 5 minutes.
A direct result of this program has been the issuance by NBS of a new Standard Reference Material (SRM), a maraging steel, for oxygen. This SRM has the lowest oxygen concentration (4.5 ppm) of any steel standard yet issued by NBS.

Mason, H. L., Editor, **Innovative metrology—key to progress,** *Proceedings of the 1970 Standards Laboratory Conference, Nat. Bur. Stand. (U.S.), Spec. Publ. 335, 132 pages (Mar. 1971) $1.50, SD Catalog No. C13.10:335.*

Key words: Metrology management; National Conference of Standards Laboratories; physical measurement; proceedings NCSL.

The biennial Standards Laboratory Conference of the National Conference of Standards Laboratories convened at the Gaithersburg facilities of the National Bureau of Standards June 15–17, 1970. The theme of the meeting, Innovative Metrology—Key to Progress, was amplified by 23 papers presented at technical sessions devoted to new technologies and applications, laboratory management and operations, new methods of optimizing calibration intervals, new ways of managing, and new international developments.

Meinke, W. W., **Standard reference materials for clinical measurements,** *Anal. Chem.* **43,** *28A–47A (May 1971).*

Key words: Clinical chemistry; organic SRMs; standard reference materials; spectrophotometry SRMs.

The NBS Program in Standard Reference Materials for Clinical Chemistry measurements is described. Each of the SRMs issued in this area in the last five years is discussed. Future directions of the program are also mentioned.

Menis, O., Editor, **Status of thermal analysis.** *Proceedings of a Symposium on the Current Status of Thermal Analysis Held at Gaithersburg, Maryland, April 21–22, 1970, Nat. Bur. Stand. (U.S.), Spec. Publ. 338, 189 pages (Oct. 1970) $1.00, SD Catalog No. C13.10:338.*

Key words: Atherosclerotic plaque; DSC; elastomers and vulcanizates; explosives; high temperature DTA; kinetics by TGA; selection of DTA parameters; temperature standards; TGA; theory of isoperibol and adiabatic shield calorimeters.

The symposium papers offer contributions in differential thermal analysis (DTA), differential scanning calorimetry (DSC), development of standards for DTA temperature scales, and applications in high temperature biochemical, polymer and explosive materials. The selection and the effect of experimental parameters on the types of information on thermal curves is described. The measurement theory of isoperibol and adiabatic shield calorimeters by the method of intermittent heating is described and the magnitude of calorimetric instrumental errors is outlined. In an analysis of a differential scanning calorimeter, three instrumental time constants are described and the necessary corrections for the various instrumental and thermal time constants are recommended. The need for and the status of temperature scale standards for DTA is discussed. An evaluation of 12 materials for use as standards by cooperating laboratories is presented. High temperature (> 1900 K) DTA, problems of high temperature calorimetry to 1300 K are discussed. The implications concerning the nature of biological membranes and decomposition of atherosclerotic plaques are derived from differential scanning calorimetry of three-component systems of phospholipid, cholesterol or one of its esters and water. A description is given of an apparatus developed for measuring the rate at which vapors are evolved during the thermal degradation of material in a modified thermogravimetric apparatus. The modifications of a DTA cell to minimize explosions is described. Data derived from the use of lead azide was used to evaluate the technique. Thermogravimetric analysis for establishing basic composition of elastomer compounds and vulcanizates were reviewed. A careful study of oxidation characteristics of carbon black in the formulation is also included.

Menis, O., Rains, T. C., **Sensitivity, detection limit, precision and accuracy in flame emission and atomic absorption spectrometry, Chapter 2, Analytical Flame Spectroscopy, Selected Topics,** R. Mavrodineanu, Ed., *pp. 47–77 (Springer-Verlag Publishing Co., New York, N.Y., 1970).*

Key words: Accuracy; atomic absorption; detection limits; differential method sensitivity; flame emission; nonaqueous media; precision; tables.

This chapter on sensitivity, detection limits, precision and accuracy in Flame Emission and Atomic Absorption spectrometry discusses the principles, definitions and methodology in establishing and evaluating these criteria. The various instrumental components and their optimum operation are described to enable the analyst to achieve these goals. Tables of data for all reported elements are presented for the current results on detection limits and sensitivity. The problem associated with the environment of the analyte and the effect of nonaqueous media are discussed from the standpoint of enhanced sensitivity. Finally the criteria for attaining improved precision and accuracy are discussed and the role of the differential method, ionization buffers and standard additions is discussed.

Moore, C. E., **Selected tables of atomic spectra. A Atomic energy levels-second edition. B Multiplet tables. C I, C II, C III, C IV, C V, C VI. Data derived from the analyses of optical spectra,** *Nat. Stand. Ref. Data Ser., Nat. Bur. Stand. (U.S.), 3, Sec. 3, 71 pages (Nov. 1970) $1.00, SD Catalog No. C 13.48:3/sec. 3.*

Key words: Atomic energy levels, carbon spectra; atomic spectra of carbon; carbon spectra; multiplet tables, carbon spectra; spectra, carbon; wavelengths, carbon spectra.

The present publication is the third Section of a series being prepared in response to the persistent need for a current revision of two sets of tables containing data on atomic spectra as derived from analyses of optical spectra. As in the the first two Sections, Part A contains the atomic energy levels and Part B the multiplet tables. All six spectra of carbon, C I through C VI are included. The form of presentation is described in detail in the text to Section 1, and need not be repeated here.

Motz, J. W., Dick, C. E., Lucas, A. C., Placious, R. C., Sparrow, J. H., **Production of high-intensity K x-ray beams,** *J. Appl. Phys.* **42,** *No. 5, 2131–2133 (April 1971).*

Key words: Beryllium to gold; electron produced; high intensity; monochromatic yields; purity; x-ray beams.

K x-ray beams are produced by direct electron excitation in beryllium, carbon, aluminum, titanium, copper, silver, and gold targets. With excitation currents of 10 milliamperes from d.c. electron accelerators or 1000 amperes from single pulse machines, the K x-ray yields are respectively 4 to 9 orders of magnitude larger than the yields produced by the conventional fluorescence method. The bremsstrahlung contamination in the K x-ray beam is minimized by observing the K x-rays at 180 degrees with respect to the incident electron beam, in order to exploit the fact that the bremsstrahlung intensities become more peaked in the forward direction as the electron energy increases. Values are given for the maximum yields and purities of the K x-ray beams with the corresponding electron energies, and a comparison is made with values obtained by other methods involving atomic ion or photon excitation of K x-rays.

Mukerjee, P., Mysels, K. J., **Critical micelle concentrations of aqueous surfactant systems,** *Nat. Stand. Ref. Data Ser., Nat. Bur. Stand. (U.S.), 36, 227 pages (Feb. 1971) $3.75, SD Catalog No. C13.48:36.*

Key words: Association colloid; bibliography; CMC; colloid; colloidal electrolyte; critical concentration; critical micelle concentration; detergent; hydrophobic bonding; Krafft point; long chain compounds; micelle; paraffin chain salts; selected values; soap; solubilization; standard values; surface active agents; surface chemistry; surface tension; surfactant.

Critical micelle concentrations (CMC's), have been collected, organized and evaluated. The literature has been scanned for numerical values from 1926 up to and including 1966. In addition, over 800 values, hitherto available only in graphical form or implied in experimental data, have been extracted from the publications and are included. Close to 5,000 entries, based on 333 references, dealing with 720 compounds are tabulated in the main tables. Whenever available, the temperature, any additives present, the method of determination and the literature source are given for each CMC value and an indication of the apparent quality of the preparation and method used are included. A shorter table gives selected values which are believed to be particularly reliable, including highly accurate ones. Among these, concordant values from at least two independent laboratories are emphasized.
Included in the Introduction is a general discussion of the importance and significance of CMC values and of methods for their determination, as well as a summary of the procedures used in the collection, evaluation and presentation of these values in the present work. Extensive indexes are provided.

Murphey, W. M., Caswell, R. S., **Analysis of results of the Bureau International des Poids et Mesures thermal neutron flux density intercomparison,** *Metrologia* **6,** *No. 4, 111–115 (October 1970).*

Key words; Data analysis; flux density; intercomparisons; least squares; standards; thermal neutrons.

The results of an international comparison of thermal neutron flux density standards sponsored by the Neutron Working Group of the Bureau International des Poids et Mesures have been analyzed using a method conceptually different from a companion analysis by Axton. Both methods, however, yield closely the same results. All individual values are within $\pm 2.6\%$ of the adjusted value, the average absolute deviation being about 1%.

Napolitano, A., Hawkins, E. G., **Standard Reference Materials: Viscosity of a standard borosilicate glass (Certification of Standard Reference Material 717),** *Nat. Bur. Stand. (U.S.), Spec. Publ. 260–23, 10 pages (Dec. 1970) 25 cents, SD Catalog No. C13.10:260–23.*

Key words: Beam-bending; borosilicate glass; glass viscosity; parallel-plate; rotating cylinder; standard reference material; viscosity; viscosity standard.

The viscosity of a borosilicate glass has been measured at the National Bureau of Standards and four other laboratories. Determinations were made in the range 10^8 to 10^{15} poises (1525 to 470 °C). Measurements were made by the rotating cylinder, fiber elongation, beam bending, and parallel-plate methods. The results have been evaluated and the glass has been issued as Standard Reference Material No. 717.

Neill, A. H., Jr., **Wet traction of tractionized tires,** *Nat. Bur. Stand. (U.S.) Tech. Note 566, 14 pages (Feb. 1971) 20 cents, SD Catalog No. C13.46:566.*

Key words: Siping; stability; stopping distance tires; traction; tractionizing.

A series of dynamic vehicle tests was performed at NBS to evaluate the performance of tractionized or siped tires. Stopping distance and lateral breakaway data is presented from a two wheel diagonally braked automobile which clearly shows that siped tires do not represent any improvement in the lateral stability or stopping distance characteristics of a typical passenger automobile.

Nimeroff, I., **Color-match classification by variable parameters, Color.** *Engr.* **9,** *No. 2, 13–17 (March-April 1971).*

Key words: Classification; color; color-match; isomerism; metamerism.

There is an increasing need for standard procedures by which to assess the nature of achieved color matches. It has been found that there are seven different classes of color matches in which the colorimetric parameters, the spectral characteristics of observer, source and specimen, are variable. The different classes result from the seven possible combinations of these three variable parameters, taken one, two and three at a time. Those matches in which one parameter varies are called, in accord with the variable parameter, observer-variable, source-variable or specimen-variable matches; those in which two parameters vary are called source-specimen-variable, source-observer-variable, or specimen-observer-variable matches; those in which all three vary are called source-specimen-observer-variable matches. Three of these classes of color match are currently designated metameric matches, one class is currently designated spectral match, while the other three classes have no current designation. The colorimetric effect of spectral differences in all of these classes of color matches may be charac- developed by Nimeroff and Yurow for matches that are currently designated metameric matches. A generalization of this index and its applications are presented.

Ogburn, F., Shives, T. R., Brady, C. H., **Calibration of a filar micrometer,** *J. Mater.* **6,** *No. 1, 60–66 (March 1971).*

Key words: Metal coatings; micrometers; microscopes; optical equipment; optical microscopes; thickness; thickness gages.

The precision with which a filar micrometer can be calibrated against a fixed interval of a stage micrometer was determined at magnifications of about 175 and 1900 for a group of 15 individuals familiar with microscopes. At each magnification the spread of measurements among the 15 operators was about 0.8 percent, whereas the spreads for the individual operators were substantially less.

Osinsky, V. I., Winogradoff, N. N., **Excitation and temperature dependence of band-edge photoluminescence in gallium arsenide,** *Phys. Rev.* **B. 3,** *No. 10, 3341–3346 (May 15, 1971).*

Key words: Gallium arsenide lasers; impurity effects; intensity dependence; radiative recombination.

Photoluminescent spectra of *n*-type GaAs were studied as a function of the excitation intensity, temperature, and doping level. The spectra consisted of two major bands representing radiative band-to-band recombination and radiative transitions through impurity centers, respectively. The intensity of the peak of the former went through a minimum and a maximum as the temperature was increased from 175 to 500 °K. The temperature corresponding to the above maximum increased as the excitation intensity was decreased or the doping level increased. These results suggest that the temperature dependence of the peak intensity in band-to-band transitions is primarily due to the thermal distribution of the carriers over the available energy states. The peak intensity would therefore normally be expected to decrease monotonically with an increase in temperature, while the above maxima and minima represent perturbations imposed by the presence of temperature dependent transitions through radiative or nonradiative impurity recombination centers.

Page, C. H., **Comments on "Nonlinear resistors that generate subharmonics,"** *Proc. IEEE Letters* **59,** *No. 2, 301 (Feb. 1971).*

Key words: Nonlinear; subharmonics.

The analysis reported by Erdey is shown to be incorrect.

Page, C. H., Vigoureux, P., Editors, **The international system of units (SI),** *Nat. Bur. Stand. (U.S.), Spec. Publ. 330, 42 pages (Jan. 1971), 50 cents, SD Catalog No. C13.10:330.*

Key words: General conference of weights and measures; international committee of weights and measures; international system of units; SI; système international des unités; units of measurement.

This translation from the French "Le Système International d' Unités", (SI) published originally by the International Bureau of Weights and Measures (BIPM) has been prepared jointly by the National Physical Laboratory, UK, and the National Bureau of Standards, USA. Included are Resolutions and Recommendations of the General Conference of Weights and Measures (CGPM) on the International System of Units, together with relevant extracts from the International Organization for Standardization (ISO) for the practical use of the system.
Appendix I gives in chronological order the decisions promulgated since 1889 by CGPM and the International Committee of Weights and Measures (CIPM) on units of measurement and on SI. Appendix II outlines the measurements, consistent with the theoretical definitions given in this document, which metrological laboratories can make to realize the units and to calibrate precision material standards.

Parks, E. J., **Thermal analysis of modified cellulose,** *Tappi* **54,** *No. 4, 537–544 (April 1971).*

Key words: Alum; aluminum; apparent activation energy; calcium; cellulose; crosslinking; differential; ion exchange; organic acid; oxycellulose; stability; sulfuric acid; thermal analysis; thermogravimetric analysis.

Differential thermal analysis (DTA) and thermogravimetric analysis (TGA) techniques have been applied to characterize thermal properties of cellulose and modifications of the type that might reasonably occur in papermaking pulps. Periodate, periodite-chlorite, chromate, chromate-chlorite, hypochlorous acid, and hypochlorous acid-chlorite oxycelluloses all were examined, as were their calcium and aluminum exchange products. In addition, the effects on thermal properties of cellulose exerted by alum, sulfuric acid, and two organic acids that cause color reversion all were investigated. The peak temperature of a massive decomposition endotherm (T_3), the apparent activation energy of this endothermic reaction (E^*) and the integral procedural decomposition temperature (ipdt) seem to be best suited of thermal variables to denote stability. Oxidation usually destabilizes cellulose slightly. An exception is exhaustive oxidation of periodate oxycellulose with chlorous acid. This causes T_3 and E^* to increase, although the ipdt drops. Exchange with calcium greatly stabilizes cellulose containing carboxyl groups, whereas aluminum destabilizes the same material. Each effect is concentration dependent. The importance of pH in these relationships is not known. Sulfuric acid has a destabilizing effect qualitatively different from that of aluminum covering carboxyls and that of alum added to cellulose. Destabilization by alum is probably a result of contributions both by sulfate and by aluminum. Organic acids have little effect.
Each treatment has resulted in a higher percentage of residue than that of cellulose, which indicates the promotion of crosslinking by oxygen, metals, and acid.

Paule, R. C., Mandel, J., **Analysis of interlaboratory measurements on the vapor pressures of cadmium and silver (Certification of Standard Reference Materials 746 and 748),** *Nat. Bur. Stand. (U.S.), Spec. Publ. 260–21, 30 pages (Jan. 1971), 35 cents, SD Catalog No. C13.10:260–21.*

Key words: Cadmium; components of error (within- and between-laboratory); heats of sublimation (second and third law); interlaboratory measurements; silver; standard errors; standard reference materials; vapor pressure.

Detailed statistical analyses have been made of results obtained from a series of interlaboratory measurements on the vapor pressures of cadmium and silver. Standard Reference Materials 746 (cadmium) and 748 (silver) which were used for the measurements have been certified over the respective pressure ranges $10^{-11}-10^{-4}$ atm and $10^{-12}-10^{-3}$ atm. The temperature ranges corresponding to these pressures are 350–594 K for cadmium and 800–1600 K for silver. The heats of sublimation at 298 K and the associated two standard error limits for cadmium and silver are 26660 ± 150 cal/mol and 68010 ± 300 cal/mol, respectively. Estimates of uncertainty have been calculated for the certified temperature-pressure values as well as for the uncertainties expected from a typical single laboratory's measurements. The statistical analysis has also been made for both the second and third law methods, and for the within- and between-laboratory components of error. The uncertainty limits are observed as functions of both the heat of sublimation and the temperature.

Peavy, S. T., Varner, R. N., Hogben, D., **Source listing of OMNITAB II program,** *Nat. Bur. Stand. (U.S.), Spec. Publ. 339, 371 pages (Dec. 1970) $4.75, SD Catalog No. C13.10:339.*

Key words: Accuracy; algorithms; ANSI FORTRAN; documentation; error checking; machine independent; OMNITAB II operating system subprograms; OMNITAB II source listing; programming techniques; transportable; user-oriented computing system.

OMNITAB II is a general-purpose interpretive computing system designed to allow a nonprogrammer to use a high-speed computer easily, accurately and effectively. The system permits the user to perform arithmetic operations including complex arithmetic, trigonometric calculations, miscellaneous function calculations, statistical analysis, Bessel function calculations, and operations on matrices and arrays.
The OMNITAB II system contains 177 subprograms written in the ANSI FORTRAN language. Every effort has been made to make the system transportable. This publication contains a complete listing of all these subprograms. The listing is preceded by a brief introduction which describes the programming techniques used; the use of system library functions; and the subprograms used to control the flow of operations in the OMNITAB system.

Phucas, C. B., **Technical Standards Coordinator, Package quantities of green olives,** *Nat. Bur. Stand. (U.S.), Prod. Stand. 40–70, 9 pages (May 1971) 10 cents, SD Catalog No. C13.20/2:40–70.*

Key words: Green olives, package quantities of; olives, green, package quantities of; package quantities of green olives.

This Voluntary Product Standard covers a range of package quantities that are recommended for green olives and establishes specific packaging requirements in terms of net drained weight. Methods of labeling products which comply with this Standard are provided.

Phucas, C. B., **Technical Standards Coordinator, Package quantities of instant mashed potatoes,** *Nat. Bur. Stand. (U.S.), Prod. Stand. 41–70, 8 pages (April 1971) 10 cents, SD Catalog No. C13.20/2:41–70.*

Key words: Instant mashed potatoes, package quantities of; mashed potatoes, instant, package quantities of; package quantities of instant mashed potatoes; potatoes, instant mashed, package quantities of.

This Voluntary Product Standard covers a range of package quantities based on servings and establishes the definition of a serving which is based on the weight of the reconstituted product.

Phucas, C. B., **Technical Standards Coordinator, Package quantities of instant nonfat dry milk,** *Nat. Bur. Stand. (U.S.), Prod. Stand. 37–70, 9 pages (April 1971) 10 cents, SD Catalog No. C13.20/2:37–70.*

Key words: Dry milk package quantities; instant nonfat dry milk; nonfat dry milk, package quantities of; package quantities of dry milk.

This Voluntary Product Standard covers package quantities of instant nonfat dry milk based on quart equivalents within the range of 3 to 20 quarts. It also establishes the weight of instant nonfat dry milk required to make 1 quart. This Standard covers all types of packages of instant nonfat dry milk intended for household use including those containing individual quart or multiquart equivalent envelopes.

Potzik, J., **A Method for determining the dynamic response of an elastic load cell element,** *Rev. Sci. Instr.* **41,** *No. 12, 1726–1731 (December 1970).*

Key words: Dynamic force; load cell; viscoelastic damping.

A method has been developed for determining the dynamic characteristics of a load cell element by subjecting it to sinusoidally time-dependent forces, and an experiment using a piezoelectric shaker is described which illustrates the feasibility of the method. At present a simple viscoelastic model is assumed for the load cell element, and relaxation times on the order of 10^{-7} seconds have been measured. The application of this information to load cells subjected to other types of dynamic forces is also discussed.

Preston, J. D., Forthofer, R. J., **Correlation of vehicle, dynamometer and other laboratory tests for brake friction materials,** *Proc. Society of Automotive Engineers Conf., Detroit, Michigan, January 11–15, 1971. Paper No. 710250, pp. 1–10 (1971).*

Key words: Brake friction materials; coefficient of friction; friction assessment screening test machine; friction materials test machine, girling scale dynamometer; inertia brake dynamometer; vehicle road tests.

The frictional properties of brake lining materials are greatly influenced by the manner in which they are used. Test procedures designed to measure the coefficient of friction of these materials can likewise produce widely differing results depending on the type of test conducted. This paper presents data illustrating the performance correlation of three commercially available brake lining materials when subjected to vehicle tests and some of the more commonly used laboratory test procedures.

Radlinski, R. W., Forthofer, R. J., Harvey, J. L., **Operating performance of motor vehicle braking systems as affected by fluid water content,** *Proc. Society of Automotive Engineering Conf., Paper No. 710253, pp. 1–11 (January 11–15, 1971).*

Key words: Automotive hydraulic brake fluids; brake fluids performance; braking systems; low temperature viscosity.

Automotive hydraulic brake fluids are known to pick up water in service. This paper shows that a major portion of the water picked up by the brake fluid in a braking system is transmitted through the hoses. It discusses two major effects of water pick-up on brake fluids performance—reduction in vapor lock temperature and increase in low temperature viscosity. Performance data for several "wet" brake fluids operating in actual braking systems at high and low temperatures are presented.

Ramboz, J. D., **A link-compensated ratio transformer bridge,** *Rev. Sci. Instr.* **42,** *No. 4, 522–524 (April 1971).*

Key words: Bridge; impedance; impedance bridge; measurement; ratio transformer; ratio transformer bridge.

A ratio transformer impedance bridge that is capable of measuring either capacitive or inductive impedances is described. It is made of commercially available laboratory apparatus and can yield measurements to an uncertainty of less than ± 0.1 percent. The unique feature is an injection transformer which reduces the effect of the interconnecting "link-resistance" between the unknown impedance and the bridge reference reactance. Five circuit variations of the bridge are shown and the equations which yield the solutions for the unknown resistance, capacitance, or inductance and phase angle are given.

Reitwiesner, G. W., **On computer performance measurement programming measuring indexing adroitness by isolating complex primes,** *Nat. Bur. Stand. (U.S.), Tech. Note 572, 25 pages (Apr. 1971) 35 cents, SD Catalog No. C13.46:572.*

Key words: Assessment; complex; composite; computer; criteria; evaluation; Gaussian primes; indexing; measurement; performance; prime; program; test.

This writing, describing a computer performance test program, is concerned not primarily with specific measurements, but rather with a procedure for making measurement regarding specific properties of computer operation.

The program is written in a particular problem-oriented programming language; therefore assessment perforce spans the effects of the computer hardware, of the programming language, and of the intervening compiler processes.

The objective of the test is to assess adroitness in certain indexing operations. Assessment is accomplished by measuring execution time of a recursive programming loop.

The test problem was chosen as a convenient artifice to use certain specific indexing-type operations in the programming employed for solution.

The test program performs a simple computation for which the solution is completely definitive, yet for which both the solution and the time for achieving it are variable under parameters whose values are introduced as program input data.

Richmond, J. C., Editor, **Space simulation.** *Proceedings of a Conference held at NBS Gaithersburg, Maryland, September 14–16, 1970. Nat. Bur. Stand. (U.S.), Spec. Publ. 336, 984 pages (October 1970), $5.25, SD Catalog No. C13.10:336.*

Key words: Ablation; particulate radiation; re-entry; space simulation; thermal radiation; vacuum; weightlessness.

This volume contains all of the papers presented at the Fifth Space Simulation Conference held at the National Bureau of Standards September 14–16, 1970, that were available for publication. The general scope of the conference was the effect of the space environment on materials, components, structures and man. The range of topics is too wide to permit a simple classification, but contamination, ablation, degradation of materials by the space environment and predictive testing account for approximately half of the papers presented. Other topics range from purely laboratory problems such as radiometry standards, calibration of vacuum gages, cryopumping and operation of space simulation facilities to gravity simulation, with neutral buoyancy for zero gravity and a man-rated centrifuge for high gravity, use of a drifting submarine to study the psychological aspects of long-duration missions in a space station, and simulation of (1) atmospheric balloon environments, (2) radiation from nuclear power sources, (3) solar wind, (4) micro-meteoroid bombardment, (5) soil friction on the moon and (6) the Martian atmosphere.

Risley, A. S., **The physical basis of Atomic Frequency Standards,** *Nat. Bur. Stand. (U.S.), Tech. Note 399, 54 pages (April 1971) 60 cents, SD Catalog No. C13.46:399.*

Key words: Atomic frequency standards; cesium beam; energy levels; hydrogen maser; hyperfine interaction; rubidium gas cell; transition probability.

A tutorial discussion of the physical basis of atomic frequency standards is given. These principles are then related to the conditions under which an atom can be used as the working substance of a stable and accurate frequency standard. The three primary examples of atomic frequency standards—the hydrogen maser, the cesium beam, and the rubidium gas cell—are then discussed in terms of these principles and conditions. The functions of the fundamental parts of each device become apparent through this development.

Robinson, D. C., **Determining of load errors in universal testing machines due to speed of testing,** *Mater. Res. Stand.* **11,** *No. 1, 14–17 (January 1971).*

Key words; Dynamic loading; load error; testing machine.

A modification of an American Society for Testing and Materials (ASTM) proposed method of determining errors in testing machines was used to measure the indicator errors caused by dynamic loading for three universal machines of different design. For each of the machines, load errors due to the lag of the indicator were found to be linearly related to the rate of applied load. Based on the experimental results, it appears that for testing machines of various design, the response of the indicating system to uniformly increasing loads resembles that of a proportional-error servomechanism which has a

"velocity-lag" steady-state error when following a ramp function input. A discussion is given of the variables which are found to be significant in determining the load errors for the three machines investigated. The essential components in the auxiliary load-measuring system were a load cell, a fast response digital voltmeter and a high speed still camera. The alternate method used was found to provide higher quality photographic information from which to determine the indicator errors than that obtained when using a moving picture camera as proposed in the ASTM procedure.

Rowland, G. A., **The increasing role of states in building codes and standards,** *Proc. 26th. Annual Conf. Reinforced Plastics, Composites Division, Washington, D.C., February 9–12, 1971, Section 5–B, pp. 1–3 (February 10, 1971).*

Key words: Interstate; intra-state; national conference of states on bldg. codes & stds.; uniformity.

Building codes promulgated, modified, and interpreted on a local basis have been deemed to be major deterrents to the development of reasonably large aggregated markets for many new or little-used materials needed in meeting the country's present and future building and housing requirements.
Since its inception in 1967, the National Conference of States on Building Codes and Standards has been increasingly active in promoting greater involvement of the States in the complex building regulatory system. The development of more competent technical procedures for accrediting new materials, including reinforced plastics, for acceptance statewide, and possibly nationwide, rather than city-by-city will be a very important contribution toward progress.
The responsibilities for health and safety constitutionally rests in the several states and the differences in their administration of this responsibility is now being seriously reviewed. The Conference in its three years of existence has been able to bring together delegates from the several states, establish working arrangements, and proceed in developing a program of study and recommendations for consideration by the Conference in solving many of the present building regulatory problems.
This national effort is a new, refreshing, coordinated approach towards what has been a rather chaotic, restrictive, individual approach to building regulations.
A current report of the National Conference of States on Building Codes and Standards and the aforementioned organizational structure and activities is presented.

Ruegg, F. C., **A circuit which expands the count storage capacity of a multichannel analyzer,** *Nucl. Instr. Methods* **92,** *7–11, (1971).*

Key words: Multichannel scaler; nuclear instrumentation; overflow counter.

A circuit has been designed which allows the experimenter to store up to 10^{10} counts/channel in a 10^5 count capacity multichannel analyzer. The circuit uses the analyzer's second subgroup to store the overflow counts of the first subgroup. The circuit was designed to be used with an analyzer operating in the multichannel scaling mode.

Scharf, K., **Spectrophotometric measurement of ferric ion concentration in the ferrous sulphate (Fricke) dosemeter,** *Phys. Med. Biol.* **16,** *No. 1, 77–86 (1971).*

Key words: Chemical dosimeter; chemical dosimetry; ferrous sulfate; ferrous sulfate dosimeter; ferric ions; Fricke dosimeter; radiation dosimeter; radiation dosimetry; spectrophotometry; spectrophotometric measurements.

A systematic error in the spectrophotometric measurement of ferric ion concentrations in the ferrous sulphate dosimeter may be made by an incorrect evaluation of a non-linear spectrophometric calibration curve. Methods are discussed for determining the radiation-produced change in molarity from the actual calibration curve, and a method of normalization of measured absorbances is suggested. Normalization factors, converting measured absorbances into normalized values, can either be calculated by choosing a reference value of the molar extinction coefficient, or can be determined by comparative absorbance measurements on two spectrophotometers, one of them to be a precision instrument. Normalized absorbances are proportional to molarity and may be considered to be free of errors due to instrumental parameters and inaccuracies in acidity and temperature of solutions, and of errors in molarity if derived by comparative measurements.

Schramm, R. E., **Corrections and calculations on a x-ray diffraction line profile: A computer program,** *Nat. Bur. Stand. (U.S.), Tech. Note 600, 34 pages (June 1971) 40 cents, SD Catalog No. C13.46:600.*

Key words: Computer programs, Fourier analysis; nickel steels; x-ray analysis; x-ray diffraction; statistics.

This computer program was written to perform corrections and make calculations on an x-ray diffraction profile before Fourier analysis. The corrections are for background and for variations of intensity with the Bragg angle. Also calculated are the separation of the $K\alpha_1 - K\alpha_2$ doublet and the centroid and position of peak maximum with their standard deviations. There is also an option to smooth the profile.

Scott, W. W., Jr., **New coaxial RF–DC ammeter,** *IEEE Trans. Instr. Meas.* **IM–19,** *No. 4, 318–323 (Nov. 1970).*

Key words: Ammeter; rf-dc, coax; thermopile radiation; infrared.

A unique new type of rf ammeter is described. The ammeter combines broad frequency coverage with broad current range and is designed for use in a 50-ohm coaxial transmission line. Thermal compensation is employed to reduce effects of most self-heating errors.
The ammeter consists of a cylindrical ellipsoidal silver reflector of infrared energy with a cylindrical thick-film heater along one focus and a heat sensing thermopile along the other focus. Advantages over older ammeter designs include a shielded construction with inherent electrical isolation between the rf and dc circuits, a large dc output (approximately 1 to 100 millivolts) corresponding to a decade dynamic range (0.5 to 5 amperes), and a frequency range from dc to about 1 GHz.
This coaxial ammeter is believed to be the first to have very low SWR (1.02) in a 50-ohm transmission line. Ammeters of lower current range can be built, but at a penalty of increased SWR due to the larger heater resistance required.

Selby, M. C., **The Bolovac and its applications,** *IEEE Trans. Instr. Meas.* **IM–19,** *No. 4, 324–331 (November 1970).*

Key words: Bolovac; microwave current measurements; microwave power measurements; microwave voltage measurements.

The Bolovac is a novel device for the standardization and measurement of TEM voltage, current, and power from below 1 MHz through 18 GHz (potentially through 36 GHz). It can be used for attentuation measurement and as a superior impedance termination at all the above-mentioned frequencies. To date it is the first and only practical means of calibrating microwave current indicators and of evaluating oscilloscopes displaying 25-ps or shorter rise-time pulses.
It is felt that application of the Bolovac will radically improve power measurements. It reduces the problems arising from mismatch-error uncertainties, one of the major present sources of concern in power measurement; measurement of complex reflection coefficients; complex computations; use of error-limit charts; and measurement of effective efficiency and calibration factors. Its application should radically increase optimum accuracy and measurement-time efficiency in calibration facilities outside the National Bureau of Standards.
The Bolovac together with an Rf generator can be used as a source of known voltage. It can also be used as an absorption power meter. It needs no RF calibration. It has a range as high as 40 dB depending on the desired precision and on whether one or more sensors (special bolometric disks) are used. Voltages down to 0.1 volt with accuracies of 0.5 percent and better (and corresponding power in 50-ohm systems) have been measured.
The paper describes the general features and application of the

Bolovac and lists references to more comprehensive papers on the subject.

Sieck, L. W., Searles, S., Ausloos, P., **High-pressure photoionization mass spectrometry. Photoionization of propane at 11.6–11.8 eV. Formation and reactivity of the $(C_3H_8)_2^+$ dimer ion,** *J. Chem. Phys.* **54,** *No. 91–95 (Jan. 1, 1971).*

Key words: Ion-molecule reaction; kinetics; mass spectrometry; photoionization; propane; radiation chemistry.

The major reaction path of the propane molecular ion with propane was found to be the formation of the dimer ion $(C_3H_8)_2^+$ via a termolecular mechanism;

$$C_3H_8^+ + C_3H_8 \xrightarrow{C_3H_8} (C_3H_8)_2^+ + C_3H_8$$

In addition, $C_3H_6^+$ and $C_3H_7^+$ were also found as minor reaction products at lower pressures. The reactions of the dimeric ions with ethylene and NO were also investigated. The charge exchange reaction

$$(C_3H_8)_2^+ + NO \rightarrow NO^+ + 2C_3H_8$$

was found in propane-NO mixtures, suggesting a recombination energy in excess of 9.24 eV. The formation of $C_3H_8NO^+$ was also detected at higher total pressures. The dimeric ion was also found to transfer H_2 to ethylene without affecting the structural integrity of the Carbon skeleton,

$$(C_3H_8)_2^+ + C_2H_4 \rightarrow C_6H_{14}^+ + C_2H_6$$

indicating that this species exhibits the chemical behavior of a saturated hydrocarbon ion.

Sixsmith, H., Giarratano, P., **A miniature centrifugal pump,** *Rev. Sci. Instr.* **41,** *No. 11, 1570–1573 (Nov. 1970).*

Key words: Centrifugal; helium; nitrogen; pump; pump design; pump performance.

A miniature centrifugal pump designed to circulate helium in a flow loop is described. It is designed to operate in the liquid helium temperature range under ambient pressures up to 100 atmospheres ($10^7 N/m^2$), producing a maximum flow rate of 50 cm^3/s and a maximum pressure rise of 0.5 psi (3400 N/m^2). The operating characteristics obtained from preliminary tests with cold nitrogen gas and an analysis of the performance are included.

Slattery, W. J., Editor, **An index of U.S. voluntary engineering standards,** *Nat. Bur. Stand. (U.S.), Spec. Publ. 329, 1,000 pages (Mar. 1971) $9.00, SD Catalog No. C13.10:329.*

Key words: Engineering standards, index of; index of standards, recommended practices, specifications, and test methods; Key-Word-In-Context index of voluntary standards; standards, voluntary, index of.

This computer-produced Index contains the permuted titles of more than 19,000 voluntary engineering and related standards, specifications, test methods, and recommended practices, in effect as of December 31, 1969, published by some 360 U.S. technical societies, professional organizations, and trade associations. The title of each standard can be found under all the significant key words which it contains. These key words are arranged alphabetically down the center of each page together with their surrounding context. The date of publication or last revision, the standard number, and an acronym designating the standards-issuing organization appear as part of each entry. A list of these acronyms and the names and addresses of the organizations which they represent are found at the beginning of the Index.

Smith, R. W., Jr., Conference Chairman, Editor, **Precoordination-basis for industrialized building,** *(Proc. Conf. Gaithersburg, Md., Sept. 24–26, 1969), Nat. Bur. Stand. (U.S.), Bldg. Sci. Ser. 32, 136 pages (Jan. 1971) $1.50, SD Catalog No. C13.29/2:32.*

Key words: Building; components; precoordination; standards.

The Conference entitled "Precoordination—Basis for Industrialized Building" was held at the National Bureau of Standards, Gaithersburg, Md., on September 24–26, 1969. The Conference was sponsored by the American National Standards Institute's Committee A62, Precoordination of Building Components and Systems, to explore the standards required to establish a basis for an industrywide system of building using interchangeable components. Coordinated components, conforming to these standards, will be compatible and interchangeable in both dimension and function and thereby offer unlimited opportunities for product and material selection as well as design flexibility.

Somes, N. F., Dikkers, D. R., Boone, T. H., **Lubbock tornado: A survey of building damage in an urban area,** *Nat. Bur. Stand. (U.S.), Tech. Note 558, 38 pages (Mar. 1971) 50 cents, SD Catalog No. C13.46:558.*

Key words: Anchorage; building performance; glazing; hailstones; masonry; mobile homes; roofs; structural engineering; wind load.

The Building Research Division of the National Bureau of Standards' Institute of Applied Technology sent a three-man team to investigate the damage to buildings and other structures caused by the tornado which struck Lubbock, Texas, on May 11, 1970. The team members—the authors of this report—carried out photographic surveys on the ground and from a helicopter on the days of May 14, 15, and 16, 1970. The report is based largely on data gathered during this period but includes some data provided by other agencies and individuals whose assistance is acknowledged in the report. The report concludes that current good practice in the design and construction of buildings and mobile homes would have greatly reduced the damage observed at Lubbock. It also notes that natural disasters provide full-scale tests of buildings and urges the development of performance criteria with respect to wind loads for certain building elements.

Spiegel, V., Jr., Murphey, W. M., **Calculation of thermal neutron absorption in cylindrical and spherical neutron sources,** *Metrologia,* **7,** *No. 1, 34–38 (Jan. 1971).*

Key words: Manganous sulfate bath; neutron source absorption; neutron source calibration; thermal neutron absorption.

A calculation of the thermal neutron self-absorption for cylindrical or spherical neutron sources has been made. The calculations are confirmed by the experimentally-measured difference in manganous sulfate bath activity for bare and cadmium-covered Pu-Be and Am-Be neutron sources. The calculation is done in single interaction approximation and assumes that the incident thermal neutron flux is isotropic. The source material may be fissionable and be covered by up to three cladding materials. A computer program has been written for the numerical calculations.

Speigel, V., Jr., Murphey, W. M., **Computer code for the calculation of thermal neutron absorption in spherical and cylindrical neutron sources,** *Nat. Bur. Stand. (U.S.), Tech. Note 576, 25 pages (May 1971) 35 cents, SD Catalog No. C13.46:576.*

Key words: Manganous sulfate bath calibration of neutron sources; neutron; neutron standards.

A computer code has been written in FORTRAN IV for the calculation of thermal neutron absorption in spherical and cylindrical neutron sources. The formalism of the calculation, the structure of the computer code, a listing of the code, and some sample results are presented. The comparison of the results of this calculation to experiment appears elsewhere (1).

Spijkerman, J. J., Travis, J. C., Pella, P. A., DeVoe, J. R., **Preliminary study on the characteristics and design parameters for a Mossbauer resonant detector,** *Nat. Bur. Stand. (U.S.), Tech. Note 541, 65 pages (Jan. 1971), 65 cents, SD Catalog No. C13.46:541.*

Key words: Conversion electrons; iron; Mössbauer Spectroscopy; resonant detector.

448-719 OL - 72 - 5

Progress in the design and fabrication of a resonant detector for Mössbauer Spectroscopy is described. This report begins with a review of all of the methods of detection for this spectroscopy and describes the expected advantages of the resonant detector. If one uses conversion electron detection, considerable enhancement in signal to noise ratio and decrease in linewidth may be realized. Efforts to produce an iron bearing resonant material are described.

Sullivan, D. B., Peterson, R. L. Kose, V. E., Zimmerman, J. E., **Generation of harmonics and subharmonics of the Josephson oscillation,** *J. Appl. Phys.* **41,** *No. 12, 4865–4873 (November 1970).*

Key words: Josephson effect; superconductivity.

The observation of harmonics and subharmonics of the Josephson oscillation is shown to be in agreement with a rather simple model of the junction. The generation of harmonics provides an explanation of induced steps in the current-voltage characteristic which occur at submultiples of the usual induced step voltages. The subharmonic oscillation is seen to be a relaxation-like process which can be easily understood in terms of a mechanical analog.

Taylor, B. N., **Report on the International Conference on Precision Measurement and Fundamental Constants,** *held at the National Bureau of Standards, Gaithersburg, Md., Aug. 3–7, 1970, Metrologia* **7,** *No. 1, 39–42 (Jan. 1971).*

Key words: Fundamental constants; least squares adjustments; precision measurements.

This is a report on the International Conference on Precision Measurement and Fundamental Constants held at the National Bureau of Standards, Gaithersburg, Maryland, August 3–7, 1970. It includes a brief discussion of the purpose and significance of the Conference as well as some of the organizational details as they pertain to the Conference sponsors, topics covered, publication of the Conference Proceedings, etc. The bulk of the report is devoted to a summary by topic of the Conference highlights and conclusions.

Thurber, W. R., **Determination of deep impurities in silicon and germanium by infrared photoconductivity,** *Nat. Bur. Stand. (U.S.), Tech. Note 570, 13 pages (Mar. 1971) 25 cents, SD Catalog No. C13.46:570.*

Key words: Deep impurities; germanium; infrared; photoconductivity; photoresponse; semiconductors; silicon.

The feasibility of using infrared photoresponse and photoconductivity measurements to study deep impurities in germanium and silicon is examined by reviewing the literature. It is concluded that photoconductivity is useful in detecting the presence of specific impurities because each impurity has a long wavelength cut off in response associated with its ionization energy. However, when there are several deep impurities in the same specimen, it is difficult to be certain of detecting each one because some have broad cut offs and many have nearly the same ionization energies. Photoconductivity as a general technique has serious limitations for determining the total concentration of deep impurities. The equations for determining impurity concentration from the magnitude of the photoconductivity signal depend on the relative influence of deep and shallow centers. Equations are derived for several situations and experimental results from the literature are discussed for each one. Only uncompensated centers are available for photoionization and therefore the total concentration can not be obtained directly. In some situations the response due to a deep center is independent of its concentration. Other techniques for studying deep impurities are discussed briefly.

Tighe, N. J., **Microstructure of fine-grain ceramics,** *(Proc. 15th Sagamore Army Materials Research Conf., Sagamore Conference Center, Raquette Lake, N.Y., Aug. 20–23, 1968), Chapter in Ultrafine-Grain Ceramics, pp. 109–133 (Syracuse University Press, Syracuse, N.Y., 1970).*

Key words: Alumina; Al_2O_3; ceramics; electron microscopy; fine-grain ceramics; ion bombardment; magnesia; MgO; microstructure; rock; zirconia.

This describes the use of transmission electron-microscopy to characterize the microstructure of fine-grain ceramics. Observations have been made on a number of polycrystalline materials including alumina, magnesia, zirconia, metal-ceramic composites, and rock specimens.
Thin sections were prepared by ion bombardment. In these sections grain boundaries, pores, impurity precipitates and dislocations could be observed directly. Crystalline second-phase material formed as grains and small precipitates could be identified by means of electron diffraction. The method of specimen preparation and the results obtained from the observation of the specimens will be discussed.

Varner, R. N., Peavy, S. T., **Test problems and results for OMNITAB II,** *Nat. Bur. Stand. (U.S.), Tech. Note 551, 190 pages (Dec. 1970) $1.50, SD Catalog No. C13.46:551.*

Key words: Accuracy; ANSI FORTRAN; computer system implementation; examples; OMNITAB II; software; test problems.

The lack of test problems and results for many software packages is a great hindrance to both the systems programmer and the general user. In this publication a set of fifty-two test problems and results for the OMNITAB II system is provided to assist individuals in checking the implementation of the OMNITAB II program on their particular computer. The general user will also find these descriptive examples instructive in the use of OMNITAB commands.

Wachtman, J. B., Jr., **Standard materials for measurements on ceramics,** *Am. Ceram. Soc. Bull.* **50,** No. 3, 242–247 *(March 1971).*

Key words: Ceramics; chemical composition; mechanical properties; pressure; properties; standard reference materials; standards; temperature; thermal.

Standard materials having well determined values of specific properties are useful in establishing the validity of techniques for characterization and property measurements on ceramics. For some properties certified materials are available "off-the-shelf"; for certain other properties certification is in progress and a few samples may be available on a collaborative basis; while for still other properties serious problems remain. Some recent progress and current work on standard materials is briefly reviewed for the areas of temperature, pressure, radiation, chemical composition, thermal emittance, thermal expansion, thermal conductivity, vapor pressure, elasticity and viscosity.

Wagman, D. D., Evans, W. H., Parker, V. B., Halow, I., Bailey, S. M., Schumm, R. H., Churney, K. L., **Selected values of chemical thermodynamic properties—Tables for elements 54 through 61 in the Standard order of arrangement,** *Nat. Bur. Stand. (U.S.), Tech. Note 270–5, 49 pages (Mar. 1971) 55 cents, SD Catalog No. C13.46:270–5.*

Key words: Enthalpy; entropy; Gibbs energy of formation; hafnium compounds; heat of formation; niobium compounds; scandium compounds; tantalum compounds; titanium compounds; vanadium compounds; yttrium compounds; zirconium compounds.

Contains tables of values for the standard heats and Gibbs (free) energies of formation, entropies and enthalpies at 298.15 K and heats of formation at 0 K for compounds of vanadium, niobium, tantalum, titanium, zirconium, hafnium, scandium, and yttrium (elements 54–61 in the Standard Order of Arrangement). These tables are a continuation of the comprehensive revision of NBS Circular 500.

Wait, D. F., **The precision measurement of noise temperature of mismatched noise generators,** *IEEE Trans. Microwave Theory Tech.* **MTT–18,** *No. 10, 715–724 (Oct. 1970).*

Key words: Compensation method; cryogenic noise generators; mismatch error; noise temperature measurement.

By refining the technique and analysis of an earlier paper, it is shown that a compensation method is the basis of the most precise measurement of noise temperature, especially for cryogenic

noise generators. The measurement system is adjusted so that it is in thermal equilibrium with the generator under test. As is typical for the compensation method, the generator under test may be mismatched and the comparison errors and the detector limitations can be verified experimentally. For generators with small reflection coefficients ($|\Gamma| \lesssim 0.1$), the comparison error is very close to the theoretical minimum, namely twice the system resolution. For reflection coefficients as large as 0.5, the comparison error increases in a typical system to about four times the system resolution.

Wallace, B., Brown, W. E., **Stoichiometric composition of whitlockite,** *J. Dental Res.* **50,** *No. 2, 343–346 (March–April 1971).*

Key words: Ca/P ratio; pyrolysis; pyrophosphate; stoichiometry; tricalcium phosphate; whitlockite.

The mineral whitlockite has been described as having Ca/P ratios of 3/2 and 10/7. This study used the pyrolytic formation of pyrophosphate and whitlockite from calcium orthophosphates and their mixtures with $CaCO_3$, to determine this Ca/P ratio. Its mean value of $1.506 \pm .015$ indicated a formula of $Ca_3(PO_4)_2$.

Walther, H., Hall, J. L., **Tunable dye laser with narrow spectral output,** *Appl. Phys. Letters* **17,** *No. 6, 239–242 (September 15, 1970).*

Key words: Birefringent filter; dye laser; frequency control.

A tunable dye laser with narrow-banded spectral output in the order of 0.01 Å or even smaller is described. This narrow spectral output is obtained by means of a birefringent filter (Lyot filter) which was inserted into the laser cavity. The properties of this laser setup have been investigated and are described.

Wampler, R. H., **A report on the accuracy of some widely used least squares computer programs,** *J. Am. Stat. Assoc.* **65,** *No. 330, 549–565 (June 1970).*

Key words: Computer programs; curve fitting; Gram-Schmidt orthogonalization; Householder transformations; iterative refinement; least squares; linear equations; orthogonalization; orthogonal polynomials; regression; rounding error; stepwise regression.

Two linear least squares test problems based on fifth degree polynomials have been run on more than twenty different computer programs in order to assess their numerical accuracy. The programs tested, all in present-day use, included representatives from several statistical packages as well as some from the SHARE library. Essentially four different algorithms were used in the various programs to obtain the coefficients of the least squares fits. The tests were run on several different computers, in double precision as well as single precision. By comparing the coefficients reported, it was found that those programs using orthogonal Householder transformations or Gram-Schmidt orthonormalization were much more accurate than those using elimination algorithms. Programs using orthogonal polynomials (suitable only for polynomial fits) also proved to be superior to those using elimination algorithms. The most successful programs accumulated inner products in double precision and made use of iterative refinement procedures. In a number of programs, the coefficients reported in one test problem were sometimes completely erroneous, containing not even one correct significant digit.

Waxler, R. M., **Laser glass composition and the possibility of eliminating electrostrictive effects,** *IEEE, J. Quantum Electron.* **QE–7,** *No. 4, 166–167 (April 1971).*

Key words: Electrostriction; glass; lasers; photoelasticity.

Many authors have stated that electrostrictive self-trapping of the light beam initiates laser damage in solid transparent dielectrics. By systematically varying composition, it may be possible to find a glass in which electrostrictive effects are eliminated.

Weiss, A. W., **A review of theoretical developments in atomic *f*-values,** *(Proc. 2nd. Intern. Conf. Beam-Foil Spectroscopy in Nuclear Instruments and Methods, Lysekil, Sweden, June 8–12, 1970), Part II, Lifetimes and transition probabilities, 25–119 in Nucl. Instr. Methods* **90,** *121–131 (North-Holland Publ. Co., Amsterdam, The Netherlands, 1970).*

Key words: Atomic lifetimes; atomic spectra; configuration interaction; oscillator strengths.

Theoretical work on atomic *f*-values are reviewed with particular emphasis on the relation to recent beam-foil measurements. One-electron models currently in use are reviewed and their limitations and range of applicability are discussed. Many-electron, or multi-configuration, models are also described and their results compared with experiment. Regularities and irregularities along isoelectronic sequences will be discussed, and some current problems will be presented.

Weiss, B. Z., Meyerson, M. R., **Fatigue crack initiation and propagation in chromium diffusion coated Ti bearing steel,** *J. Iron Steel Inst.* **208,** *No. 12, 1069–1077 (December 1970).*

Key words: Chromium diffusion coating; columnar grains; fatigue crack initiation; fatigue crack propagation; residual stress; titanium bearing steels.

Chromium diffusion coatings on Ti-bearing steel frequently lead to columnar growth beneath the Cr-rich layer. The grains are preferentially oriented. The depth of the columnar zone does not depend on the chromizing time. A high rate of cooling prevents columnar growth. No grain boundary diffusion or carbide formation at the grain boundaries was observed. The Cr-rich later is structurally homogenous and consists of α-solid solution. The hardness of the coating does not vary with the chromizing time.
Compressive residual stresses were found in the Cr-rich later. The stresses, whose magnitude does not change with the depth of the layer, may be decreased by additional heat treatment.
Three modes of fatigue crack nucleation were observed all beneath the Cr-rich layer. Cracks were formed after 10% to 18% of total fatigue lifetime. Crack propagation in its initial stages is primarily dependent on the mode of nucleation. In the later stage propagation is dependent on stress and grain size. Fatigue properties may be improved considerably by a factor of 3 to 5 by additional "normalizing" after chromizing.

West, E. D., **Data analysis for isoperibol laser calorimetry,** *Nat. Bur. Stand. (U.S.), Tech. Note 396, 34 pages (Feb. 1971) 40 cents, SD Catalog No. C13.46:396.*

Key words: Calorimetry; laser; laser calorimetry; laser energy; laser power.

Isoperibol calorimeters (those operating in a constant-temperature environment) are used to measure the power and energy in laser beams relative to electrical standards. The derivation of the basic formula is reviewed. Two methods are presented for analyzing the data taken at equal time intervals: (1) An approximate manual method with criteria for avoiding significant errors of approximation and (2) A least squares method for use with automatic digital computers.

White, H. J., Jr., **Federal information processing standards index, January 1, 1971,** *Nat. Bur. Stand. (U.S.), Fed. Info. Process. Stand. Publ. (FIPS Pub) 12, 143 pages, $1.50, SD Catalog No. C13.52:12.*

Key words: American National Standards; computers, data elements and codes; data processing systems; Federal Information Processing Standards; management information systems; International Organization for Standardization; standards; U.S. Government.

This publication provides material concerning standardization activities in the area of information processing at the Federal, National and International levels. Also included are related policy and procedural guideline documents. A list of Federal Government participants involved in the development of Federal Information Processing Standards is provided.

Wiederhorn, S. M., Johnson, H., **Effect of pressure on the fracture of glass,** *J. Appl. Phys.* **42,** *No. 2, 681–684 (Feb. 1971).*

Key words: Deep submergence; fracture; fracture energy; glass; high pressure; strength.

The fracture surface energies of three glass compositions were measured as a function of ambient pressure and were found to be independent of pressure, to 20 kbar, suggesting no change in the fracture mechanism. The mechanical behavior of glass thus differs from that of plastics or metals which are observed to become stronger and more ductile with increasing pressure. The difference in fracture behavior is believed due to the fact that fracture of glass is essentially a volume conserving process in contrast to metals and plastics for which volume expansion occurs.

Woelfel, J. B., Paffenbarger, G. C., **Expanding and shrinking 7-year-old dentures: report of cases,** *J. Am. Dental Assoc.* **81,** *No. 6, 1342–1348 (December 1970).*

Key words: Acrylic; adaption; contraction; dentures; epoxy; expansion; hard rubber; retention; serviceability; stability.

A set of complete dentures made of hard rubber shrank and warped during seven years of observation. The greatest shrinkage occurred on the lower molar-to-molar span 1.47% (0.75 mm) and the least 0.13% (0.09 mm) on the upper flange-to-flange span. A similar set of complete dentures made of an epoxy resin expanded but warped very little during the seven years. The greatest expansion 1.12% (0.56 mm) occurred on the lower molar-to-molar span and the least 0.86% (0.60 mm) on the upper flange-to-flange span. There was little or no difference in the serviceability of these dentures as judged by changes in centric and eccentric occlusion, stability, retention, and condition of the tissues and by the dentist's and patient's appraisals. Both sets of dentures deteriorated about the same in service. The apposition of the supporting tissues and the dentures were about the same as determined by pressure indicator paste patterns. The conclusion is, therefore, that the supporting tissues followed the dimensional changes in the dentures to a great extent.

Yakowitz, H., Fiori, C. E., Michaelis, R. E., **Standard reference materials: Homogeneity characterization of Fe-3Si alloy,** *Nat. Bur. Stand. (U.S.), Spec. Publ. 260–22, 30 pages (Feb. 1971) 35 cents, SD Catalog No. C13.10:260–22.*

Key words: Fe–3Si alloy; homogeneity testing; metallography; microprobe analysis; spectrometric analysis; standard reference materials.

An alloy of iron-3.22 wt. pct. silicon (Fe-3Si) was characterized with regard to chemical homogeneity of iron and silicon at the micrometer level of spatial resolution. This alloy is satisfactory for use as a homogeneous standard for electron probe microanalysis. The samples were cut from coarse-grained sheet stock to a final size of about 3 mm x 3 mm x 0.28 mm thick. Homogeneity was checked by means of quantitative raster scanning in which a square matrix (1.1 mm x 1.1 mm) of individual points is analyzed by the microprobe. Each matrix represents 400 separate analyses. Usually, the same matrix was rerun so that each point was sampled twice. The coefficient of variation for both the iron and silicon is less than one percent. Quantitative microprobe analysis was also carried out on this alloy giving a silicon content of 3.14% and an iron content of 96.9%.

Yokel, F. Y., Dikkers, R. D., **Strength of load bearing masonry walls,** *J. Struct. Div. Am. Soc. Civil Engineers* **97,** *No. ST5, 1593–1609 (May 1971).*

Key words: Bricks; buckling; deflection; loads; forces; masonry; moments; slenderness ratio; stability; structural engineering; walls.

A theory is presented, for the rational analysis of masonry walls under eccentric vertical compressive load, or under a combination of vertical compressive and transverse load. The theory is based on established concepts, which have been modified to account for the properties of masonry. Similar methods of rational analysis have been adopted for the design of steel columns and are in the process of being adopted for reinforced concrete columns. An investigation of the results of 192 tests of full-scale walls of various types of masonry construction established the feasibility of applying this theory to closely predict the strength of these walls. The analysis accounts for variables not presently considered in the design of masonry structures. The correlation between test results and theory is illustrated by several typical examples.

Yokel, F. Y., Mathey, R. G., Dikkers, R. D., **Compressive strength of slender concrete masonry walls,** *Nat. Bur. Stand. (U.S.), Bldg. Sci. Ser.* **33,** *32 pages (Dec. 1970) 40 cents, SD Catalog No. C13.29/2:33.*

Key words: Buckling; compressive strength; concrete block walls; elastic stability; flexural strength; masonry walls; reinforced concrete masonry walls; slenderness effect; structural stability.

Sixty reinforced and unreinforced concrete masonry walls of different slenderness ratios were tested to failure under vertical loads applied axially and at various eccentricities. Prism specimens, made of similar masonry units and mortars, were also tested under the same loading conditions. Analysis of test results indicates that wall strength can be conservatively predicted by evaluating cross-sectional wall capacity on the basis of prism strength and reducing the capacity for slenderness effects by evaluating the added moments attributable to wall deflection. Test results were also compared with allowable loads computed in accordance with the current NCMA standard.

Yokel, F. Y., Mathey, R. G., Dikkers, R. D., **Strength of masonry walls under compressive and transverse loads,** *Nat. Bur. Stand. (U.S.), Bldg. Sci. Ser.* **34,** *74 pages (Mar. 1971) 70 cents, SD Catalog No. C.13.29/2:34.*

Key words: Brick; cavity walls; composite walls; compressive strength; concrete block; flexural strength; masonry; mortar; slenderness effects; standards; structural stability; walls.

Ninety walls of 10 different types of masonry construction were tested under various combinations of vertical and transverse load. It is shown that the effect of vertical load and wall slenderness on transverse strength can be predicted by rational analysis. The analysis is based on established theory which has been extended to account for the properties of masonry. Similar methods of rational analysis have been adopted for the design of steel structures and are presently being considered for reinforced concrete structures.

Zimmerman, J. E., **Recent Developments in superconducting devices,** *J. Appl. Phys.* **42,** *No. 1, 30–71 (Jan. 1971).*

Key words: Cardiography; instrumentation; Josephson effect; magnetometry; superconductivity.

A simple model of the electrical characteristics of thin-film bridge, point contact, and tunnel junction Josephson devices is given, along with some comments on their relative performance at very low and at very high frequencies. A particular example is the dc IV characteristic of a point contact at the center of a parallel-disc microwave cavity. Some recent developments in devices and the application of a point-contact loop (SQUID) device to magnetocardiography is described.

Other NBS Publications

J. Res. Nat. Bur. Stand. (U.S.), 75A (Physics & Chemistry), No. 2 (March–April 1971), SD Catalog No. C13.22/sec. A:75/2. $1.25.

Tentative set of key values for thermodynamics—Part I. Report of the ICSU–CODATA Task Group on Key Values for Thermodynamics, October, 1970. S. Sunner.

Expanded formulation of thermodynamic scaling in the critical region. M. J. Cooper.

Table of spin-orbit energies for *p*-electrons in neutral atomic (core) np configurations. W. C. Martin.

Heat capacities of *cis*-1,4-polyisoprene from 2 to 360 K. S. S. Chang and A. B. Bestul.

Combined low-pressure and high-pressure measurements of density and bulk modulus of aviation instrument oil and 2-methylbutane and their mixtures. J. C. Houck and P. L. M. Heydemann.

Crystal structure of $Ca_3Na_2(CO_3)_3$ (shortite). B. Dickens, A. Hyman, and W. E. Brown.

J. Res. Nat. Bur. Stand. (U.S.), 75A (Physics & Chemistry), No. 3 (May–June 1971), SD Catalog No. C13.22/sec.A:75/3. $1.25.

The solid phase photolysis and radiolysis of ethylene at 20 and 77 K. R. Gorden, Jr., and P. Ausloos.

Kinetic mass spectrometric investigation of the ion-molecule reactions occurring in C_4 and C_5 alkanes following photoionization at 106.7 and 104.8 nm. L. W. Sieck, S. K. Searles, and P. Ausloos.

An alumina standard reference material for resonance frequency and dynamic elastic moduli measurement. I. For use at 25 °C. R. W. Dickson and J. B. Wachtman, Jr.

Optical and mechanical properties of some neodymium-doped laser glasses. R. M. Waxler, G. W. Cleek, I. H. Malitson, M. J. Doge, and T. A. Hahn.

Effect of environment of viscous flow in inorganic oxide glasses. J. H. Simmons and P. B. Macedo.

Phase relations in the SrO-IrO_2-Ir system in air. C. L. McDaniel and S. J. Schneider.

The crystal structure of $BaCa(CO_3)_2$, (barytocalcite). B. Dickens and J. S. Bowen.

Ionization of hydrofluoric acid at 25 °C. P. R. Patel, E. C. Moreno, and J. M. Patel.

Vapor pressure equation for water in the range 0 to 100 °C. A. Wexler and L. Greenspan.

J. Res. Nat. Bur. Stand. (U.S.), 75A (Physics and Chemistry), No. 4 (July–August 1971), SD Catalog No. C13.22/sec. A:75/4. $2.00.

Inclusions in laser materials. H. S. Bennett.

Heat diffusion near absorbing centers in laser materials. H. S. Bennett.

Thermal conductivity, electrical resistivity, and thermopower of aerospace alloys from 4 to 300 K. J. G. Hust, D. H. Weitzel, and R. L. Powell.

Refractive indices of fused silica at low temperatures. R. M. Waxler and G. W. Cleek.

High-speed (subsecond) measurement of heat capacity, electrical resistivity, and thermal radiation properties of tungsten in the range 2000 to 3600 K. A. Cezairliyan and J. L. McClure.

The calculated continuous emission of a LTE hydrogen plasma. J. R. Roberts and P. A. Voight.

The second spectrum of nickel (Ni II) (addenda and errata). A. G. Shenstone.

Tables of second virial coefficients and their first and second derivatives for the Stockmayer (m, 6, 3) potential function. J. S. Gallagher and M. Klein.

J. Res. Nat. Bur. Stand. (U.S.), 75A (Physics and Chemistry), No. 5 (September–October 1971), SD Catalog No. C13.22/ sec. A:75/5. $1.25.

Measurement of the relative enthalpy of pure α-Al_2O_3 (NBS heat capacity and enthalpy standard reference material No. 720) from 273 to 1173 K. D. A. Ditmars and T. B. Douglas.

High-precision coulometric titrations of boric acid. G. Marinenko and C. E. Champion.

Determination of trace elements in ruby laser crystals by neutron activation analysis. B. A. Thompson and E. C. Miller.

Crystallography of some double sulfates and chromates. H. F. McMurdie, M. C. Morris, J. deGroot, and H. E. Swanson.

Discrimination between equations of state. J. R. Macdonald and D. R. Powell.

New absorption bands and isotopic studies of known transitions in CO. J. D. Simmons and S. D. Tilford.

A study of line shape of CO infrared emission lines. J. A. Dowling, S. Silverman, W. S. Benedict, and J. W. Quinn.

Ionization quantum yields and absorption coefficients of selected compounds at 58.4 and 73.6–74.4 nm. R. E. Rebbert and P. Ausloos.

Kinetic mass spectrometric investigation of the reactions of *t*-$C_4H_9^+$ ions with some simple polar molecules at thermal energies. L. Hellner and L. W. Sieck.

Energy levels, wave functions, dipole and quadrupole transitions of trivalent gadolinium ions in sapphire. P. H. E. Meijer.

J. Res. Nat. Bur. Stand. (U.S.), 75B (Mathematical Sciences), Nos. 1 & 2 (January–June 1971), SD Catalog. No. C13.22/ sec. B:75/1 & 2. $1.25.

Bounds to truncation errors in biorthogonal polynomial approximations, with illustrative applications to gamma ray transport distributions. L. V. Spencer.

A theorem on matrix commutators. J. M. Smith.

A special permutation matrix decomposition for combinatorial design incidence matrices. E. C. Johnsen and T. F. Storer.

The Casimir check for the algebraic matrices of the configuration $(d+s)^n_\nu$. C. Roth.

Convex homotopy. W. A. Horn.

The powers of a connected graph are highly hamiltonian. Vasanti N. Bhat and S. F. Kapoor.

Exact solutions of linear equations with rational coefficients. A. S. Fraenkel and D. Loewenthal.

An improvement of the Fischer inequality. R. Merris.

On the Smith normal form. M. Newman.

On certain optimal quadrature formulas. S. Haber.

Abramowitz, S., Levin, I. W., Raman spectra of the hexahalogenated benzenes in the solid phase, Spectrochim. Acta. **26A,** 2261–2268 (1970).

Allpress, J. G., Roth, R. S., Structural studies by electron microscopy: Polymorphism of $ZrO_2 \cdot 12Nb_2O_5$, J. Solid State Chem. **2,** 366–376 (1970).

Armstrong, G. T., Gibbs energy vs. free energy, Chem. Eng. News, Letter to the Editor, p. 3 (April 26, 1971).

Ausloos, P., Rebbert, R. E., Sieck, L. W., Ion-molecule reactions in the radiolysis of ethane, J. Chem. Phys. **54,** No. 6, 2612–2618 (March 15, 1971).

Baker, D. V., Editor, 1970 Technical Highlights of the National Bureau of Standards, Annual Report, Fiscal Year 1970, Nat. Bur. Stand. (U.S.), Spec. Publ. 340, 258 pages (February 1971) $1.50. SD Catalog No. C13.10:340.

Ballard, D., Yakowitz, H., Spectrometer shield for stray iron x-ray radiation in the scanning electron microscope, Rev. Sci. Instr. **42,** No. 1, 14–15 (January 1971).

Bennett, H. S., F centers in ionic crystals: Semicontinuum-polaron models and polarizable-ion models, Phys. Rev. **B. 3,** No. 8, 2763–2777 (April 15, 1971).

Bowman, R. R., Quantifying hazardous electromagnetic fields: Practical considerations, Nat. Bur Stand. (U.S.), Tech. Note 389, 15 pages (April 1970) 30 cents.

COM–71–00781. (For further information concerning availability, write to National Technical Information Service, Springfield, Virginia 22151.

Brenner, A., Anderson, H. J., Note on the preparation of rhenium oxychlorides, J. Electrochem. Soc. **118,** No. 2, 373–374 (February 1971).

Brower, W. S., Jr., Parker, H. S., Growth of single crystal cuprous oxide, J. Crystal Growth **8,** 227–229 (1971).

Brown, R. L., An upper limit for the rate of destruction of $O_2(^1\Delta_g)$ by atomic hydrogen, J. Geophys. Res. Space Phys. **75,** No. 19, 3935–3936 (July 1, 1970).

Carter, R. S., Editor, Reactor Radiation Division: Annual Progress Report for the Period Ending October 31, 1970, Nat. Bur. Stand. (U.S.), Tech. Note 567, 66 pages (Mar. 1971) 70 cents, SD Catalog No. C13.46:567.

Chappell, S. E., Humphreys, J. C., Energy deposition in surface layers of silicon by monoenergetic electrons, Proc. 4th Intern. Conf. Electron and Ion Beam Science and Technology, May 10–14, 1970, Los Angeles, Calif., pp. 655–666 (The Electrochemical Society, Inc., New York, N.Y., 1970).

Collin, G. J., Ausloos, P., Ion-molecule reactions in the condensed-phase radiolysis of hydrocarbon mixtures. III. Reactions of *i*-$C_4H_9^+$ and *tert*-$C_4H_9^+$ ions originating from neopentane, J. Am. Chem. Soc. **93,** No. 6, 1336–1340 (March 24, 1971).

Colwell, J. H., Mangum, B. W., Thornton, D. D., Low-temperature magnetic susceptibility and heat capacity of $GdAsO_4$, Phys. Rev. **B. 3,** No. 11, 3855–3861 (June 1, 1971).

Cooper, J. W., Conneely, M. J., Smith, K., Ormonde, S., Resonant structure of lithium between the 2^2S and 2^2P thresholds, Phys. Rev. Letters **25,** No. 22, 1540–1543 (November 30, 1970).

Costrell, L., CAMAC instrumentation system-introduction and

general description (Proc. Nuclear Science Symp., New York, N.Y., Nov. 6, 1970), IEEE Trans. Nucl. Sci. **NS-18**, No. 2, 1-6 (April 1971).

Currie, L. A., Rodriguez-Pasquées, R. H., Photonuclear tritium yields at 90 MeV, Nucl. Phys. **A157**, 49-60 (1970).

Czyz, W., Maximon, L. C., Coulomb effects in high energy He^4-He^4 elastic scattering, Ann. Phys. **60**, No. 2, 484-486 (October 1970).

Danos, M., Gibson, B. F., Very high-momentum components in nuclei and far "subthreshold" production of quarks, Phys. Rev. Letters **26**, No. 8, 473-476 (Feb. 22, 1971).

Danos, M., Gillet, V., Evidence for quartet structure in medium and heavy nuclei, Physics Letters **34B**, No. 1, 24-26 (Jan. 18, 1971).

Danos, M., Spicer, B. M., Quartet structure in light nuclei, Z. Physik **237**, 320-326 (1970).

Day, G. W., Linear and nonlinear optical properties of trigonal selenium, Appl. Phys. Letters **18**, No. 8, 347-349 (April 15, 1971).

Day, G. W., Gruzensky, P. M., Some optical properties of cesium cupric chloride, Appl. Opt. **9**, No. 12, 2794-2795 (December 1970).

Dibeler, V. H., Walker, J. A., McCulloh, K. E., Photoionization study of chlorine monofluoride and the dissociation energy of fluorine, J. Chem. Phys. **53**, No. 12, 4414-4417 (December 15, 1970).

Dibeler, V. H., Photoionization studies and thermodynamic properties of some halogen molecules, (Proc. Intern. Conf. on Mass Spectroscopy, Kyoto, Japan, Sept. 8-13, 1969), Chapter in Recent Development in Mass Spectroscopy, K. Ogata and T. Hayakawa, Ed., pp. 781-790 (University of Tokyo Press, Tokyo, Japan, 1970).

Dillon, T. A., Smith, E. W., Cooper, J., Mizushima, M., Semiclassical treatment of strong collisions in pressure broadening, Phys. Rev. **A2**, No. 5, 1839-1846 (November 1970).

Domalski, E. S., Thermochemical properties of peroxyacetyl (PAN) and peroxybenzoyl nitrate (PBN), Environ. Sci. Tech. Communications, **5**, 443-444 (1971).

Durst, R. A., Editor, Electrochemical analysis section: Summary of activities—July 1969 to June 1970, Nat. Bur. Stand. (U.S.), Tech. Note 543, 92 pages (Nov. 1970) $1.00, SD Catalog No. C13.46:543.

Ederer, D. L., Lucatorto, T., Madden, R. P., Autoionization spectra of lithium, Phys. Rev. Letters **25**, No. 22, 1537-1540 (November 30, 1970).

Edqvist, C., Lindholm, E., Selin, L. E., Asbrink, L., Kuyatt, C. E., Mielczarek, S. R., Simpson, J. A., Fischer-Hjalmars, I., Rydberg series of small molecules VIII photoelectron spectroscopy and electron spectroscopy of NO_2, Phys. Scrip. **1**, 172-178 (1970).

Evans, B. J., Swartzendruber, L. J., Mossbauer study of local molecular fields, cation distributions, and recoilless fractions in Sb substituted lithium ferrite, J. Appl. Phys. **42**, No. 4, 1628-1630 (March 15, 1971).

Fatiadi, A. J., Oxidative cleavage of aromatic azines with periodic acid: e.s.r. evidence for the liberation of nitrogen dioxide, Chem. Ind. pp. 64-66 (January 9, 1971).

Fickett, F. R., Clark, A. F., Longitudinal magnetoresistance anomalies, J. Appl. Phys. **42**, No. 1, 217-219 (Jan. 1971).

Franklin, A. D., Bennett, H. S., Editors, ARPA-NBS program of research on high temperature materials and laser materials, Reporting Period July 1 to December 31, 1970, Nat. Bur. Stand. (U.S.), Tech. Note 574, 44 pages (May 1971) 50 cents, SD Catalog No. C13.46:574.

Freeman, D. H., Zielinski, W. L. Jr., Editors, Separation and purification section: Summary of activities, July 1969 to June 1970, Nat. Bur. Stand. (U.S.), Tech. Note 549, 86 pages (Jan. 1971) 75 cents, SD Catalog No. C13.46:549.

Gadzuk, J. W., A comparison between the Fermi-Thomas and quantum dielectric response of a metal surface to a static point charge, Surface Sci. **23**, 58-68 (1970).

Gadzuk, J. W., Plummer, E. W., Hot-hole-electron cascades in field emission from metals, Phys. Rev. Letters **26**, No. 2, 92-95 (Jan. 11, 1971).

Garvin, D., The information analysis center and the library, Spec. Libraries **62**, No. 1, 17-23 (January 1971).

Gebbie, K. B., Thomas, R. N., On the dependence of T_e upon quantity versus quality of the radiation field in a stellar atmosphere, Astrophys. J. **161**, No. 1, 229-241 (July 1970).

Geltman, S., Burke, P. G., Electron scattering by atomic hydrogen using a pseudo-state expansion. II. Excitation of $2s$ and $2p$ states near threshold, J. Phys. B: Atom. Molec. Phys. **3**, No. 8, 1062-1072 (August 1970).

Godfrey, J. T., Vidal, C. R., Smith, E. W., Cooper, J., Effect of time ordering in the unified theory, Phys. Rev. **A. 3**, No. 5, 1543-1546 (May 1971).

Green, M. S., Cooper, M. J., Sengers, J. M. H. L., Extended thermodynamic scaling from a generalized parametric form, Phys. Rev. Letters **26**, No. 9, 492-495 (March 1, 1971).

Greenspan, M., Comment on "Response of ideal circuit elements to sinusoidal excitations," Am. J. Phys. **39**, No. 5, 586-587 (May 1971).

Hastie, J. W., Hauge, R. H., Margrave, J. L., Infrared spectra and geometries of heavy metal halides: $SrCl_2$, $BaCl_2$, $EuCl_2$, EuF_2, $PbCl_2$, and UCl_2, High Temp. Sci. **3**, No. 1, 56-71 (Jan. 1971).

Hellwig, H., Vessot, R. F. C., Levine, M. W., Zitzewitz, P. W., Allan, D. W., Glaze, D. J., Measurement of the unperturbed hydrogen hyperfine transition frequency, IEEE Trans. Instr. Meas. **IM-19**, No. 4, 200-209 (November 1970).

Herron, J. T., Huie, R. E., Mass spectrometric studies of the reactions of singlet oxygen in the gas phase, Ann. N.Y. Acad. Sci. **171**, Article 1, 229-238 (Oct. 15, 1970).

Hummer, D. G., Rybicki, G. B., Non-coherent scattering—VII. Frequency-dependent thermalization lengths and scattering with continuous absorption, Monthly Notices Roy. Astron. Soc. **150**, No. 4, 419-434 (1970).

Hussmann, E. K., A holographic interferometer for measuring radiation energy deposition profiles in transparent liquids, Appl. Opt. **10**, No. 1, 182-186 (January 1971).

Hustvedt, E. H., Conference Coordinator, Friend, M. L., Editor, Proceedings of joint meeting of government operations research users and producers, Held at the National Bureau of Standards, Gaithersburg, Maryland, June 5-6, 1969. Nat. Bur. Stand. (U.S.), Spec. Publ. **347**, 164 pages (May 1971) $1.25, SD Catalog No. C13.10:347.

Jacox, M. E., Milligan, D. E., Infrared spectrum and structure of the species CO_3, J. Chem. Phys. **54**, No. 3, 919-926 (February 1, 1971).

Julienne, P. S., Predissociation of the $H_2D^1\Pi_g$ state, Chem. Phys. Letters **8**, No. 1, 27-28 (January 1, 1971).

Kelley, R. D., Klein, R., Scheer, M. D., Isotope effects in the hydrogen-atom addition to olefins at low temperatures, J. Phys. Chem. **74**, No. 25, 4301-4309 (1970).

Kidnay, A. J., Hiza, M. J., The purification of helium gas by physical adsorption at 76 °K, AIChE J. **16**, No. 7, 949-954 (Nov. 1970).

Kieffer, L. J., Low energy electron collision cross section data. Part II. Electronic excitation level and line cross sections, Atomic Data **1**, No. 2, 121-287 (Nov. 1969).

Klein, M., Hanley, H. J. M., The m-6-8 potential function, J. Chem. Phys. **53**, No. 12, 4722-4723 (Dec. 15, 1970).

Klose, J. Z., Mean lives and absolute f-values in neutral iron, Astrophys. J. **165**, No. 3, 637-642 (May 1, 1971).

Kuriyama, M., Miyakawa, T., Primary and secondary extinctions in the dynamical theory for an imperfect crystal, Acta Cryst. **A26**, Part 6, 667-673 (November 1970).

Kurylo, M. J., Peterson, N. C., Braun, W., Absolute rate of the reaction $H+H_2S$, J. Chem. Phys. **54**, No. 3, 943-946 (February 1, 1971).

Lane, N. F., Geltman, S., Differential elastic and rotational excitation cross sections for electron-H_2 scattering, Phys. Rev. **184**, No. 1, 46-51 (Aug. 5, 1969).

Latanision, R. M., Ruff, A. W., The temperature dependence of stacking fault energy in Fe-Cr-Ni alloys, Met. Trans. **2**, 505-509 (February 1971).

Laufer, A. H., Keller, R. A., Lowest excited states of ketene, J. Am. Chem. Soc. **93**, No. 1, 61-63 (January 1971).

Lightbody, J. W., Jr., Electron scattering sum rule for ^{12}C-experiment and theory, Physics Letters **33B**, No. 2, 129-132 (September 28, 1970).

Linsky, J. L., Avrett, E. H., The solar H and K lines, Astron. Soc. Pacific **82**, 169-248 (April 1970).

McClellan, B. E., Menis, O., Kinetics and mechanism of extraction of iron(III) with β-isopropyltropolone, Anal. Chem. **43**, No. 3, 436-438 (March 1971).

Madey, T. E., Yates, J. T., Jr., Electron-stimulated desorption and work function studies of clean and cesiated (110) GaAs, J. Vacuum Sci. Technol. **8**, No. 1, 39-44 January-February 1971.

Maki, A. G., Olson, W. B., Sams, R. L., HCN rotational-vibrational energy levels and intensity anomalies determined from infrared

measurements, J. Mol. Spectry. **36,** No. 3, 433–447 (December 1970).

Matarrese, L. M., Evenson, K. M., Improved coupling to infrared whisker diodes by use of antenna theory, Appl. Phys. Letters **17,** No. 1, 8–10 (July 1, 1970).

Meijer, P. H. E., Influence of the dipole-dipole coupling on the specific heat of cesium titanium alum, Phys. Rev. B **3,** No. 1, 182–185 (January 1, 1971).

Meinke, W. W., The universal analytical instrument, Proc. 5th Annual National Conference on Industrial Research, Applying Emerging Technologies, Industrial Research, Inc., Chicago, Ill., September 18, 1969, pp. 31–41 (1970).

Menis, O., McClellan, B. E., Bright, D. S., Determination of the formation constants of iron(III) and vanadium(V) with β-isopropyltropolone using the extraction method, Anal. Chem. **43,** No. 3, 431–435 (March 1971).

Merris, R., Pierce, S., A class of representations of the full linear group, J. Algebra **17,** No. 3, 346–351 (March 1971).

Milligan, D. E., Jacox, M. E., Infrared spectrum and structure of intermediates in the reaction of OH with CO, J. Chem. Phys. **54,** No. 3, 927–942 (February 1, 1971).

Missoni, G., Dick, C. E., Placious, R. C., Motz, J. W., Inelastic atomic scattering of 0.1-, 0.2-, 0.4-, and 3.0-MeV electrons, Phys. Rev. A. **2,** No. 6, 2309–2317 (December 1970).

Mohan, R., Danos, M., Biedenharn, L. C., Isospin impurities in the nuclear ground states, Phys. Rev. C. **3,** No. 2, 468–479 (February 1971).

Moore, C. E., Annual report on spectorscopy, July 1, 1969–June 30, 1970, Bull. Am. Astron. Soc. **3,** No. 1, 154–155 (1971).

Mountain, R. D., Comment on "Rotational diffusion of spherical-top molecules in liquids," J. Chem. Phys. **54,** No. 7, 3243 (April 1, 1971).

Noack, M., Kokoszka, G. F., Gordon, G., Dynamic Jahn-Teller effects and magnetic anisotropies in aqueous solutions and water-ethanol glasses of copper(II) solvates and complexes with 2,2′-dipyridine, J. Chem. Phys. **54,** No. 3, 1342–1350 (February 1, 1971).

Olson, W. B., Papousek, D., High-resolution infrared spectra of ethanelike molecules and the barrier to internal rotation: The ν_9,ν_{13} band of dimethylacetylene, J. Mol. Spectry. **37,** No. 3, 527–534 (March 1971).

Pecker, J. -C., Thomas, R. N., Personal libraries and publication policies, Atoms **25,** 37–38 (Jan. 1970).

Peterson, R. L., Numerical study of deformation-potential scattering of electrons by optical phonons in a longitudinal magnetic field, Phys. Rev. B. **2,** No. 10, 4135–4144 (November 15, 1970).

Pierce, S., Orthogonal groups of positive definite multilinear functionals, Pacific J. Math. **33,** No. 1, 183–189 (1970).

Plummer, E. W., Gadzuk, J. W., Surface states on tungsten, Phys. Rev. Letters **25,** No. 21, 1493–1495 (November 23, 1970).

Redding, R. W., Hougen, J. T., Calculation of the Eulerian angles and large amplitude vibrational coordinate corresponding to an arbitrary instantaneous molecular configuration, J. Mol. Spectry. **37,** No. 2, 366–370 (February 1971).

Robertson, B., Mitchell, W. C., Equations of motion in nonequilibrium statistical mechanics. III. Open systems, J. Math. Phys. **12,** No. 3, 563–568 (March 1971).

Rosenstock, H. M., Botter, R., Franck-Condon principle for the ionization of polyatomic molecules (Proc. Intern. Conf. on Mass Spectroscopy, Kyoto, Japan, Sept. 1969), Chapter in Recent Development in Mass Spectroscopy, K. Ogata and T. Hayakawa, Ed., pp. 797–806 (University of Tokyo Press, Tokyo, Japan, 1970).

Santoro, A., Absorption correction for diffraction measurements in complex cases (Proc. Intern. Summer School organized by the Commission on Crystallographic Computing of the Intern. Union of Crystallography, Ottawa, Canada, August 4–11, 1969), Chapter in Crystallographic Computing, F. R. Ahmed, S. R. Hall, and C. P. Huber, Ed., pp. 283–290 (Munksgaard, Copenhagen, Denmark, 1970).

Santoro, A., Mighell, A. D., Reimann, C. W., The crystal structure of a 1:1 cupric nitrate-pyrazine complex $Cu(NO_3)_2$ ($C_4N_2H_4$), Acta Cryst. **B26,** 979–984 (July 7, 1970).

Schaffer, R., Editor, Organic Chemistry Section: Summary of Activities, July 1969 to June 1970, Nat. Bur. Stand. (U.S.), Tech. Note **547,** 134 pages (Nov. 1970) $1.25, SD Catalog No. C13.46:547.

Schroeder, L. W., Rush, J. J., Neutron diffraction study of the structure and thermal motion of phosphonium bromide, J. Chem. Phys. **54,** No. 5, 1968–1973 (March 1, 1971).

Scribner, B. F., Editor, Activities of the NBS Spectrochemical Analysis Section, July 1969 to June 1970, Nat. Bur. Stand. (U.S.). Tech. Note **542,** 114 pages (Nov. 1970) $1.25, SD Catalog No. C13.46:542.

Simmons, J. H., Macedo, P. B., Analysis of viscous relaxation in critical oxide mixtures, J. Chem. Phys. **64,** No. 3, 1325–1331 (February 1, 1971).

Smith, C. E., Milligan, D. E., Jacox, M. E., Matrix-isolation study of the vacuum-ultraviolet photolysis of chlorofluoromethane. The infrared and ultraviolet spectra of the free radical ClCF, J. Chem. Phys. **54,** No. 7, 2780–2793 (April 1, 1971).

Swartzendruber, L. J., Localized moments on Fe impurities in Nb-Mo alloys: Mössbauer-effect absorber study, J. Appl. Phys. **42,** No. 4, 1 (March 15, 1971).

Tate, E. L., Improving library collections by weeding, Proc. U.S. Department of Interior, 1970 Departmental Library Workshop, Washington, D.C., Sept. 28–Oct. 2, 1970, pp. 54–61 (U.S. Department of Interior, Office of Library Services, Washington, D.C., Feb. 1971).

Taylor, J. K., Editor, Microchemical Analysis Section: Summary of Activities, July 1969 to June 1970, Nat. Bur. Stand. (U.S.), Tech. Note. 545, 126 pages (Dec. 1970) $1.25, SD Catalog No. C13.46:545.

Tech, J. L., A high-dispersion spectral analysis of the Ba II Star HD 204075 (ζ Capricorni), Nat. Bur. Stand. (U.S.), Monogr. 119, 174 pages (March 1971) $3.25, SD Catalog No. C13.44:119.

Tipson, R. S., Brady, R. F., Jr., West, B. F., Cyclic acetals of ketoses. Part IV. Re-investigation of the oxidation of 1,2:4,5-Di-*O*-isopropylidene-β-D-fructopyranose with methyl sulfoxide-acetic anhydride, Carbohydrate Res. **16,** 383–393 (March 1971).

Tjon, J. A., Gibson, B. F., O'Connell, J. S., Trinucleon form factors calculated from realistic local potentials, Phys. Rev. Letters **25,** No. 8, 540–542 (August 24, 1970).

U.S. Metric Study Report. International Standards, Nat. Bur. Stand. (U.S.), Spec. Publ. 345–1, 157 pages (Dec. 1970) $1.25, SD Catalog No. C13.10:345–1.

Uzgiris, E. E., Hall, J. L., Barger, R. L., Precision infrared Zeeman spectra of CH_4 studied by laser-saturated absorption, Phys. Rev. Letters **26,** No. 6, 289–293 (Feb. 8, 1971).

Van Blerkon, D., Hummer, D. G., The normalized on-the-spot approximation for line transfer problems, J. Quant. Spectrosc. Radiat. Transfer Note, **9,** No. 11, 1567–1571 (Nov. 1969).

Van Brunt, R. J., Kieffer, L. J., Angular distribution of O^- from dissociative electron attachment to O_2, Phys. Rev. A, **2,** No. 5, 1899–1905 November 1970).

Van Brunt, R. J., Kieffer, L. J., Angular distribution of protons and deuterons produced by dissociative ionization of H_2 and D_2 near threshold, Phys. Rev. A **2,** No. 4, 1293–1304 (October 1970).

Vidal, C. R., Cooper, J., Smith, E. W., Hydrogen stark broadening calculations with the unified classical path theory, J. Quant. Spectry. Radiative Transfer **10,** No. 9, 1011–1063 (September 1970).

Vidal, C. R., Cooper, J., Smith, E. W., Unified theory calculations of stark broadened hydrogen lines including lower state interactions, Nat. Bur. Stand. (U.S.), Mongr. 120, 45 pages (Jan. 1971), 50 cents, SD Catalog No. C13.44:120.

Vidal, C. R., Cooper, J., Smith, E. W., Unified theory calculations of stark broadened hydrogen lines including lower state interactions, (Short Version), J. Quant. Spectry. Radiative Transfer **11,** 263–281 (1970).

Watson, R. E., Bennett, L. H., Carter, G. C., Weisman, I. D., Comments on the Knight shift in bismuth and other *p*-band diamagnetic metals, Phys. Rev. B. **3,** No. 1, 222–225 (January 1971).

Weber, L. A., Density and compressibility of oxygen in the critical region, Phys. Rev. A. **2,** No. 6, 2379–2388 (Dec. 1970).

Weber, L. A., Some vapor pressure and *P, V, T* data on nitrogen in the range 65 to 140 K, J. Chem. Thermodynamics **2,** No. 6, 839–846 (Nov 1970).

Weir, C. E., Piermarini, G. J., Block, S., On the crystal structures of Cs II and Ga II, J. Chem. Phys. **54,** No. 6, 2768–2770 (March 15, 1971).

Weiss, A. W., Symmetry-adapted pair correlations in Ne, F^-, Ne^+, and F, Phys. Rev. A. **3,** No. 1, 126–129 (January 1971).

Weiss, M. J., Kuyatt, C. E., Mielczarek, S., Inelastic electron scattering from formaldehyde, J. Chem. Phys. **54,** No. 10, 4147–4150 (May 15, 1971).

Weiss, M. J., Mielczarek, S. R., Kuyatt, C. E., Inelastic electron

scattering from nitrous oxide between 5.0 and 20.0 eV energy loss, J. Chem. Phys. **54,** No. 3, 1412–1414 (Feb. 1, 1971).

Wiese, W. L., Atomic transition probabilities—A survey of our present knowledge and future needs, (Proc. 2nd. Intern. Conf. Beamfoil Spectroscopy in Nuclear Instruments and Methods, Lysekil, Sweden, June 8–12, 1970). Part II, Lifetimes and transition probabilities, 25–119 in Nucl. Instr. Methods **90,** 25–33 (North-Holland Publ. Co., Amsterdam, The Netherlands, 1970).

Wiese, W. L., Kelleher, D. E., On the cause of the redshifts in white-dwarf spectra, Astrophys. J. **166,** L59–L63 (June 1, 1971).

Wright, J. C., Moos, H. W., Colwell, J. H., Mangum, B. W., Thornton, D. D., $DyPO_4$: A three-dimensional Ising antiferromagnet, Phys. Rev. B. **3,** No. 3, 843–858 (February 1, 1971).

Yates, J. T., Jr., Madey, T. E., Interactions between chemisorbed species: H_2 and N_2 on (100) tungsten, J. Vacuum Sci. Technol. **8,** No. 1, 63–68 (January–February 1971).

**Publications for which a price is indicated are available by purchase from the Superintendent of Documents, U.S. Government Printing Office, Washington, D.C. 20402 (foreign postage, one-fourth additional). The NBS non-periodical series are also available from the National Technical Information Service (NTIS), Springfield, Va. 22151, which was formerly the Clearinghouse. Reprints from outside journals and the NBS Journal of Research may often be obtained directly from the authors.*

JOURNAL OF RESEARCH of the National Bureau of Standards—C. Engineering and Instrumentation
Vol. 75C, Nos. 3 and 4, July–December, 1971

INDEX TO VOLUME 75C

January to December, 1971

A

Accurate ... 185
Accurate microwave high power measurements using a cascaded coupler method ... 185
AC–DC difference ... 145
Acoustical pulse ... 33
Adaptor ... 177
Adiabatic saturation ... 69
Adsorption ... 165
Analytic solutions ... 79
Apparatus for impact-fatigue testing ... 95
Archival film ... 19
Argon, compressibility factor of ... 165
Attenuator ... 1
Axisymmetrical ... 155

B

Bedard, A. J., Jr., Seismic response on infrasonic microphones ... 41
Boundary conditions ... 79
Bramall, Kenneth E., Accurate microwave high power measurements using a cascaded coupler method ... 185
Burnett apparatus for the accurate determination of gas compressibility factors and second virial coefficients, and evaluation of its capability based on some results for argon and carbon dioxide ... 165
Burnett data reduction ... 165
Burns, G. W., Hurst, W. S., A program in refractory metal thermocouple research ... 99

C

Calibration ... 89, 185
Carbon dioxide, second virial coefficient of ... 165
Cezairliyan, A., Design and operational characteristics of a high-speed (millisecond) system for the measurement of thermophysical properties at high temperatures ... 7
Cezairliyan, A., Rotating adjustable transmission optical step attenuator ... 85
Cezairliyan, A., Rotating optical attenuator for the generation of subsecond duration sawtooth shape radiance pulses ... 29
Comparator ... 145
Compensation ... 41
Compressibility factor ... 165
Computation of the temperature distribution in cylindrical high-pressure furnaces ... 79
Computation, temperature distribution ... 79
Connector ... 177
Connectors ... 89
Corrosion ... 107
Corrosion pit depth ... 107
Corrosion rate ... 107
Cryostat ... 95

D

Densitometer ... 23
Design and operational characteristics of a high-speed (millisecond) system for the measurement of thermophysical properties at high temperatures ... 7
Dew point temperature ... 69
Directional coupler ... 185
Disturbed ... 107
Durcholz, R. L., Schramm, R. E., Reed, R. P., Apparatus for impact-fatigue testing ... 95

E

Efficiency ... 177
Elastic ... 155
Electrochemical ... 107
EMF-temperature relationship ... 99
Engen, G. F., An extension to the sliding short method of connector and adaptor evaluation ... 177
Engen, G. F., An improved method for microwave power calibration, with application to the evaluation of connectors ... 89
Experiment ... 155
Extension to the sliding short method of connector and adaptor evaluation ... 177

F

Fatigue ... 95
Finite-element analysis ... 155
Fisher, C. R., Mitchell, R. A., Woolley, R. M., Formulation and experimental verification of an axisymmetrical finite-element structural analysis ... 155
Force transducer ... 155
Formulation and experimental verification of an axisymmetrical finite-element structural analysis ... 155
Furnace ... 99
Furnaces, high-pressure ... 79

G

Gas ... 165
Gas, compressibility factor of ... 165
Gas on metal ... 165
Gas, PVT properties of ... 165
Greenspan, L., Heated air adiabatic saturation psychrometer ... 69
Ground motion ... 41

H

Hastings, J. R., Waxman, M., A Burnett apparatus for the accurate determination of gas compressibility factors and

Page

second virial coefficients, and evaluation of its capability based on some results for argon and carbon dioxide..... 165
Hastings, J. R., Waxman, M., Computation of the temperature distribution in cylindrical high-pressure furnaces..... 79
Heated air adiabatic saturation psychrometer..... 69
High power..... 185
High-pressure furnaces..... 79
High pressure research..... 79
High-speed measurements..... 7, 85
High-speed methods..... 29
High temperature..... 99
High temperatures..... 7
High temperature, steady state..... 79
Humidity..... 69
Hurst, W. S., Burns, G. W., A program in refractory metal thermocouple research..... 99
Hussman, M., McLaughlin, W. L., Rosenstein, M., Lantz, J. J., Jr., A scanning densitometer for continuous recording of spectral transmission density at low spatial contrast..... 23
Hygrometer..... 69
Hypo..... 19

I

Impact..... 95
Improved method for microwave power calibration with application to the evaluation of connectors..... 89
Infrasonic microphones..... 41
Instantaneous..... 107

K

Kinder, B. J., Little, W. E., Larson, W., A rotary-vane attenuator with an optical readout..... 1

L

Lantz, J. J., Jr., McLaughlin, W. L., Rosenstein, M., Hussman, E. K., A scanning densitometer for continuous recording of spectral transmission density at low spatial contrast..... 23
Larson, W., Little, W. E., Kinder, B. J., A rotary-vane attenuator with an optical readout..... 1
Light attenuator..... 29
Little, W. E., Larson, W., Kinder, B. J., A rotary-vane attenuator with an optical readout..... 1
Longitudinal and shear sound waves..... 33
Low temperature..... 95

M

McLaughlin, W. L., Rosenstein, M., Hussman, E. K., Lantz, J. J., Jr., A scanning densitometer for continuous recording of spectral transmission density at low spatial contrast... 23
Measurement..... 185
Measurements..... 165
Mechanical property equipment..... 95
Microdensitometer..... 23
Microfilm..... 19
Microwave..... 1, 185
Mismatch..... 89
Mitchell, R. A., Woolley, R. M., Fisher, C. R., Formulation and experimental verification of an axisymmetrical finite-element structural analysis..... 155
Mixing ratio..... 69
Mixo..... 69
Moist gas..... 69

N

New method of determining residual thiosulfate in processed photographic film..... 19

O

Optical attenuator..... 85

P

Page

Permanent record film..... 19
Photometry..... 29, 85
Pitting factor..... 107
Polarization..... 107
Polarization measurements as related to the corrosion of underground steel piling..... 107
Pope, C. I., A new method of determining residual thiosulfate in processed photographic film..... 19
Power equation..... 89
Power measurement..... 89
Power dissipation..... 79
Precision..... 1
Proctor, T. M., Jr., Sound speed measurements on solids; absolute accuracy of an improved transient pulse method... 33
Program in refractory metal thermocouple research..... 99
Psychrometer..... 69

R

Radiance..... 85
Radiance modulation..... 29
Radiation..... 29
Radiochromic dye films..... 23
Reed, R. P., Schramm, R. E., Durcholz, R. L., Apparatus for impact-fatigue testing..... 95
Refractory metals..... 99
Rosenstein, M., McLaughlin, W. L., Hussman, E. K., Lantz, J. J., Jr., A scanning densitometer for continuous recording of spectral transmission density at low spatial contrast..... 23
Rotary vane..... 1
Rotary-vane attenuator with an optical readout..... 1
Rotating adjustable transmission optical step attenuator..... 85
Rotating optical attenuator for the generation of subsecond duration sawtooth shape radiance pulses..... 29

S

Scanning densitometer for continuous recording spectral transmission density at low spatial contrast..... 23
Schramm, R. E., Durcholz, R. L., Reed, R. P., Apparatus for impact-fatigue testing..... 95
Schwerdtfeger, W. J., Polarization measurements as related to the corrosion of underground steel piling..... 107
Second virial coefficient..... 165
Seismic response..... 41
Seismic response on infrasonic microphones..... 41
Sensor..... 99
Sliding short..... 107
Soil..... 107
Soil undisturbed..... 107
Solids sound speed..... 33
Sound speed accuracy..... 33
Sound speed measurements in solids; absolute accuracy of an improved transient pulse method..... 33
Spectral transmission density..... 23
Speed of sound..... 33
Stainless steel..... 95
Steel piling..... 107
Stiffness matrix..... 155
Structural analysis..... 155

T

Temperature gradients..... 79
Temperature irregularities..... 79
Temperature variation..... 79
Thermal conductivity..... 79
Thermal voltage converters and comparator for very accurate AC voltage measurements..... 145
Thermocouple..... 99
Thermodynamics..... 7
Thermoelement..... 145
Thermoelements..... 99

Page

Thermophysical properties 7
Transfer voltmeter 145
Transient pulse-acoustical 33

U

Ultra high vacuum 99

V

Vapor pressure 69
Voltage measurements 145

W

Page

Waxman, M., Hastings, J. R., A Burnett apparatus for the accurate determination of gas compressibility factors and second virial coefficients, and evaluation of its capability based on some results for argon and carbon dioxide 165
Waxman, M., Hastings, J. R., Computation of the temperature distribution in cylindrical high-pressure furnaces 79
Weight loss 107
Williams, E. S., Thermal voltage converters and comparator for very accurate AC voltage measurements 145
Woolley, R. M., Mitchell, R. A., Fisher, C. R., Formulation and experimental verification of an axisymmetrical finite-element structural analysis 155
W-Re alloys 99

U.S. GOVERNMENT PRINTING OFFICE : 1972 OL—448–719

UNITED STATES
GOVERNMENT PRINTING OFFICE
PUBLIC DOCUMENTS DEPARTMENT
WASHINGTON, D.C. 20402

OFFICIAL BUSINESS
PENALTY FOR PRIVATE USE, $300

POSTAGE AND FEES PAID
U.S. GOVERNMENT PRINTING OFFICE

JOURNAL OF RESEARCH of the National Bureau of Standards — Vol. 75C, Nos. 3 & 4 — July–December 1971
C. Engineering and Instrumentation

Contents

Page

Thermal voltage converters and comparator for very accurate AC voltage measurements. E. S. Williams. 145

Formulation and experimental verification of an axisymmetrical finite-element structural analysis. R. A. Mitchell, R. M. Woolley, and C. R. Fisher. 155

A Burnett apparatus for the accurate determination of gas compressibility factors and second virial coefficients, and an evaluation of its capability based on some results for argon and carbon dioxide. Meyer Waxman and John R. Hastings. 165

An extension to the sliding short method of connector and adaptor evaluation. Glenn F. Engen. 177

Accurate microwave high power measurements using a cascaded coupler method. Kenneth E. Bramall. 185

Publications of the National Bureau of Standards. 193

Index to volume 75C, January–December 1971. 217

Library of Congress Catalog Card Number: 62–3900

For sale by the Superintendent of Documents, U.S. Government Printing Office, Washington, D.C. 20402. (Order by SD Catalog No. C 13.22/sec. C: 75 (3 & 4). Price $1.25 (single copy). Subscription price: $5.00 a year; $1.25 additional for foreign mailing.
UNITED STATES GOVERNMENT PRINTING OFFICE, WASHINGTON : 1972